ASSESSMENT OF SOME TRIGGERING MECHANISMS ASSOCIATED WITH SUBMARINE SLOPE FAILURES ON CONTINENTAL SLOPES UTILIZING CENTRIFUGE TESTING

STERLING PARSONS

ASSESSMENT OF SOME TRIGGERING MECHANISMS ASSOCIATED WITH SUBMARINE SLOPE FAILURES ON CONTINENTAL SLOPES UTILIZING CENTRIFUGE TESTING

by

© Sterling Parsons, B.Eng.

A thesis submitted to the

School of Graduate Studies

in partial fulfilment of the

requirements for the degree of

Master of Engineering

Faculty of Engineering and Applied Science
Memorial University of Newfoundland

May 2005

St. John's Newfoundland

Your file Votre référence
ISBN: 978-0-494-31296-4
Our file Notre référence
ISBN: 978-0-494-31296-4

ABSTRACT

The conditions leading to submarine slope failures on continental slopes are not fully understood. A research program utilizing centrifuge modelling was developed to provide insight into the understanding of submarine slope failures on continental slopes. The primary research objectives were to develop methodologies for the modelling of submarine slope failures caused by static loadings on continental slopes, and to show that the test data obtained simulates prototype conditions.

Based on experience from previous demonstration tests, the testing program consisted of three centrifuge tests. The study investigated the triggering mechanisms in normally consolidated submarine slopes under static loads induced by two basic phenomena: sediment erosion and excess pore water pressure. Slope stability analysis using limit equilibrium methods was completed to evaluate the results of the centrifuge tests.

Due the high excess pore pressures required to initiate slope failures in the centrifuge and the restrictions imposed by the finite size of the centrifuge model, the centrifuge tests probably did not simulate actual natural submarine failure conditions. However, this research has provided new insights and allowed the development of new methodologies for the modelling of submarine slope failures, and has demonstrated the possible usefulness of the geotechnical centrifuge for this type of research. Further centrifuge testing and analysis is recommended.

ACKNOWLEDGEMENTS

I would like to thank my supervisor, Dr. Ryan Phillips, for his guidance and financial support throughout this program. I would also like to give many thanks to all the employees at the C-CORE Centrifuge Centre: Ms. Susan Pfister for her supervision and assistance as an experienced centrifuge user, Mr. Don Cameron and Mr. Derry Nicholl for their assistance with package preparation and practical advice, Mr. Karl Tuff and his workterm students for their electronic expertise, Dr. Bipul Hawlader for his technical assistance with the geotechnical analysis and a special thanks goes to Mr. Vincent Morgan for his continuous guidance and support.

I would also like to my parents for their sacrifices and moral support throughout my post-secondary education.

Finally I would like to thank my wife, Gina, if it weren't for her love and encouragement, the completion of this thesis would not have been possible.

TABLE OF CONTENTS

LIST OF TABLES

LIST OF FIGURES

LIST OF ABBREVIATIONS AND SYMBOLS

a	Acceleration
a	Cone net area ratio
A	Ratio of pore pressure to hydrostatic
b	Width of slice
c	Cohesion
c'	Effective cohesion
c_u/σ_v'	Normalized undrained strength ratio
CPT	Cone penetration test
d	Depth of wave
d	Geometric parameter of each slice
d	Particle size
e	Void ratio
E	Compressibility time
E	Interslice normal force
f	Perpendicular offset of the normal force from the centre of rotation of a slice
f_o	Correction factor
$f(x)$	Function that varies with respect to x
Fs	Factor of safety
g	Acceleration due to gravity
h	Height of slice
h_c	Capillarity
h_m	Depth of model
H	Height of wave
k	Permeability
k	Pseudo-static horizontal body force
l	Model length
l	Length of slice
L	Length of wave
LVDT	Linear voltage displacement transducer
N	Number of earth gravitations, g
N	Slice base normal force
N_{kt}	Empirical cone factor
P	Total normal force on base of slice
PPT	Pore pressure transducer
q_c	Measured cone tip resistance
r_u	Excess pore pressure ratio
r_d	Stress reduction factor
R	Radius or moment arm associated with the mobilized shear force of a slice

s	Available shear strength
s_u	Undrained shear strength
s_r	Saturation
SPT	Standard penetration test
SST	Slope stability test
t_1	Inertia
t_2	Laminar flow
t_3	Creep
u	Pore water pressure
u_b	Pore pressure acting on the cone tip
u_e	Excess pore water pressure
u_o	Hydrostatic pore water pressure referenced from the seabed level
W	Weight of slice
x	Angle between the tangent to the centre of the base of each slice and the horizontal
X	Interslice shear force
z	Soil depth

β	Angle of soil slope
ϕ	Particle friction
ϕ'	Internal angle of friction
γ'	Submerged unit weight of soil
γ_w	Unit weight of water
η	Viscosity
λ	Constant evaluate in solving the factor of safety
Λ	Normalized undrained shear strength constant
θ	Angle of the resultant interslice force from the horizontal
ρ	Density of soil
ρ_l	Liquid density
σ'	Effective normal stress
σ_c	Particle strength
σ_o	Total overburden pressure
σ'_o	Effective overburden pressure
σ_t	Surface tension

σ_v Total vertical stress acting on the cone tip

σ_v Vertical stress

τ Shear stress

τ_w Wave-induced shear stress

τ_h/σ_o' Cyclic stress ratio

ω Geometric parameter of each slice

LIST OF APPENDICES

1.0 INTRODUCTION

This thesis describes a research program utilizing centrifuge modelling to provide further insight into the understanding and mechanics associated with submarine slope failures on continental slopes. The study investigated the triggering mechanisms in normally consolidated submarine slopes under static loads induced by two basic phenomena: sediment erosion and excess pore water pressure. The primary research objectives were to develop methodologies for the modelling of submarine slope failures, conduct centrifuge tests investigating the behaviour of submarine slope failures, and show that the test data obtained reasonably simulate actual submarine slope failure conditions.

The progression of oil and gas exploration and development onto the continental slope, or in even deeper waters, has increased pressure for a greater understanding of submarine mass movements and their triggering mechanisms (Locat et al., 2000). The increasing need for seafloor transport and communication routes, the pressure on coastal developments, the protection of marine environment, and the impact of global changes are additional reasons why the understanding of submarine mass movements and their consequences have become such important issues.

After many decades of research, the conditions leading to failure, as well as the triggering of many large submarine slides throughout the world are still not fully understood (Laberg et al., 2003). Centrifuge modelling is one particular tool that can provide information into the mechanisms associated with submarine slope failures. Centrifuge

modeling is a method for reduced-scale physical modelling of gravity-dependent phenomena, such as submarine slope stability. Although centrifuge modelling is widely accepted for modelling many prototype events, there is no well-accepted methodology to model the stability of submarine slopes (Zhou et al., 2002).

The work presented in this thesis demonstrates methods of modelling submarine slope failures in the centrifuge. The overall objectives were to improve the current state of knowledge of submarine slope instabilities, and to demonstrate the usefulness of the centrifuge for this type of research.

2.0 LITERATURE REVIEW

2.1 General

Submarine slope instability is a common widespread phenomenon that imposes many constraints on marine engineering projects. Evidence of submarine slope failures can be observed in a variety of offshore environments, such as, shallow water regions, near-shore zones, continental slopes, and beyond to the deep ocean floors. This literature review will focus on the stability of slopes located on continental slopes, and in particular, submarine slope failures on low-sloped stratified silty clay deposits.

Submarine slope failures on continental slopes have been documented since the 19th century. Milne (1897) reported that landsliding was the probable reason for the breaking of communication cables off Newfoundland bank in 1884. This is quite possible considering the overwhelming evidence of the 1929 Grand Banks slide. Until the existence of remote sensing acoustic tools in the 1930s, the breaking of communication cables was the best evidence of submarine slope failures on continental slopes.

Since the 1930s, the development and improvement of offshore remote exploration technologies has significantly advanced. These technologies include high-resolution seismic profiling, side-scan sonar, and multibeam bathymetry, which can provide accurate sea floor or sub-bottom data. These technologies have greatly increased our understanding of submarine slope instabilities, and have allowed researchers to focus on particular triggering mechanisms that initiate slope failures.

Utilizing centrifuge modelling, this thesis attempts to provide insight into the mechanisms that cause submarine slope failures. First of all, an overview of how submarine slopes are assessed to be stable or unstable will be explained. The possible triggering mechanisms associated with submarine slope instabilities, the modelling of soil behaviour in the centrifuge, and previous centrifuge tests simulating the behaviour of submarine slope failures will also be discussed.

2.2 Analysis of Submarine Slope Stability

2.2.1 General

There are three major driving forces that affect the stability of a submarine slope: gravity forces, hydraulic forces and earthquake forces (Poulos, 1988). Gravity forces provide a mechanism for general mass movement, and slope failure. Hydraulic forces are the result of currents, tides, surface waves, and internal waves. The forces exerted due to earthquakes are the result of a sudden release of energy from a fault or fault complex.

To analyse these driving forces, significant advances have been made in the past few decades in the area of static and dynamic stability, and deformation analyses. The increased availability of microcomputers has contributed to extensive changes in the computational aspects of slope stability analysis. Analyses can be completed with enhanced efficiency, and can incorporate comprehensive soil mechanics than was not possible without computers.

This increase in computational power has led to the widespread use of finite-element methods for detailed analyses of soil slopes. Slope stability methods such as limit equilibrium methods, and continuum mechanics solutions also benefited from microcomputers. These methods are not as comprehensive as the finite-element method, but due to their simplicity they are widely used. These methods will now be discussed in further detail.

2.2.2 Limit Equilibrium Method

Limit equilibrium methods are widely used methods to assess the stability of slopes. The basic principle of limit equilibrium methods is the comparison of the overturning moments or forces acting on a supposedly unstable soil volume to the resisting moments or forces. In a deterministic analysis, the factor of safety against failure is the ratio of the resisting to overturning moments or forces. If the factor of safety is greater than one, then the slope is presumed to be stable. Probabilistic approaches can also be applied whereby, uncertainties in the loading and shear strength of the sediments are accounted for.

The analysis of a slope's stability subjected to gravity forces is often determined using limit equilibrium methods with a circular failure surface. However, for most submarine slopes, infinite slope analysis is often used (Lee & Edwards, 1986). This is due to the fact that the failure is assumed to occur parallel to the surface, and often the large size of submarine slides. To conduct an analysis, one of the three situations may occur: the

undrained condition, which may be relevant in cases of rapid deposition or erosion; the fully drained conditions whereby no excess pore pressures are present; the partially drained condition, in which some pore pressure dissipation has occurred and excess pore pressure exists (Poulos, 1988).

2.2.2.1 Infinite Slope Analysis

Infinite slope analysis is the most widely used method to assess submarine slope stability. This method utilizes force equilibrium between the shearing stress exerted by the buoyant weight of the soil mass, and the shear resistance the soil creates along a potential failure plane. In the instance of the shearing stress equalling the shearing resistance of the soil along the failure surface, submarine slope failure is initiated. The ratio between the shearing resistance, and the shearing stress of a potential failure plane is known as the factor of safety against sliding for that particular plane.

The infinite slope analysis method assumes that the sliding surface is parallel to the slope surface, and yields a relatively low depth to length ratio. The factor of safety can be calculated as,

$$Fs = \frac{s}{\tau} \tag{2.1}$$

where Fs is the factor of safety against sliding, s is the available soil shear strength or shear resistance and τ is the shear stress caused by the weight of the soil mass (Hampton et al., 1996). Assuming drained conditions, the shear strength of soil can be expressed in terms of effective stresses as,

$$s = c' + \sigma' \tan\phi' \tag{2.2}$$

where σ' is effective normal stress, ϕ' is the internal angle of friction and c' is the effective cohesion. For a linear slope with angle β, the shear stress and the normal stress acting on the sliding plane at a depth, z, below the seabed are,

$$\tau = \gamma' z \cos\beta \sin\beta \qquad\qquad \sigma' = \gamma' z \cos^2\beta \tag{2.3}$$

where γ' is the submerged unit weight of the soil. Substituting the expressions for available soil shear strength and shear stress into Equation 2.1 yields,

$$Fs = \frac{c' + \gamma' z \cos^2\beta \tan\phi'}{\gamma' z \cos\beta \sin\beta}. \tag{2.4}$$

For normally consolidated sediments, the effective cohesion may be approximately zero, therefore, the slope angle at failure is roughly equal to the drained angle of friction ϕ'. In most instances ϕ' is greater than 20 degrees, which demonstrates that drained failure under gravity forces alone would be an unlikely mechanism of failure for most continental slope failures, since continental slopes usually have angles of 1° – 10° (Menard, 1964).

For an undrained submarine slope stability analysis ($\phi' = 0$) the factor of safety against sliding becomes,

$$Fs = \frac{s_u}{\gamma' z \cos\beta \sin\beta} = \frac{2s_u}{\gamma' z \sin 2\beta} \tag{2.5}$$

or

$$Fs = \frac{2s_u}{\sigma_z' \sin 2\beta} \tag{2.6}$$

where s_u is the undrained shear strength. For slopes in normally consolidated soils, the factor of safety for infinite slope analysis is independent of the depth of the sliding surface since the undrained shear strength of a normally consolidated soil increases almost linearly with depth, and the vertical effective stress increases linearly with depth.

The presence of excess pore pressures in a submarine slope deposit can significantly decrease the stability of the slope. The effect of pore pressure on marine slope stability can also be estimated using the infinite slope analysis method. Quéméneur et al. (1998) shows that the shear strength of normally consolidated sediments can be expressed as,

$$s_u = \Lambda \sigma_z' = \Lambda \gamma' z \tag{2.7}$$

where Λ is the normalized undrained shear strength ratio, which is usually greater than 0.2.

When excess pore pressure exists the undrained shear strength can be written as,

$$s_u = \Lambda(\gamma' z - u_e) = \Lambda \gamma' z(1 - r_u) \tag{2.8}$$

where u_e is excess pore water pressure and r_u is the excess pore pressure ratio, which is defined as $r_u = u_e / \sigma_z'$. Therefore substituting Equation 2.8 into Equation 2.6 yields,

$$Fs = \frac{2\Lambda \gamma' z(1 - r_u)}{\sigma_z' \sin 2\beta} = \frac{2\Lambda(1 - r_u)}{\sin 2\beta}. \tag{2.9}$$

The ratio $(1-r_u)$ is a proportionality factor between normally consolidated and underconsolidated factors of safety. Quéméneur et al. (1998) states that due to the presence of excess pore pressure, undrained slope failure may occur at low slope angles. For example, gravity failure can occur at slopes lower than 6 degrees when r_u is greater than 0.6.

Consequently, since the slope gradients of continental slopes are relatively low, long-term and short-term gravity failures seem to be improbable in the sliding plane if the sediments are saturated and normally consolidated. Therefore, the existence of excess pore pressure is necessary to trigger infinite plane sliding. Also, the conditions are such that drained failures are not possible due to the presence of excess pore pressures, as a result, gravity hazards can only occur under undrained conditions.

Morgenstern (1967) proposed standard infinite slope stability equations for large, shallow submarine slopes that assess the factor of safety of a particular slope accounting for pore water pressure at the base of the strata. The factor of safety can be defined as,

$$Fs = \frac{\tan\phi'}{\tan\beta}[1-r_u] \tag{2.10}$$

where ϕ' is the internal angle of friction of the underlying soil layer, β is the slope angle, and r_u is the excess pore pressure ratio. Morgenstern's infinite slope stability equation assumes no influence from the boundary conditions and that all soil movement occurs in plane strain along a surface parallel to the slope.

Undrained submarine slope failures cannot only occur from gravity hazards, but also from dynamic loadings due to earthquakes. Morgenstern (1967) incorporated the cyclic loading of an earthquake in an infinite slope stability analysis by introducing a pseudo-static horizontal body force, k, as a percentage of gravity. Introducing the horizontal body force to an infinite slope analysis, the factor of safety can be expressed as,

$$Fs = \frac{c' + (\gamma' z \cos^2 \beta - u_e - k\gamma z \cos\beta \sin\beta)\tan\phi'}{\gamma' z \cos\beta \sin\beta + k\gamma z \cos^2 \beta} \tag{2.11}$$

where u_e is the excess pore water pressure (in excess of hydrostatic) generated during earthquake loading (Morgenstern, 1967).

It should be mentioned that the value of k is greatly influenced by local geological conditions and soil properties, and is empirically selected in terms of earthquake intensity. Lee and Edwards (1986), Lee et al. (1999), Barnes et al. (1991), and Rahman and Jaber (1991) all propose methods to assess the stability of submarine slopes subjected to cyclic loading caused by earthquakes.

Mello and Pratson (1999) proposed a method to assess regional slope stability based on two-dimensional state of stress in an infinite slope. This method incorporates cohesion and constant pore pressure with depth, and yields the principal stresses and possible slip-plane directions along a possible failure plane. The approach allows for a greater understanding of the general geometry and relative motion of mass movements, which is not considered by one-dimensional analyses.

2.2.2.2 Method of Slices

The method of slices has not been as widely used to assess the stability of offshore continental slopes as the infinite slope method, however analyses have been completed. Based on a static slope stability assessment of the Trænadjupet slide area on the mid-Norwegian margin, Leynaud & Mienert (2003) concluded both the method of slices and the finite element method yielded similar factors of safety.

A variety of analytical techniques for the method of slices have been developed. The primary difference between these methods is the expressions used to satisfy the static equations, the interslice normal and shear forces, and the assumed relationship between the interslice forces (Krahn, 2003). Figure 2.1 illustrates a typical slice in a potential sliding mass with the forces acting on the slice. Normal and shear forces act on the slice base, and the left and right sides of the slice.

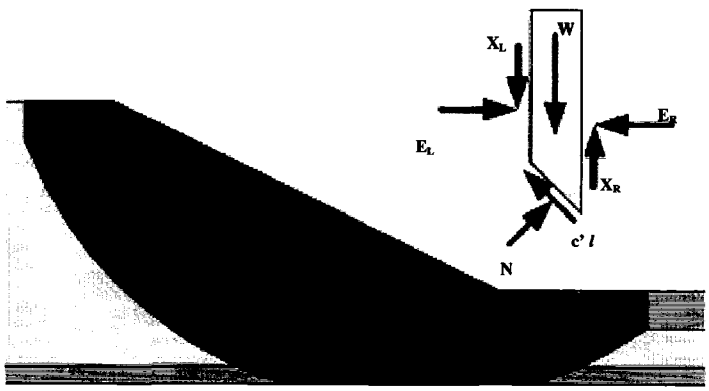

Figure 2.1: Slices and forces in a sliding mass.
(adapted from Krahn, 2003)

The static equilibrium of forces in two directions, and also the moments are used to determine the factor of safety of a particular slope. However, these relationships are insufficient to make the problem determinate, therefore, more information is required about either the normal force distribution, or the interslice force distribution (Fredlund and Krahn, 1976). Therefore, additional elements of physics, or an assumption should also be applied. Based on different assumptions various methods of analysis have been developed.

The most common methods of slices include the Ordinary method, Bishop's simplified method, Janbu's simplified method, Spencer's method, and the Morgenstern-Price method. Other methods have also been developed, but these methods are less common. Fredlund and Krahn (1976) developed the general limit equilibrium formulation, which encompasses the key elements of all methods previously listed. The general limit equilibrium formulation is based on two factors of safety expressions, and can incorporate a variety of interslice shear-normal force conditions. One expression provides a factor of safety satisfying moment equilibrium, and the other satisfying horizontal force equilibrium. These equations are all expressed in terms of effective stresses.

The general limit equilibrium factor of safety equation considering moment equilibrium is,

$$Fs_m = \frac{\sum \{c' lR + (N - ul) R \tan \phi'\}}{\sum Wx - \sum Nf} \tag{2.12}$$

and the factor of safety equation considering horizontal force equilibrium is,

$$Fs_f = \frac{\sum \{c' l \cos\beta + (N - ul)\tan\phi' \cos\beta\}}{\sum N \sin\beta} \tag{2.13}$$

where W is the total weight of the slice of width b and height h, N is the total normal force on the base of the slice over a length l, R is the radius or the moment arm associated with the mobilized shear force, u is the pore water pressure, f is the perpendicular offset of the normal force from the centre of rotation, x is the horizontal distance from the slice to the centre of rotation, and β is the inclination of the slice base.

The factor of safety equations described by Fredlund and Krahn (1976) included components to allow for the effects of earthquake loadings, partial slope submergence, and line loading of a slope. However, for simplicity these factors were omitted.

A key variable for both Equations 2.12 and 2.13 is the normal force, N. The normal force can be calculated from the equilibrium of vertical forces, which yields,

$$N = \frac{W + (X_R - X_L) - \frac{c' l \sin\beta + ul \sin\beta \tan\phi'}{Fs}}{\cos\beta + \frac{\sin\beta \tan\phi'}{Fs}} \tag{2.14}$$

where X is the interslice shear force acting on the right or left side of an individual slice, Fs is Fs_m when N is substituted into the moment equilibrium factor of safety equation, and Fs is Fs_f when N is substituted into the force equilibrium factor of safety equation.

The key point of a slice method is how the slice base normal is dependent on the interslice shear forces X_R and X_L on either side of the slice. The slice base normal differs between the previously listed methods in how each method accounts for the interslice shear forces. These methods will now be investigated in further detail.

Ordinary or Fellenius Method

The ordinary method of slices is the simplest method since it is the only analysis technique that incorporates a linear factor of safety expression. In this method, the interslice forces are neglected in this approach (Fellenius, 1936). Summing the moments about a common point derives the factor of safety for a given slope. Introducing the failure criteria and the normal force, the factor of safety can be expressed as,

$$Fs = \frac{\sum \{c'lR + (N - ul)R\tan\phi'\}}{\sum Wx - \sum Nf}. \qquad (2.15)$$

However, neglecting the interslice forces does not satisfy Newton's laws of physics between slices. The indiscriminate change in direction of the resultant interslice force from one slice to the next can result in factor of safety errors up to 60% (Whitman and Bailey, 1967).

Bishop's Simplified Method

The method of slices proposed by Bishop (1955) neglects the interslice shear forces, therefore, assuming that a normal or horizontal force adequately defines the interslice forces. The summing of forces in the vertical direction derives the normal force on the base of each slice:

$$N = \frac{W - \left(\frac{c'l \sin\beta + ul \sin\beta \tan\phi'}{Fs_m} \right)}{\cos\beta + \frac{\sin\beta \tan\phi'}{Fs_m}} \tag{2.16}$$

which is similar to Equation 2.14 except for the absence of the interslice shear forces.

The factor of safety is determined by summing the moments about a common point. Hence, the substitution of Equation 2.16 into Equation 2.12 of the general limit equilibrium formation will yield the Bishop's method factor of safety.

Janbu's Simplified Method

Janbu et al. (1954) proposed a correction factor, f_o, to account for the effect of interslice shear forces. The correction factor considers the effects of cohesion, angle of internal friction, and the shape of the failure surface. The normal force is expressed by summing the vertical forces, and ignoring the interslice shear forces. The normal force is expressed similarly as Equation 2.16 defined by Bishop's method.

Janbu's simplified method derives the factor of safety by utilizing horizontal force equilibrium. The factor of safety, Fs_f as expressed in Equation 2.13, is used to designate the factor of safety uncorrected for interslice shear forces. The corrected factor of safety is then,

$$Fs = f_o Fs_f . \tag{2.17}$$

Spencer's Method

This method assumes a constant relationship between the magnitude of the interslice shear force, and the interslice normal forces, E (Spencer, 1967). This relationship can be expressed as,

$$\tan\theta = \frac{X_L}{E_L} = \frac{X_R}{E_R} \tag{2.18}$$

where θ is the angle of the resultant interslice force from the horizontal. Summing the forces perpendicular to the interslice forces, Spencer (1967) derives the normal force accounting for forces in the vertical and horizontal directions as,

$$N = \frac{W - (E_R - E_L)\tan\theta - \left(\frac{c'l\sin\beta + ul\sin\beta\tan\phi'}{Fs}\right)}{\cos\beta + \frac{\sin\beta\tan\phi'}{Fs}}. \tag{2.19}$$

Spencer (1967) expressed two factors of safety, one based on the summation of moments about a common point, and the other summing the forces in the direction parallel to the interslice forces. They can be expressed similarly to Equations 2.12 and 2.13 of the general limit equilibrium formation. At some angle of the interslice forces the two factors of safety will be equal, at that point both the moment and force equilibrium are satisfied.

Morgenstern-Price Method

When developing their method, Morgenstern and Price (1965) assumed an arbitrary mathematical function to express the direction of the interslice forces as,

$$\lambda f(x) = X/E \tag{2.20}$$

where λ is a constant to be evaluated in solving the factor of safety, and $f(x)$ is a function that varies with respect to x. When the function is constant, the Morgenstern-Price method is identical to Spencer's method.

Similarly to Spencer's method, the general limit equilibrium equations effectively describe the expressions described by Morgenstern and Price (1965). The normal force is derived from vertical force equilibrium, as in Equation 2.15. However, differing from Spencer's analysis, the vertical shear forces are computed using an assumed λ value and side force function,

$$X = E\lambda f(x). \tag{2.21}$$

The Morgenstern-Price method calculates two factors of safety, one satisfying the conditions of moment equilibrium, and the other satisfying the conditions of force equilibrium. These expressions are similar to Equations 2.12 and 2.13 of the general limit equilibrium. The moment and force equilibrium factors of safety are solved for a range of λ values and a particular side force function. For some value of λ the two factors of safety will equal, therefore, satisfying both moment and force equilibrium.

2.2.3 Continuum Analyses

Analytical solutions from linear elasticity or viscoelasticity and continuum mechanics yield a number of procedures that have been developed to calculate stresses and

displacements in soil due to ocean waves (Hsiao and Shemdin, 1980; Seed and Rahman, 1978; Yamamoto, 1978) and earthquake loadings (Seed and Idriss, 1971). Methods in the literature assume the soil to be either a semi-infinite homogeneous elastic half-space, or a single homogeneous elastic layer of finite thickness. Those methods were followed by procedures that allowed for non-homogeneous soils (Booker et al., 1985a, b) or layered anisotropic profiles (Small and Booker, 1982) to be determined without a large amount of computation.

The principal idea of continuum analyses is to compute the shear stresses that are developed in the soil at different depths by wave or earthquake loading. The shear stresses are then compared with the shear strength of the soil at the equivalent depths. The shear strength is computed accounting for the effects of cyclic and/or dynamic loading. When the shear stress reaches the magnitude of the shear strength, failure is assumed to occur (Poulos, 1988).

To express wave-induced cyclic loading, Seed and Rahman (1978) proposed a form of the following expression using the wave-induced shear stress, τ_w, as a function of the depth of the sediment and wave properties, which contributes to the prediction of the effects of wave-induced instability. The expression is,

$$\frac{\tau_w}{\gamma' z} = \sin\beta + \frac{\pi\gamma_w H}{\gamma' L \cosh\left(\frac{2\pi d}{L}\right)} \tag{2.22}$$

where γ' is the submerged unit weight of the sediment, β is the slope angle, γ_w is the unit weight of water, H is the height of the wave, d is the depth of the water, and L is the length of the wave.

Simplified approaches to evaluate liquefaction potential under earthquake loading have been published by Seed and Idriss (1971), Ishihara (1977), Seed et al. (1983), Robertson and Campanella (1985), Robertson and Wride (1998), and Youd et al. (2001). The first three authors propose methods that utilize mostly empirical relationships based on results from standard penetration tests to determine the stress conditions required to cause liquefaction. The latter three authors use techniques that apply empirical relationships based on cone penetration test data. Youd et al. (2001) incorporate empirical relationships and in-situ penetration test techniques to provide state-of-the-art liquefaction potential procedures for standard industry practice.

Seed et al. (1983) propose a relatively straightforward approach. The cyclic stress ratio, τ_h/σ_o', created in the soil due to earthquake loading is approximated using the following expression,

$$\frac{\tau_h}{\sigma_o'} \cong 0.65 \frac{a_{\max}}{g} \frac{\sigma_o}{\sigma_o'} r_d \tag{2.23}$$

where $a_{\max}$ is the peak acceleration at the ground surface, g is the acceleration due to gravity, σ_o is the total overburden pressure neglecting the hydrostatic pressure due to

water overlying the seabed, $\sigma_o^{'}$ is the effective overburden pressure, and r_d is the stress reduction factor, which can be approximated by,

$$r_d = 1.0 - 0.015z \tag{2.24}$$

where z is the depth of soil in metres.

The cyclic stress ratio can be determined from a modified penetration test and the earthquake magnitude. Seed et al. (1984) propose a modified correction value to adjust the standard penetration test (SPT) value for overburden pressure, and standardize the energy ratio applied from the drill rods.

Finn (2002) provides state-of-the-art liquefaction assessment charts based on various penetration tests and in-situ shear wave velocity. The charts can be utilized for engineering practise based on the standard penetration test, the cone penetration test, the Becker penetration test, or measured in-situ shear wave velocities.

2.2.4 Finite Element Method

The finite element method is a numerical method that can be used to solve problems in many engineering applications. The finite element method is useful for problems involving complicated geometries, loadings, and material properties, where analytical mathematical solutions are not possible to obtain. These analytical problems generally require the solution of ordinary or partial differential equations that are not easily

computed. The use of numerical methods, such as the finite method is often necessary to obtain acceptable solutions (Logan, 2002).

The finite element method has been widely accepted as a technique to analyse geotechnical problems. The method can utilize elastic-plastic constitutive laws that can capture the non-linearity of soils, and the development of pore pressure under various loading conditions. To approximate the non-linear stress-strain curves, incremental and iterative techniques are used to compute the stresses and strains in each element.

The application of the finite element method to assess the stability of submarine slopes has been documented by numerous authors (Towhata and Ryull, 1990; Azizian and Popescu, 2001; Azizian and Popescu, 2003; Biscontin et al., 2003; and Leynaud and Mienert, 2003). One of the major advantages offered by the finite element method is that it predicts seabed movements, and provides an indication of the overall stability of a slope. It can also compute the stability of slopes of non-homogeneous or anisotropic soils in a relatively straightforward manner. However, it is difficult obtaining the required soil properties with the level of confidence comparable with the accuracy provided by the method (Poulos, 1988).

2.3 Discussion of Triggering Mechanisms Associated with Submarine Slope Failures

2.3.1 General

Utilizing exploration techniques, on-site investigations of specific mass movements must be conducted to effectively investigate the possible triggering mechanisms associated with submarine slope failures on continental slopes. Typically, submarine mass movements originate in many different climatic and geomorphic environments. Due to the variety of submarine environments globally, mass movements occur in areas with a wide range of physical characteristics.

Submarine mass movements can range in volumes of several tens of cubic metres to enormous slides such as the Agulhas Slide. Occurring off the coast of South Africa, the Agulhas Slide is the largest known submarine slide with an estimated volume of 20,000 km^3 (Hampton et al., 1996). The thickness of submarine slides also varies over a wide range. Piper and McCall (2003) observed rotational slumps on the St. Pierre Slope with a thickness of 5 – 10 m, whereas Bugge et al. (1987) documented that the Storegga slide was up to 450 m in thickness. Continental slopes can have gradients that range from 1° to 10° (Menard, 1964), however slopes of 3° to 6° are typical (Shepard, 1963).

Although continental slopes do have relatively gentle gradients, submarine canyons, which are often included in the topography of a continental slope, generally have steeper slopes. The presence of submarine canyons on continental slopes can contribute to

submarine slope failures. The possibility of sediment accumulation on the head of submarine canyons, and the channel effect they provide for the flow of sediments can initiate slope instability (Morgenstern, 1967).

According to Driscoll et al. (2000), an understanding of slope instability failure mechanisms is necessary to improve the ability to forecast potential hazards posed to structures and populations. In recent years, many researchers have concentrated on the development of tsunamis due to large submarine mass movements (Lynett et al., 2003; Trifunac and Todorovska, 2003; Walder and Watts, 2003; Watts, 2003). Through increased study, researchers are increasing their ability to forecast potential risks to structures and populations based on the probability of a significant tsunami event.

As previously mentioned, there are three major driving forces that affect the stability of a submarine slope, they include: gravity forces, hydraulic forces, and earthquake forces. Researchers have subdivided these forces into many possible mechanisms that may initiate submarine landslides, these include: tectonic oversteepening, seismic loading, storm-wave loading, rapid accumulation and underconsolidation, diapirism, gas hydrate disassociation and gas charging, sediment erosion, low tides and seepage, glacial processes, volcanic island processes, and creep (Locat and Lee, 2000; Hampton et al., 1996). It should be noted that quite often slope instability on low slopes is caused by more than one triggering mechanism (Lee, 2003; Bryn et al., 2004).

Although this thesis concentrates on the stability of slopes on the continental slope, there are many other submarine environments in which slope failures can occur. These areas include: fjords, active river deltas on the continental margin, submarine canyon-fan systems, and oceanic volcanic islands (Hampton et al., 1996). Several of the mechanisms previously mentioned do not significantly affect the stability of continental slopes, however, they do create slope stability concerns in other submarine environments. When applicable, submarine environments other than continental slopes will be utilized to demonstrate the effects of certain triggering mechanisms on slope stability.

2.3.2 Tectonic Oversteepening

The tectonic activity associated with faulting can lead to an increase of slope angle caused by warping and faulting. Large slides have been identified in the submarine environment, due to the oversteepening and subsequent increase of gravity forces associated with tectonic scraping and warping (Morgenstern, 1967; Prior and Coleman, 1984).

Schwab et al. (1991) described a large amphitheatre-shaped scarp approximately 55 km across, which was discovered on the northern insular slope of Puerto Rico. The large slide is believed to be caused by tectonic oversteepening, generating a mass movement in excess of 1500 km^3 of material. It is alleged that the upper part of the slope uplifted a few hundred metres resulting in a final water depth of approximately 3000 m. The toe of

the slope subsided more than 4000 m, thus generating a 4.5° regional slope, and large enough shear stresses to initiate slope failure.

Booth and Garrison (1978) conclude that faulting is a major feature on the Mississippi delta. They conclude that faulting was the probable cause of retrograde slumping in the area. Hampton et al. (1978), Johns et al. (1986) and Evans et al. (1996) also conclude that oversteepening is one of several major factors that can initiate slope failure.

2.3.3 Seismic Loading

Another tectonic activity that is attributed to slope failure is earthquakes. The application of vertical and horizontal acceleration stresses due to strong earthquakes significantly jeopardises the stability of a submarine slope (Morgenstern, 1967). As explained by Poulos (1988), strong earthquakes will generally cause large accelerations, velocities, and displacements leading to consequent slope failure. Based on studies by Boulanger et al. (1998), smaller non-failure earthquakes can actually strengthen the sediment matrix by developing excess pore water pressure during seismic loading and thereby allowing drainage and densification after the end of earthquake.

The governing factor affecting slope stability from earthquakes is the development of cyclic lateral motions that occur primarily in the underlying bedrock. The generated motions create shear stresses in the overlying soils deposits that are both dynamic and cyclic in nature. Failure may occur when the lateral displacements in the bedrock layer

fall out of phase with those in the soil layer, creating large lateral strains and subsequent excess pore pressure in the soil.

The direct link between earthquakes and submarine slope instability is widely accepted and numerous events have been well documented (Prior and Coleman, 1984). One of the most well known failures is the 1929 Grand Banks failure off the coast of Newfoundland. The main triggering mechanism known to initiate the mass movement was a large earthquake. The earthquake had a magnitude of 7.2 on the Richter scale and the epicentre was located on the western margin of the St. Pierre Slope at a depth of 2000 m. Along with severing several cables, a turbidity current traveled at a velocity of 19 m/s, and the total sediment transported was estimated to be in excess of 150 km^3 (Piper et al., 1999).

Well-known slides that occurred on the continental slope offshore of Norway are the Trænadjupet Slide (Laberg and Vorren, 2000) and the Andøya Slide (Laberg et al., 2000). The initiation of these slope failures can be attributed to strength reduction due to earthquake loading. It is believed that other potential contributing factors may have also caused shear strength reduction for the Trænadjupet and Andøya slides.

Hampton et al. (1978) describe a large submarine slope failure that occurred on the continental shelf and continental slope in the Gulf of Alaska. They accredit the slope failure to a variety of circumstances. However, the major triggering factor was the creation of excess pore pressure due to earthquake loadings.

2.3.4 Storm Wave Loading

In shallow water near shore and on continental shelf systems, the migration of large surface waves applies relatively large hydraulic forces on the seabed. These waves create dynamic water pressures on the ocean floor, and can create shear stresses, strains, and excess pore pressures that can create possible seabed instability (Zen et al., 1991).

The stability of the seabed subjected to wave-induced stresses and excess pore pressures has had considerable attention (Poulos, 1988). The nature of wave-induced liquefaction can be categorised into two main processes of how excess pore pressures are created. Similar to earthquake-induced liquefaction, the first process is liquefaction caused by the cyclic shear stress that produces the steady increase of excess pore pressure in the seabed (Zen et al., 1991). The second process contributing to wave-induced liquefaction is the spatial difference in pore pressures within the seabed. One cause of this spatial difference is the damping and phase lag in the propagation of pore pressures. Another cause is the upward seepage flow created in the seabed due to the rapid lowering in the sea surface during the passage of wave troughs.

Wave effects are significant, and can cause potential risks to near shore structures, though pressure amplitudes decrease with increasing water depth. Bottom pressure anomalies due to storm waves are not a major factor affecting slope stability for water depths greater that 500 m. Therefore, on continental slopes, where water depths are regularly larger than 500 m, wave-induced loadings can often be ignored in the stability analysis (Hampton et al., 1978; Edwards et al., 1980; Piper and McCall, 2003). However,

canyons heads that are often at water depths of 100 – 200 m are susceptible to cyclic loading from wave effects.

2.3.5 Rapid Accumulation and Underconsolidation

Underconsolidation does not exist under normal static steady state conditions (Quéméneur et al., 1998). The static equilibrium of sediments corresponds to normally or overconsolidated sediment states. The development of underconsolidated sediments is associated with dynamic processes that create the existence of excess pore water pressure. There are numerous causes for underconsolidation, such as seismic activity, storm waves, tides, hydrothermalism, gas generation, and the recent/rapid deposition of sediments.

On deltaic areas that are supplied from fjords, sediment accumulation is associated with submarine slope failures. The rapid deposition on deltas can outpace the expulsion of pore water, causing a state of underconsolidation and subsequent low shear strength (Terzaghi, 1956; Hampton et al., 1996). Johns et al. (1986) describe local slope failures on the delta-front slope at Kitimat Fjord, British Columbia, stating that rapid deposition is a possible explanation for slope failures.

The point source supply of sediment from a river mouth onto the continental margin can generate areas where deltaic deposits are commonly subjected to submarine slope failures. Studies of the Mississippi River delta (Terzaghi, 1956; Coleman & Prior, 1978;

Prior & Coleman, 1978; Prior & Coleman, 1984) have shown that large amounts of sediment, as much as 6 million tons is deposited into the ocean annually. Fine sands typically accumulate at or near the migrating distributary mouths, and silt-clay sediments accumulate mainly beyond the distributaries onto the exterior regions of the delta. The fine-grained sediments when deposited have very high water contents, and are extremely underconsolidated.

High sedimentation rates associated with times of glaciation can be related to slope failures on continental slopes. Describing the Trænadjupet Slide event, Laberg and Vorren (2000) conclude that periods of high sedimentation during glacial periods promoted instability of the glacigenic sediments, and inhibited fluid dissipation from the relatively thin layers of interglacial and interstadial sediments. Since water/gas dissipation was inhibited, the build-up excess pore pressure proceeded, and the interglacial and interstadial sediment interfaces behaved as the planes of failure. However, as previously stated, it is believed that earthquake loading was the triggering mechanism that ultimately initiated the slope failure.

One of the largest submarine slides known is the well-documented Storegga Slide located on the 0.5 - 2.0° continental slope offshore of Norway (Bugge et al., 1987). The slide is believed to have occurred as one main event approximately 8,200 years ago and resulted in a slide scar of approximately 300 km. The rapid loading of glacial clays onto sensitive marine clay layers is believed to have created excess pore pressures of 20 to 30% above

hydrostatic. This process is regarded as the main destabilization factor of the mass movement (Byrn et al., 2004).

Rapid deposition can also create oversteepening of the slope, which subsequently can lead to slope failure. In the western Mediterranean, Casas et al. (2003) state that submarine mass movements on the Ebro slope are a result of relatively high sediment supply to the area.

2.3.6 Diapirism

In many submarine basins, the creation of salt or mud diapiric structures can vary widely in scale and in intensity of movement. Often becoming several kilometres in area, diapiric structures can reach heights of 300 m to 500 m. Continued vertical movement of the diapiric formations can cause local oversteepening of sediments, which can lead to widespread sediment instability (Prior and Coleman, 1984).

There are numerous examples of submarine mass movements in which diapirism is considered a governing failure mechanism. Almagor (1980) describes slope failures on the continental slope off the coast of northern Sinai-southern Israel. He states that considerably large deposits of buried evaporites created slope oversteepening and eventual slope failures. Carlson et al. (1993) concludes that the emergence of mud diapirs on the Umnak Plateau in the southern Bering Sea led to the oversteepening that ultimately caused failure of the seafloor.

2.3.7 Gas Hydrate Disassociation and Gas Charging

The dissociation of gas hydrates in underlying submarine slopes is believed to contribute to slope instability. Gardner et al. (1999) points out that gas hydrates were discovered downslope of the Humboldt slide of the coast of California. Sediment samples were recovered from the upper zone of the slide containing high concentrations of methane rich gas. They conclude that the resulting mass movement was related to excess pore pressures with a direct reduction in strength. It was believed that the gas formations significantly contributed to failure, however, were not the exclusive cause.

Gas hydrates are ice-like materials that contain natural gas and water. Under certain pressures and temperatures associated with seafloor conditions, gas hydrates are considered stable. When temperatures increase or pressures decrease, the stability of the sediment may decrease since the hydrate may disassociate and release bubble-phase natural gas. If pore water movement is obstructed due to low sediment permeability, the gas charging may cause excess pore pressure, and promote slope instability (Locat and Lee, 2000).

Piper and McCall (2003) state that the dissociation of gas hydrates is thought to contribute to slope instability, yet their actual role is still uncertain. New studies are steadily developing theoretical models to assess the stability of submarine slopes in gas hydrate regions. Sultan et al. (2003) presents a model of the thermodynamic chemical equilibrium of gas hydrates that accounts for the influences of temperature, pressure, and pore water chemistry. Utilizing their model, they conclude that the melting of gas

hydrates may have caused a decrease in sediment strength, contributing to the Storegga slide.

Based on an extensive study of the Storegga slide, Bryn et al. (2004) conclude that even though geophysical surveys indicated the possibility of gas hydrates in some areas, their presence was not confirmed in any geoborings, also the gas saturation pressure sampled in the pore water was low. The authors do concur that the melting of gas hydrates may have contributed to the destabilization of sediments of the Storegga slide (Bryn et al., 2004).

Along with gas hydrates, the presence of free gas within sediments can create gas charging, which can decrease sediment shear strength and lead to slope failure (Locat and Lee, 2000). In most cases the gas is methane, which originates from sediments containing organic materials. The methane bubbles have been attributed as a mechanism promoting slope failure at many sites. The Humboldt slide (Gardner et al., 1999) and the region instability in the Gulf of Alaska (Hampton et al., 1978) are just some examples of gas charging being identified as a possible mechanism for decreasing sediment shear strength.

2.3.8 Sediment Erosion

The erosion of the seafloor by strong currents can jeopardise the stability of a slope. Currents in canyons can create erosion along the entire escarpment, which can lead to

fault-bounded translational slides (Hampton et al., 1996). The slope failure eventually occurs because the erosion of sediments create slope oversteepening, whereby, the gravitational driving forces would then exceed the sediment shear strength.

Sangrey and Marks (1981) state that geophysical studies indicate that several seafloor features show erosional undercutting by currents in the Baltimore canyon region. The authors conclude that a particular group of submarine mass movements were likely due to these erosional undercuttings.

2.3.9 Low Tides and Seepage

Submarine mass movements occur frequently due to the effects of low or rapidly changing sea level at nearshore or intertidal areas (Hampton et al., 1996). Similar to the passing of a waves trough, the rapid decrease in sea level decreases the overlying hydrostatic pressure that is experienced by the seabed. This relatively instantaneous decrease in pressure creates differential pressures in the seabed that can cause upward seepage of pore water in the seabed. The upward seepage of pore waters can decrease the effective stress and hence the shear strength of the soil, which can lead to possible seafloor instability (Zen and Yamazaki, 1991).

Johns et al. (1986) conclude that numerous shallow rotational and translational mass movement events that occurred at Kitimat Fjord, British Columbia were the result of tidal

effects on the delta-front region. Among other factors, rapid tidal drawdown appeared to be one of the contributing reasons resulting in failure.

The effect of tidal variations on gassy deposits of loose Fraser River sand was studied by Atigh and Byrne (2004). Tidal variations can cause unequal pore-pressure generation with depth and time in unsaturated sediments. Such changes reduce the effective stresses during low tides and may induce liquefaction flow of slopes due to partial drainage conditions. Using an effective stress approach, a fully coupled analysis was carried out to assess the potential of liquefaction resulting in retrogressive flow slides, similar to those observed on the Sand Heads at the front of the Fraser delta.

The failure of submarine slopes due to rapid drawdown is one example of the effects water seepage. Seepage can also occur beyond the immediate coastline through coastal aquifers and other pore fluid migration processes. Christian et al. (1995) state that based on geophysical logging of deep boreholes on the Fraser River delta, the presence of freshwater was noted within the sediments. They concluded that the freshwater was possibly creating artesian conditions within the underlying deposits contributing to slope failure. Robb (1984) completed a study off the coast of New Jersey providing evidence that groundwater discharge contributed to mass movements on parts of the lower Atlantic continental slope.

Another event that can cause seepage effects in seafloor sediments is sediment subduction at plate boundaries. This process can initiate the seepage conditions necessary to cause slope failure (Locat and Lee, 2000).

2.3.10 Glacial Processes

Regional glaciation may also contribute to submarine slope instability. Governing factors may include warping and flexing of the crust, greatly altering drainage and groundwater seepage, rapid sedimentation of sediments, and rapid emplacement of moraines and tills (Locat and Lee, 2000; Hampton et al., 1996). Mulder and Moran (1995) discuss several ice-margin events, the most significant is bearing capacity failure. The loading of glacial ice may have created large shear stresses on the seafloor causing slope failures.

Based on site geotechnical investigations, Dimakis et al. (2000) discovered areas of instability in the Svalbard-Barents Sea margin. They contribute the instability to rapid sedimentation that occurred mostly during periods of maximum glaciation with the ice front located along the shelf edge. It is thought that the sediment was delivered to the upper continental slope as deformational till. Also, the sediment was believed to have been transported out beneath the ice in a conveyor belt fashion, and deposited in front of the ice margin.

2.3.11 Volcanic Island Processes

Volcanic islands are a common geologic feature that cause submarine slope instability and create some of the largest mass movements on the planet (Locat and Lee, 2000). The large movements can reach distances of 200 km and giant slumps can create ground vibrations equivalent to M7 earthquakes, which may induce tsunamis and create immediate hazards to structures and lives.

The mechanisms of failure due to volcanic processes are not well understood. Nevertheless, the presence of magma near the failure surface, the physical properties of rapidly deposited igneous rock, and the magma or gas pressures located within the core of the islands are all thought to contribute to slope instability. Moore et al. (1989) describe the slope failure events on the young submarine Loihi Volcano, south of Hawaii. The authors explain that more than half of the volcano's surface has experienced mass movements due to the active processes of the volcano.

2.3.12 Creep

Submarine mass movements due to gravitational loading, other than those caused by incomplete consolidation, may be classified as either basic instability or creep (Poulos, 1988). When shear stresses in the seabed are equal to the sediments shear strength, slope failure may occur. The mass movements associated with this condition are often rapid, and usually involve the movement of large amounts of sediment in a relatively short amount of time.

On the other hand, the creep of submarine slopes may arise under constant stress in clay soils. The rate of strain is dependent on the ratio of applied shear stress to shear strength. At low ratios, the rate of strain may accumulate at a decreasing rate with time. However, at high ratios the strains may accumulate rapidly, and result in slope failure. This type of slope failure is generally known as creep rupture.

Based on a multibeam survey of the Scotian slope, Pickrill et al. (2001) conclude that spreading creep developed a few tens of metres in the seabed. It was observed that sediment creep occurred when the toe of the creep slab had become removed due to retrogressive slumping or valley widening.

2.3.13 Retrogressive Failure of Submarine Slopes

A major feature of many submarine slides is retrogressive slope failure (Mulder and Cochonat, 1996). Gardner et al. (1999) conclude that the presence of numerous typical characteristics indicate that the Humboldt slide was retrogressive in nature. The turbidity current associated with the 1929 Grand Banks slope failure was believed to have originated from a downslope retrogressive rotational slump (Piper et al., 1999).

Hampton et al. (1996) describes retrogressive failure as sliding that occurs serially as numerous adjacent failures progress upslope. Retrogressive slope failures can occur in sediment deposits that may include sand, silt, or sensitive clays. A retrogressive slope failure in a loose sandy and silty deposit is described by Terzaghi (1956), while Bryn et

al. (2004) describes the Storegga slide as a retrogressive failure having occurred in marine and glacial clays.

2.3.14 Other Factors Affecting Submarine Slope Failures

A common submarine geotechnical stratigraphy feature associated with submarine slope failures is the presence of sediment layering. Sediment layering can confine excess pore pressures within underlying soil layers that can cause seabed instability. As previously discussed in Section 2.3.5, Laberg and Vorren (2000) conclude that due to high sedimentation rates, the build-up of excess pore pressure within underlying interglacial and interstadial sediment layers contributed to the loss of soil strength.

The existence of in situ excess pore pressures within sediment layering can significantly decrease the stability of a submarine slope. Researchers have expressed the effects of excess pore pressures in sediment layering in terms of the excess pore pressure ratio, r_u. Cayocca et al. (1998) state that a translational mass movement on the 4° continental slope in the Gulf of Guinea was initiated due to several triggering mechanisms. They conclude that at r_u values of 0.78 to 0.90, seepage may have created liquefied zones within the slide.

Due to the significant difficulty measuring the excess pore pressures associated with submarine slope failures, there is limited literature published. Since submarine slope failures are often large, where the failure surface is hundreds of meters in thickness,

(Casas et al., 2003; Bryn et al., 2004) retrieving sediment samples and peizometer data is often difficult. For instance, the Humboldt slide involved sediment failure at depths of at least 65 m below the seafloor (Gardner et al., 1999). The authors' inability to collect geotechnical data at those depths restricted them from completing a rigorous stability analysis. Therefore, they were not able to speculate the excess pore pressures necessary to cause slope instability.

In their discussion of submarine mass movements on the Canadian eastern margin, Piper and McCall (2003) state that excess pore pressures may play a role in sediment failure. They note that excess pore pressures might be generated on the mid Scotian slope by rapid loading by till tongues on the upper slope. However, they conclude that the role of pore pressures in failure is still poorly understood and their research does not throw new light on the issue.

Although the relationship of excess pore pressures and slope failure are not well understood, many authors attribute slope failure to increases in pore pressures. Tripsanas et al. (2003) state that due to the deposition from upslope mass-transport flows on the northwestern continental slope of the Gulf of Mexico, a sudden increase of overburden pressure was applied to the underlying layers. Since the local geotechnical stratigraphy consisted of alternating sand/silt and mud layers/laminae overlying noncohesive layers of sediments, the overlying impermeable mud layers acted as seals, preventing dissipation of pore pressures from the noncohesive layers. The increase of pore pressures led to a

significant reduction of shear strength of the weak layers, which contributed to a retrogressive slide.

Another retrogressive submarine slide associated with sediment layering and excess pore pressures is the Storegga slide (Bryn et al. 2004). As a result of glacial and interglacial cycles, most of the slope sequence consists of alternating weak marine and stronger glacial clay layers. As previously stated in Section 2.3.5, the rapid loading of glacial clays onto sensitive marine clay layers is regarded as the main destabilization factor of the mass movement. Bryn et al. (2004) state that based on numerical simulation and sediment sampling, the excess pore pressures of the intact shelf were to the degree of 20 to 30% above hydrostatic at the time of the Storegga slide.

Elaborating further, Bryn et al. (2004) state that the Storegga slide was probably caused by the initial movement of sediment material in the lower slope due to rapid sediment deposition. The initial sediment removal unloaded the headwall upslope causing strain concentration zones in the toe area of the headwall. In the concentration zones, large shear strains caused strain-softening in the sensitive marine clay layer that developed into progressive failure along the layer. Glide planes were formed within the marine clays, allowing the overlying glacial deposits to act as the main driving force for the sliding.

As demonstrated by the events of the Storegga slide, the strain-softening behaviour of marine clays is another important factor in understanding the failure and retrogressive slide processes in low angle slopes of the continental margin (Bryn et al. 2004). A strain-

softening clay may fail progressively when the peak shear strength is equaled and starts to loose strength. Progressive failure in normally consolidated clays has been documented (Puzrin et al., 2004). Progressive failure is commonly associated with the long-term stability of slopes in overconsolidated clays, however, short-term stability can be also affected.

2.4 Modelling of Soil Behaviour

2.4.1 General

Modelling plays a vital role in geotechnical engineering. Physical modelling attempts to replicate phenomena that exist in the prototype, whereby, the model may be a reduced scale version of the prototype, or a full-scale model. The events occurring in the model and prototype should be similar, and their similarity should be related by appropriate scaling laws. The development of model laws can be accomplished through dimensional analysis, or from differential equations that influence the phenomena, however, a combination of both can also be used.

When modelling any material, it is essential to consider the following three fundamentals:

- All significant influences should be modelled in similarity,
- all phenomena not modelled in similarity should be established secondarily by experimental evidence, and
- any phenomena that is unknown should be disclosed or confirmed insignificant by utilizing the test results (Fuglsang and Ovesen, 1988).

A challenge of geotechnical modelling is the importance of replicating soil behaviour in terms of strength and stiffness (Taylor, 1994). In geotechnical engineering, the behaviour of soil can greatly vary from one particular problem to another. There are two significant reasons why the soil behaviour may vary. First, since soil is often deposited in layers, it is possible to observe different soil strata affecting a particular problem in various ways. Second, the in-situ stresses of a soil deposit change with increasing depth. It is the second reason that centrifuge modelling has become an effective tool for the study of geotechnical problems.

2.4.2 Centrifuge Modelling

Centrifuge modelling enables the geotechnical engineer to study and analyse design problems using geotechnical materials. A centrifuge is an advanced load frame whereby soil samples can be tested under increased gravity. In order to apply the increased gravitational force, soil models are rotated at the end of a centrifuge arm. This rotation creates an inertial radial acceleration, applying a gravitational acceleration field much larger in magnitude than the Earth's gravitation field (Schofield, 1980).

The application of the increased gravitational field allows a free unstressed soil surface, while as the soil depth increases the magnitude of soil stresses and strength increase. In most circumstances, the prototype soil material should be used in the model due to the fact that different soils display very different stress-strain relationships (Taylor, 1994). Therefore, it is necessary that model stresses equal prototype stresses. Based on this primary relationship, laws of similarity are developed.

Two main issues concerning centrifuge modelling are scaling laws and scaling errors. As previously mentioned in Section 2.4.1, scaling laws can be derived utilizing a combination of both dimensional analysis and governing differential equations. Combinations of both are also used to define the scaling relationships for centrifuge modelling.

To develop laws of similarity for static stress, if N is considered the multipler of earth gravity g, applied to a material having density ρ, with a vertical stress σ_{vm} (subscript m represents the model), and a model depth of h_m, then the vertical stress in the model can be represented by,

$$\sigma_{vm} = \rho N g h_m \tag{2.25}$$

therefore, for the prototype (subscript p represents the prototype) the vertical stress would be,

$$\sigma_{vp} = \rho g h_p \tag{2.26}$$

Since, it is necessary for the model stresses and prototype stresses to equal,

$$\rho N g h_m = \rho g h_p \tag{2.27}$$

therefore,

$$h_m = \frac{1}{N} h_p . \tag{2.28}$$

From this relationship the scale factor (model : prototype) for linear dimensions is 1: N. Since the height model-prototype relationship is linear, then displacements will also have

a scale factor of 1: N. Table 2.1 provides a list of scaling factors covering the basic soil parameters used in centrifuge modelling.

Table 2.1: Scaling factors in centrifuge tests.
(Adapted from Fuglsang and Ovesen, 1988)

Parameter	Symbol	Dimensionless Number	Similarity Requirement	Scaling Factor
acceleration	a		$N_a =$	n
model length	l		$N_l =$	$1/n$
soil density	ρ		$N_\rho =$	1
time	t		$N_t =$	$1/n^2$
particle size	d	d/l	$N_d =$	1
void ratio	e	e	$N_e =$	1
degree of saturation	S_r	S_r	$N_S =$	1
liquid density	ρ_l	ρ_l/ρ	$N_{\rho_l} = N_\rho =$	1
surface tension	σ_t	$\frac{\sigma_t}{\rho_l a d l}$	$N_\sigma = N_\rho N_a N_d N_l =$	1
capillarity	h_c	$\frac{h_c \rho_l a d}{\sigma_t}$	$N_h = N_d N_\rho^{-1} N_a^{-1} N_d^{-1} =$	$1/n$
viscosity	η	$\frac{\eta}{\rho_t d \sqrt{al}}$	$N_\eta = N_\rho N_d N_a^{1/2} N_l^{1/2} =$	1
permeability	k	$\frac{k\eta}{d^2 \rho_t a}$	$N_k = N_d^2 N_\rho N_a N_\eta^{-1} =$	n
particle friction	φ	φ	$N_\varphi =$	1
particle stress	σ_c	$\frac{\sigma_c}{\rho a l}$	$N_\sigma = N_\rho N_a N_l =$	1
cohesion	c	$\frac{c}{\rho a l}$	$N_c = N_\rho N_a N_l =$	1

As previously stated, for most instances the prototype soil should be used as the model soil. However, the scaling factor for the particle size should be equivalent to the model length scaling relationship, 1: N. The prototype material introduces a discrepancy of the scaling factor on particle size, which may distort test results (Taylor, 1994). Therefore, the effects of particle size should be assessed by modelling the soil behaviour at different model scales.

Two different methods for determining the scale effects in centrifuge tests are modelling of models and modelling of prototypes (Schofield, 1980; Fuglsang and Ovesen, 1988). The modelling of models utilizes centrifuge models at different scales, which are tested under appropriate accelerations to correspond to the same prototype dimensions. The models should yield the same results, and provide an internal check of the modelling procedure. This procedure provides confidence, but not certainty to the applicability of the model test results in understanding actual prototype events. The modelling of models is often used to check the effects of particle size and other known scale effects in centrifuge testing. As previously stated, the effects of particle size can be assessed by modelling the soil behaviour at different model scales.

The direct comparison of model to prototype behaviour should have obvious advantages over the modelling of models with respect to drawing more certain conclusions about scale effects. However, the prototype testing environment is often difficult and very expensive to control.

Centrifuge modelling has often been criticised as having considerable errors due to the non-uniform acceleration field, and that the detail and complexity of the prototype are often not represented in centrifuge models. Therefore, when studying the soil behaviour of geotechnical events using centrifuge modelling, an appreciation of the limitations of the modelling exercise must be clearly understood. The main errors imposed by the centrifugal acceleration field when simulating earth's gravitational field, are the varying acceleration and stress levels in the model, the direction of acceleration, the Coriolis

effect, and Earth's natural gravitational acceleration field (Schofield, 1980; Taylor, 1994).

The varying acceleration throughout the centrifuge model is created since the applied centrifugal acceleration field is not uniform throughout the model. The acceleration is a function of the angular rotational velocity, ω and the radius r, from the center of rotation. The acceleration field increases as the distance from the centre increases, which is expressed as ωr^2. Since r is a squared term in the acceleration field its magnitude increases nonlinearly with depth in the model. Therefore, the magnitude of the stress profile in soil model is directly affected

The error experienced due to the nonlinear stress profiles is minor and can be minimized. This can be achieved by allowing the exact stresses to exist in the model and prototype at two-thirds the model depth. Therefore, the region of maximum effective vertical stress in the model soil profile would be the bottom one-third of the model depth. Most often this error has been found to be less than 3% of the stresses experienced in the prototype (Taylor, 1994).

The direction of acceleration is a source of error because as the centrifuge rotates, the acceleration is directed radially away from the center of rotation. This phenomenon leads to a change in the direction of acceleration field, from the center of the model to the sidewalls. At the center of the model the acceleration field is normal to the model surface, but as the distance from center increases the direction of the acceleration

becomes inclined from this normal and away from the center of rotation. The effects of this error should be minimized since it can create significant errors. To decrease the effects the performance of any major testing events should occur in the centre of the model, allowing the acceleration field to be normal to the model.

The Coriolis effect occurs whenever there is a model movement with velocity in the radial direction within the plane of rotation of the arm. Seepage movement or slope failures are examples of this type of movement. Although Coriolis effects can be significant, its effects can be easily predicted and therefore can be readily accommodated in any interpretation of a model test.

The error contributed by the Earth's natural gravitational acceleration field is another error that is experienced by the model. As previously stated, gravitational effects can be modelled by imposing centrifugal acceleration experienced by an object in circular flight path at the end of a rotating beam. As the centrifuge speed increases, a model basket with a frictional hinge typically swivels upward as the imposed gravitational acceleration applied to the model increases. During this increase, the direction of the imposed centrifugal gravitational acceleration is perceived in the horizontal plane. However, the model surface is not actually normal to the horizontal plane.

Due to the vertical effects of the Earth's gravitational acceleration it applies a gravitational acceleration perpendicular to the horizontal acceleration imposed by the centrifuge. As a result, the model does not experience gravitation acceleration

completely vertical, which is experienced by the prototype. The model does experience an acceleration that is very close to vertical since the magnitude of the gravitational acceleration applied by the centrifuge is often quite larger than gravitational acceleration created by the Earth. The affects of this error are usually insignificant.

2.5 Previous Centrifuge Modelling Simulating the Behaviour of Submarine Slope Failures

2.5.1 Static Modelling

Previous centrifuge testing that has specifically concentrated on the consequences of static loading on submarine slope stability has been limited. Phillips (2001) states that centrifuge modelling has been used to simulate many loading conditions and relevant soil conditions in seafloor studies. However, there is still no well-accepted method to estimate the stability of submarine slopes with applied static loadings (Zhou et al., 2002). Subsequently, the centrifuge modelling of subaerial slope stability has been relatively extensive. Slope stability was studied extensively in the early beginnings of centrifuge modelling testing. Model slopes were subjected to increasing acceleration levels before reaching a critical height at which undrained failure was observed. Slope stability was often studied since little instrumentation was needed, and slope failures could be back calculated using limit equilibrium methods (Take and Bolton, 2002).

Zhou et al. (2002) conducted centrifuge tests to determine the critical gradient of submarine slopes that consisted of silty sand and fine sand. The tests relied on gradually

increasing the slope height for each separate model test by physically tipping the model, while maintaining a relatively constant model scale ranging from N = 140 to 160. The results showed that the critical slope gradient of silty sand is larger than that of fine sand, the height of underwater slopes of silty sand have no influence on the critical slope gradient, and the critical slope gradient of fine sand is almost not influenced by the g-level in centrifuge modelling.

The centrifuge modelling of flow liquefaction caused by static loading on submarine slopes is described by Phillips and Byrne (1995). The centrifuge test series consisted of a 16° submerged slope of low-density oil sand tailings with a prototype slope height of 8.8 m. Slope failure was initiated by loading a steel plate onto the slopes crest causing the slope to liquefy, and flow to an angle of approximately 7°. The authors concluded that the measured results from the centrifuge testing showed good agreement with numerically predicted results, and that static liquefaction and strain softening responses due to excess pore pressures can be effectively modelled in a centrifuge.

An important consideration in centrifuge modelling of slope stability and plane strain problems is the minimization of side friction, and its effects on model results (Khoo et al., 1994). Santamarina & Goodings (1989) observed side boundary friction effects in reinforced sand retaining walls loaded to failure by increasing self-weight in a centrifuge. Based on their observations, they recommended that to minimize side friction effects on the observed failure mechanisms, the model width should be at least 4 times the model wall height.

Khoo et al. (1994) states the use of grease alone to eliminate side fiction is relatively ineffective. This is attributed to the fact that sand particles can penetrate the grease, and can directly contact the frictional surface. They suggest to prevent this, sand can be separated from the surfaces by two layers of ultra-thin polyethylene sheets with a coating of grease between them. Durable rubber membranes and silicone grease were used by Taniguchi et al. (1988) for stiff sands, however, if the soil is soft, the stiffness of the rubber membrane may significantly alter the deformation pattern of the soil adjacent to the sidewalls.

2.5.2 Dynamic Modelling

The dynamic response of submarine slopes and submerged embankments during earthquakes and other dynamic loadings have been the focus of many centrifuge studies (Astaneh et al., 1994). The Verification of Liquefaction Analysis using Centrifuge Studies (VELACS) project was conducted to analyse and improve the methods for analysis of the consequences of soil liquefaction (Arulanandan et al., 1994). Comparing numerical and physical model predictions from centrifuge studies, several universities tested nine different models that were loaded using simulated earthquake motions. One particular model assessed the stability of a 2° sandy submarine slope subjected to earthquake motions. Based on the results from several centrifuge centres, the results showed that dynamic modelling of submarine slope stability can be modelled with acceptable repeatability in the centrifuge.

Astaneh et al. (1994) describe a centrifuge study investigating the soil behaviour of submerged embankment dams that experience liquefaction due to earthquake loading. Simulating earthquake loadings in the centrifuge, the test series concluded that the acceleration, pore pressure, and displacement records were in good agreement with each other. Another test series involves investigating the effects of confining pressure on permanent displacement of submarine slope failures due to sediment liquefaction (Nagase et al., 1994). The centrifuge tests utilized a shake table to simulate submarine slope instabilities caused by earthquake loadings.

More recently, Malvick et al. (2002) completed centrifuge tests studying the role of void redistribution on the cyclic and post-liquefaction shear behaviour of saturated sand with an embedded silt seam. The results from the earthquake simulated centrifuge tests showed that under certain conditions, large localized shear strains could develop below the silt seam in the centrifuge model.

The results also found the parameters that influenced the amount of void redistribution included initial relative density, base motion duration, volume of sand below the silt seam, and the shaking sequence. Other factors, such as the permeability contrast of the soils, the maximum excess pore pressure ratio developed, the slope geometry, and the soil stratigraphy were also believed to be influential factors.

Along with earthquake loading, wave loading is another dynamic process that greatly affects the stability of submarine slopes. As previously stated, due to the depths of

offshore continental slopes, the effects of wave loading are not considered a significant factor to generate seabed instability. However, a brief discussion is warranted for a complete review of dynamic centrifuge modelling.

Although the centrifuge modelling of wave-induced liquefaction has not received the great attention as that of earthquake modelling, it has been studied by several researchers (Sekiguchi et al., 1993; Sassa and Sekiguchi, 1999; Sekiguchi et al., 2000; Miyamoto et al., 2002). These centrifuge studies provide experimental insight into the mechanisms that contribute to wave-induced seabed liquefaction. This information can then be directly used to assess the stability of submarine slopes.

3.0 RESEARCH FACILITIES

3.1 The C-CORE Centrifuge Centre

Located on the St. John's campus of Memorial University of Newfoundland, the C-CORE Centrifuge Centre is a research facility positioned between the Captain Robert A. Bartlett building and the S.J. Carew Building. Funding for the centrifuge centre was contributed by the Canada/Newfoundland Offshore Development Fund, the Technology Outreach Program of Industry, Science, and Technology Canada, and the Natural Sciences and Engineering Research Council Canada.

The C-CORE centrifuge centre is also equipped with cold regions capabilities. The cold regions modeling capability of the machine reflects the national need to manage the resources of Canada. The centrifuge has a refrigeration system that can deliver temperatures reaching -30°C.

The two-story centrifuge centre is comprised of offices, and a soils laboratory on the upper level. The lower level consists of a model preparation area, and a containment structure that houses an Acutronic 680-2 geotechnical centrifuge. The model preparation area also includes a machine shop, a sand-raining room, an electronics lab, a coldroom and, an x-ray facility.

The containment structure includes three separate levels. The upper level provides a stiff ceiling for the main centrifuge chamber, which dampens the aerodynamic excitation

created by the centrifuge during rotation. The electrical slipring capsule and related interfaces are also housed in the upper level. The intermediate level is the main centrifuge chamber. The main chamber is accessible by forklift, and its physical dimensions are 13.5 m in diameter and 4.2 m in height. Its walls are 300 mm thick reinforced concrete, and are surrounded by an outside rockberm. The lower level of the containment structure is an underground area containing the centrifuge drive unit and the refrigeration unit.

3.2 The Acutronic 680-2 Geotechnical Centrifuge

The C-CORE Acutronic 680-2 centrifuge is shown in Figure 3.1. The Acutronic 680-2 centrifuge is designed for a maximum rotational speed of 189 rpm, corresponding to an imposed acceleration of 200 g. The centrifuge has a 5.5 m radius to the floor of the platform, typically the centroid of a test model is at a working radius of approximately 5 m. The maximum payload capacity of the Acutronic 680-2 is 100 g x 2.2 tonnes = 220 g-tonnes at a working radius of 5 m. At 200 g, the platforms self-weight increases sufficiently to reduce the maximum payload capacity to 130 g-tonnes. Figure 3.2 provides the specifications of the Acutronic 680-2 centrifuge. The maximum allowable dimension of a model package is 1.4 m long and 1.1 m wide by at least 1.1 m high.

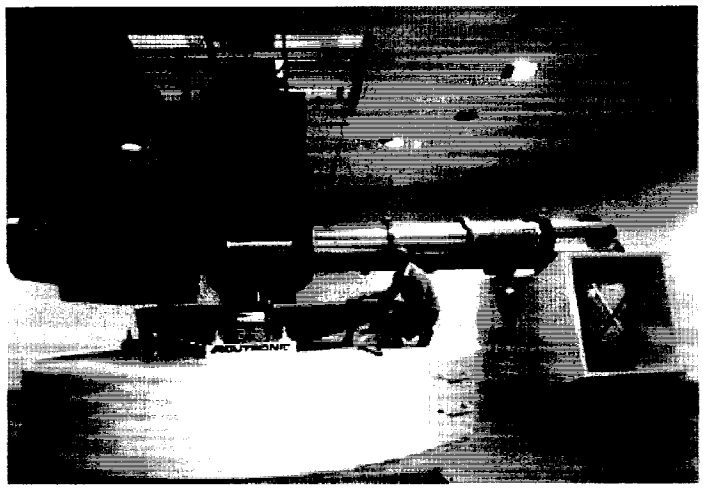

Figure 3.1: C-CORE Acutronic 680-2 geotechnical centrifuge.

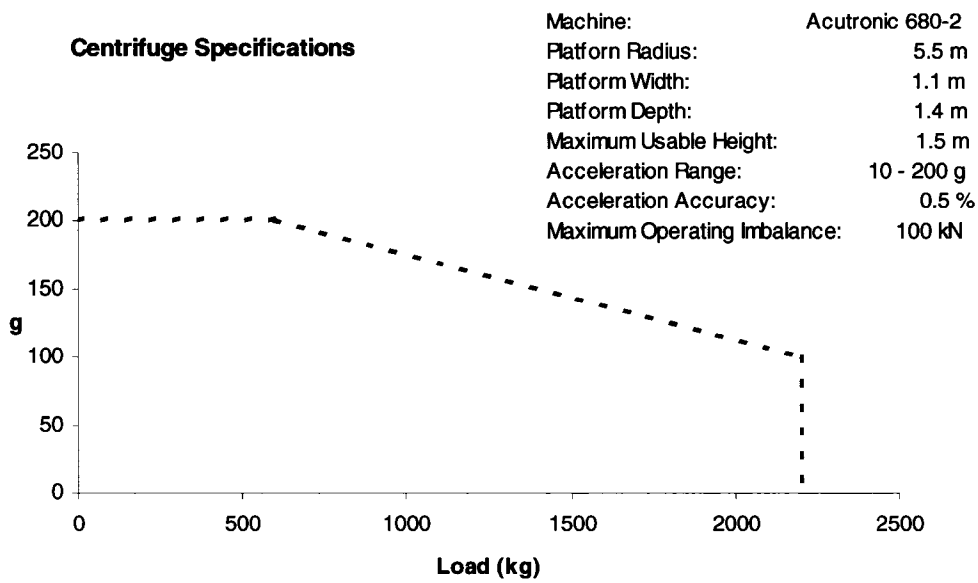

Figure 3.2: C-CORE centrifuge specifications.
(After Hurley, 1999)

The arm of the centrifuge is comprised of two parallel steel tubes that are supported apart by a central drive box and spacers as shown in Figure 3.3. At the end of the steel tubes, the swinging platform is suspended on bushings. The swinging platform is enclosed by

an aluminium aerodynamic shroud designed to reduce drag. The payload and platform are balanced by a 20.2 tonne mass counterweight.

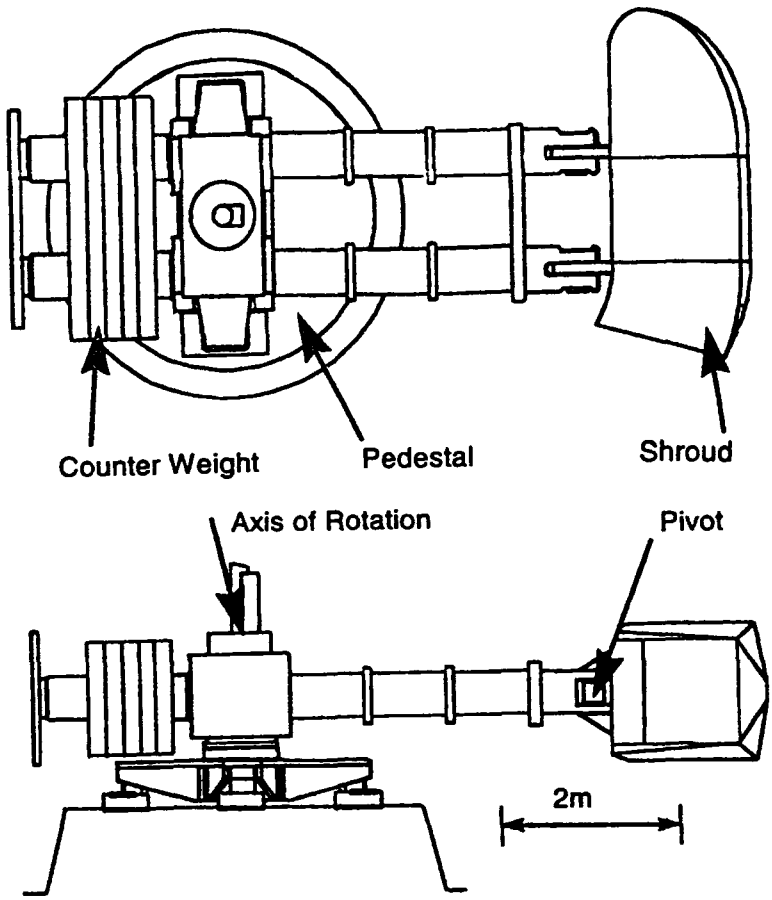

Figure 3.3: Acutronic 680-2 geotechnical centrifuge.
(After Hurley, 1999)

The centrifuge arm rotates on a set of tampered roller bearings inside the central drive box, and is mounted on a stationary shaft. The shaft is connected to the centrifuge containment through a four branch star support suspended on four springs. Each of the four springs is strained gauged to measure centrifuge imbalance to within 10kN. The

centrifuge drive unit includes a 450kW AC variable speed motor connected directly to a 9:1 gear reducer. Two 250kW invertors energise the variable speed motor.

The centrifuge is equipped with two rotary joints that allow fluids to flow through the central axis of the machine to the platform. Six fluid passages are contained in the rotary joints: two passages are designed for high pressure hydraulic fluid, two permit the passage of either air or water, and the remaining two are dedicated to the refrigeration unit.

Data collected from the test model is sent to a shielded cabinet that is attached to a 64 channel multiplexer. From the multiplexer, information is then feed to a PC based ANALOGIC HSDAS-16 (16 bit A/D convertor). The data acquisition PC located in the slipring room utilizes SNAP-Master data acquisition software. The slipring room PC is connected via a thinwire ethernet to the control room data acquisition PC (Phillips et al., 1994).

4.0 CENTRIFUGE MODEL TESTS

4.1 Introduction

Utilizing centrifuge modelling, several mechanisms associated with submarine slope failures were investigated. The primary research objective was to develop methodologies for the modelling of submarine slope failures caused by static loadings on continental slopes, to conduct centrifuge tests simulating the behaviour of submarine slope failures, and to demonstrate that the test data obtained reasonably model actual submarine slope failure conditions.

4.2 Design of Centrifuge Model Tests

4.2.1 General

Physical modelling in the geotechnical centrifuge was used to investigate different potential slope instability mechanisms. The design of the centrifuge tests covered several main areas: the triggering mechanism, the model material, the slope geometry, the model equipment, and the model instrumentation.

Continental submarine slopes typically consist of complex sediment deposits, each of which often have varying stress histories. Continental slopes, in their simplest form, can often be classified as having normally consolidated soil profiles (Booth & Garrison, 1978; Olsen et al., 1982; Baraza et al., 1990), therefore, it was desirable to have a normally consolidated model soil profile.

Erosional undercutting of lower slope sediments significantly affects the stability of the upper slope sediments. As previously discussed in Section 2.3.14, the Storegga slide was caused by the initial movement of sediment material in the lower slope due to rapid sediment deposition. The initial sediment removal unloaded the headwall upslope causing retrogressive slope failure. Based on relevance to offshore conditions and limitations in the centrifuge, slope failure caused by sediment erosional undercutting was simulated in the centrifuge.

Sediment layering exists in many deepwater offshore locations, and under specific conditions they are believed to be a critical geotechnical stratigraphy characteristic for many submarine slope failures (Bugge et al., 1987; Piper et al., 1999; Laberg et al., 2003; Tripsanas et al., 2003; Bryn et al., 2004). The effect of increased pore water pressure within distinct sediment layers can lead to loss of effective strength, thereby creating a weak layer.

The creation of increased pore pressure in sediment layers can be generated by several different factors. These may include earthquakes, the influence of aquifers, gas charging, the dissociation of gas hydrates, and rapid sedimentation. Based on relevance to offshore conditions and limitations in the centrifuge, slope failure caused by excess pore pressures confined within sediment layering was simulated in the centrifuge.

The centrifuge modelling program was conducted at C-CORE's centrifuge centre. Based on experience gained from previous demonstration tests, the testing program consisted of

three centrifuge tests. The first centrifuge test, designated Slope Stability Test 1 (SST 1), simulated slope failure due to sediment erosional undercutting. The second and third tests, entitled Slope Stability Test 2 (SST 2) and Slope Stability Test 3 (SST 3), respectively, both simulated slope failure due to excess pore pressures generated within sediment layering.

4.2.2 Soil Properties

The centrifuge tests utilized two types of model materials for testing: a fine-grained soil and a coarse-grained soil. Due to the commonality of silty clays on continental slopes (Baraza et al., 1990; Booth & Garrison, 1978; Bryant et al., 2000; Casas et al., 2003; Olsen et al., 1982; Robb, 1984), the fine-grained model material selected was Speswhite kaolin clay. Speswhite kaolin is a silty clay that has sufficient sensitivity and low enough permeability such that undrained conditions can be achieved during a rapid slope failure.

Speswhite kaolin clay is available in powder form from a highly consistent source with well-known controlled properties. Based on analyses by Al-Tabba (1987) and Lin (1995), properties are provided in Table 4.1, and the grain size distribution is given in Figure 4.1. For model preparation of each test, kaolin was mixed under vacuum at approximately 90% moisture content, yielding a fully saturated slurry with the consistency of a thick fluid.

Table 4.1: Physical properties of Speswhite kaolin clay.
(Adapted from Al-Tabba, 1987 and Lin, 1995)

Property	Units	Value
Clay Content (< 2μm)	%	75
Mean Grain Size, D_{50}	mm	0.0005
Plastic Limit	%	35
Liquid Limit	%	65
Plasticity Index	%	30
Specific Gravity	-	2.62
Permeability	m/s	0.5 to 2.0 x 10^{-9}
Coefficient of Consolidation	mm^2/s	0.1 to 0.5
Coefficient of Lateral Earth Pressure During One-Dimensional Normal Consolidation (K_{onc})	-	0.64

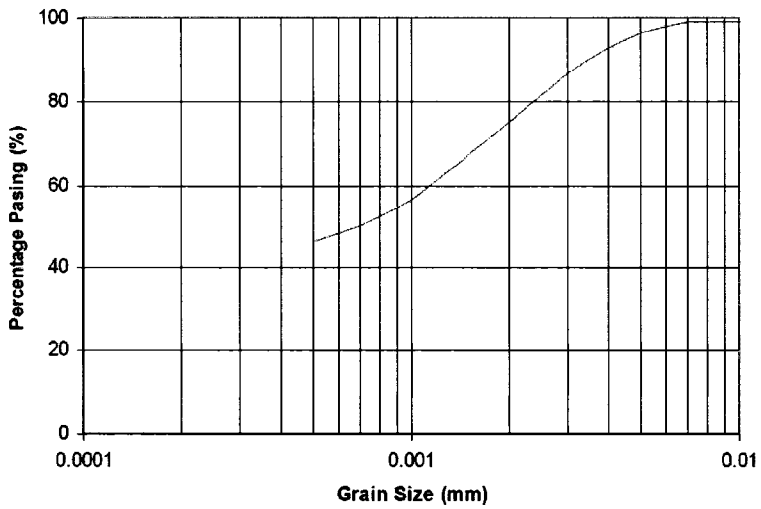

Figure 4.1: Grain size distribution of Speswhite kaolin clay.

The coarse-grained model material used for SST 1 was Fraser River Sand. Due to availability, #00 Alwhite silica sand was selected for SST 2 and SST 3. Unlike the selection of the fine-grained model material, the coarse-grained material was a secondary

design constraint. The main design concern was to ensure the permeability of the intermediate sand layer was greater than the clay layers. Assuming that the sand was loose, the internal friction angle for Fraser River sand and for #00 Alwhite silica sand is 35°.

Table 4.2: Physical properties of Fraser River sand and Alwhite silica sand.
Adapted from Vaid and Sivathayalan, 1996; C-CORE, 2004; and C-CORE, 2005.

Property	Fraser River Sand	#00 Alwhite Silica Sand
Max. dry density, γ_{max} (kN/m^3)	16.4	15.8
Min. dry density, γ_{min} (kN/m^3)	13.7	12.7
Mean grain size, D_{50} (mm)	0.26	0.32
Internal angle of friction, ϕ'	35°	35°

4.2.3 Model Description

Centrifuge test models were constructed in a plain strain rectangular strongbox with the dimensions, 900 mm x 300 mm in plan, and 400 mm in depth. The strongbox is constructed of a steel and aluminium frame on three sides of the box, and is fitted with various ports for fluid control. The remaining side consists of an 88 mm thick Perspex sheet that allows observation of the models during centrifuge testing. A typical test package is shown in Figure 4.2

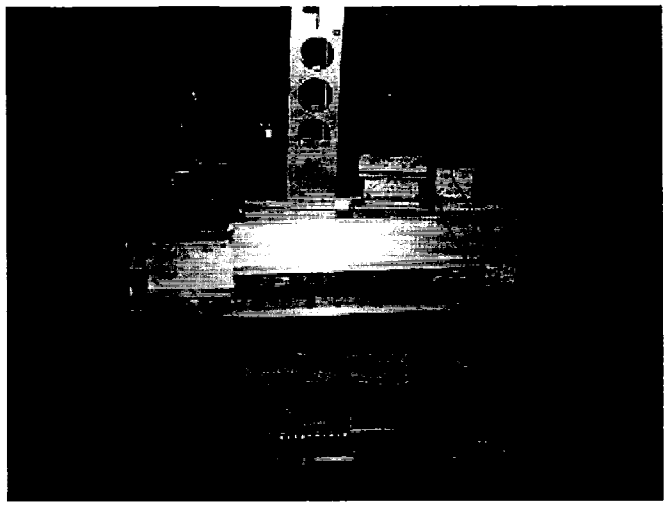

Figure 4.2: Photo of typical centrifuge test package.

Creating a normally consolidated soil with a layered profile required a three-stage preparation technique. Figure 4.3 displays the basic soil profiles involved in a model 8° slope. Although an 8° slope is relatively steep for continental slopes, it was chosen to ensure slope failure would occur in the model. The strongbox was prepared with a base layer of drainage sand, and a thin layer of Vaseline brand petroleum jelly or Tri-Flow brand Teflon-lubricant spray on the sidewalls to minimize boundary effects. The clay slurry was poured into the strongbox that was inclined at 4° on the plywood wedge. Due to the fluid characteristics of the clay slurry, it maintained a horizontal surface, as shown in Figure 4.3 (a).

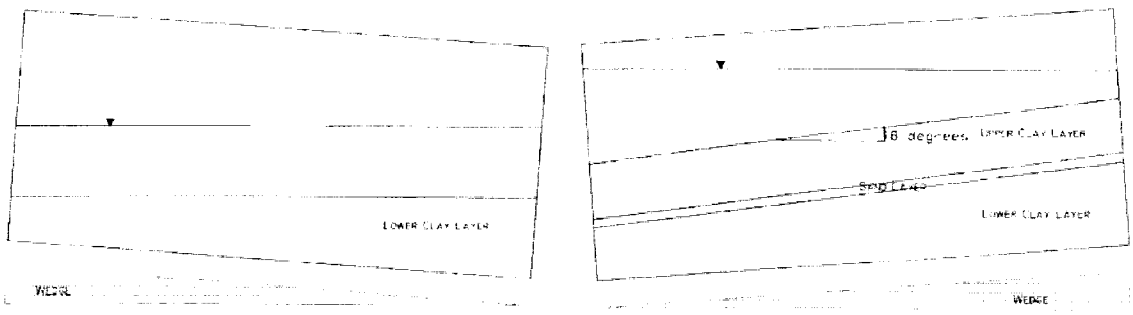

(a) (b)

Figure 4.3: Method of test package preparation to create 8° slope.

The lower clay layer was then uniformly consolidated in a consolidation loading frame at 1 g in the laboratory, as shown in Figure 4.3(a). The loading pressure selected allowed the lower clay layer to maintain a normally consolidated profile due to the overburden pressure of the overlying soil layers. The consolidation process in the loading frame allowed the lower clay layer to obtain sufficient strength to support an intermediate sand layer without impregnation.

After the preparation of the lower clay layer in the loading frame, a 10-30 mm intermediate sand layer was added, followed by a top clay slurry layer. The complete soil model was submerged with municipal water to provide submarine conditions and prevent drying of the soil surface. The soil slurry was then consolidated to 90% of its effective stress equilibrium in the centrifuge at 100 g acceleration, creating a horizontal normally consolidated sediment profile. Using a linear voltage displacement transducer (LVDT) on the soil surface, and pore water pressure transducers (PPT) embedded within the three

soil layers, the degree of consolidation was estimated using the square-root-of-time method. The PPTs and LVDTs were positioned at critical locations within the model. After the soil profile was consolidated in the horizontal position, the 4° wedge was rotated 180° below the strongbox. This procedure resulted in a soil surface inclined at approximately 8°, as shown in Figure 4.3 (b). Figure 4.3 (b) provides a typical soil profile, however, SST 1 included an aluminium insert as a means of triggering slope failure.

After the 4° plywood wedge was rotated, the head of the slope was cut to provide a horizontal surface for the LVDT. The model was reconsolidated in the centrifuge to equilibrium conditions at 100 g acceleration. Due to the soil strength developed during the initial consolidation process, the soil slope was maintained.

Experience gained from previous demonstration tests showed that during the reconsolidation of the model slope, the model could not be initially subjected to high gravitation levels, or premature slope failure would occur from the excess pore pressures generated by the increase in self weight. To allow the dissipation of excess pore water pressures, the model was initially accelerated to 10 g for the first half hour, and increased by 10 g increments every half hour thereafter. Once reaching 100 g the model was reconsolidated to 90% consolidation, which was confirmed using LVDT and PPT readings. The length of each consolidation phase took approximately 8 hours.

The complete test package, as shown in Figure 4.2, was fitted with headworks fastened to the top of the strongbox. Equipment included a CPT vertical drive actuator, LVDT brackets, and a servo-motor. Water flow was controlled to and from the model package using a system of motor operated valves. The surface water, the pore water in the sand layer and bottom drainage layer were all connected to a standpipe and overflow that could expel water from the package. The plumbing schematics for each test are illustrated in each test's specific section.

Due to the relatively high rate of evaporation from the surface water, water was periodically added to ensure a consistent hydrostatic water level. During the slope failure triggering event, valves were closed to prevent water dissipation from the intermediate sand layer.

Spaghetti strands were inserted into the soil model, allowing the failure plane of the simulated slope failures to be visually observed. Since spaghetti has negligible strength when it softens in the presence of water, it allowed failure planes to be defined. At regular intervals, spaghetti was inserted vertically adjacent to the Perspex window to allow visual observation of any possible failure planes. Spaghetti was also fitted with metallic solder strips, and inserted in the centre of the strongbox. Following the test, the test package was x-rayed. The presence of the soldered spaghetti strands allowed for soil movement to be visualized without disturbing the soil bed. Any difference between the centre and edge markers accounted for the effects of sidewall friction in the model.

A cone penetration test (CPT) was completed prior to the application of any triggering mechanism. The rate of cone penetration for each test was 3 mm/s. Once the CPT was completed, the application of a slope failure trigger mechanism was carried out.

An onboard colour closed circuit camera was installed to allow observation of any mass movements through the Perspex window in real time. A second black and white closed circuit camera was fastened to the headworks, providing a plan view of the soil model. Each camera was connected to a television in the control room, and slope failure events were recorded on videocassette.

After each test had been completed, the test model was promptly returned to the main laboratory for analyses. Shear strength was immediately measured using a 33 mm diameter Pilcon hand vane, and Shelby tube (50 mm diameter) samples were taken to provide moisture content profiles.

4.2.4 Instrumentation

Instrumentation was used to measure the soil and pore water responses during consolidation, and triggering events in the test model. The test package included Trans-Tek Series 240 (Model #: 0243-0000) linear voltage displacement transducers with a working range of ± 0.5 inches to measure soil surface movement. To record pore water responses, Druck pore pressure transducers (Model #: PDCR 81) were positioned at

critical locations within the centrifuge model. Appendix A presents the detailed specifications of the instruments.

The cone used to perform CPTs was a Fugro 1 cm^2 miniature piezocone (Type: F0.5CKEW2/V) that provided data on the soil strength profile. Shear strength was interpreted from the CPT data using standard correlation formulae,

$$q_{kt} = q_c + (1-a)u_b \tag{4.1}$$

$$c_u = \frac{(q_{kt} - \sigma_v)}{N_{kt}} \tag{4.2}$$

where q_c is the measured cone tip resistance, a is the cone net area ratio (0.52 for the C-CORE piezocone), u_b is the pore pressure acting on the cone tip, σ_v is the total vertical stress acting on the cone tip, and N_{kt} is the cone factor for shear strength interpretation. Due to the relatively shallow depths of the slope profiles, boundary effects will significantly affect the CPT results, but the methods of interpretation using Equations 4.1 and 4.1 is taken to be acceptable.

An N_{kt} value of 10.66 was applied to obtain the shear strength profile. This value was based on previous experimental correlations of CPT resistance and vane strengths.

4.3 Slope Stability Test 1

4.3.1 General

The design of Slope Stability Test 1 (SST 1) considered slope toe undercutting leading to retrogressive slope failure. Two separate triggering mechanisms were incorporated into the centrifuge model. The primary triggering mechanism was designed to simulate sediment undercutting by vertically extracting an aluminium wedge that was embedded in the toe of the slope. The removal of the wedge would cause an unsupported soil face to be exposed, triggering slope failure. The triggering event was designed to simulate significant toe erosional undercutting of the slope that may be created by several natural phenomena. Such events may include substantial erosion due to ocean currents, diapirism, or by a head scarp created by a downslope mass movement.

As a secondary method to initiate slope failure, municipal water was also connected to a sand layer within the soil profile. If required, the pressurization of the sand layer could cause a reduction of soil strength leading to slope failure. The inclusion of the sand layer also provided a trial of the procedure that would later be used in SST 2 and SST 3.

4.3.2 Model Preparation and Testing Procedure

Figure 4.4 displays the configuration of the test package after the addition of the sand layer, and the top layer of clay slurry. The soil cross-section and the positions of the LVDT, aluminium wedge, and PPTs, excluding the headworks are also shown in Figure 4.4. Figure 4.5 shows the configuration following the rotation of the wedge, and the

creation of the 8° slope. As shown in Figure 4.5, all PPTs were embedded within the soil profile except PPT 1 and PPT 10. PPT 1 was positioned inside the standpipe, which was located outside the model package. PPT 10 was connected on top of the aluminium wedge. Figure 4.5 also shows that the sand layer was not completely parallel with the soil surface. This was due inconsistencies when creating the soil profile.

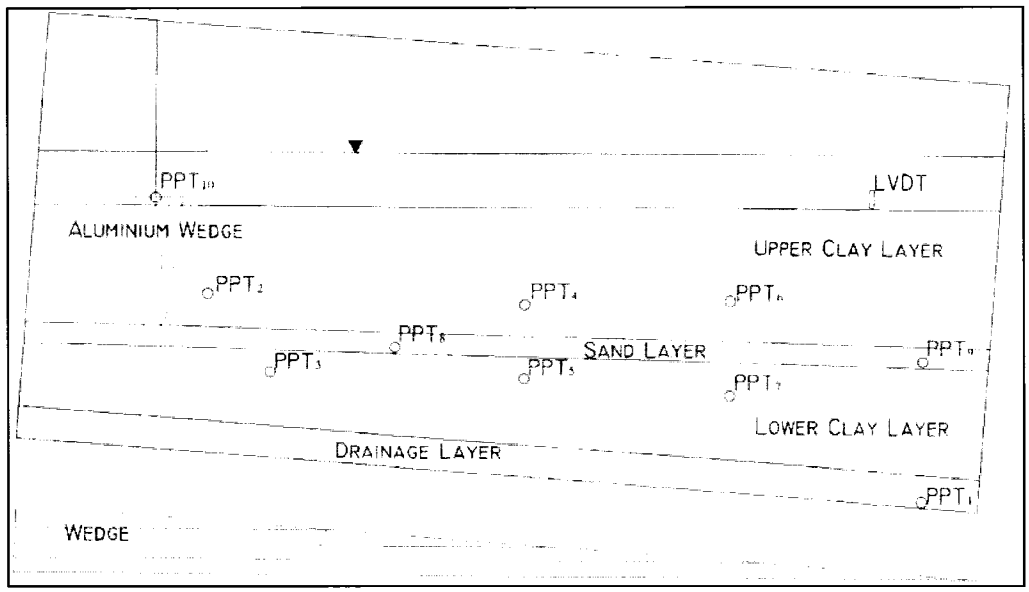

Figure 4.4: SST 1 profile of three soil layers prior to wedge rotation.

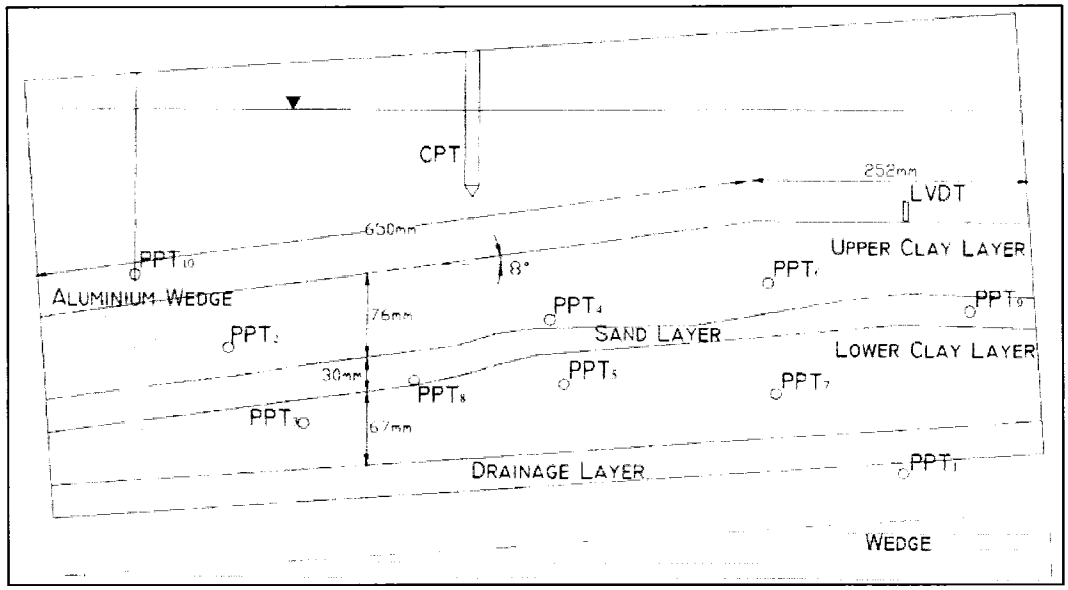

Figure 4.5: SST 1 model slope profile after rotation of wedge.

Water flow was controlled to and from the model package using a system of motor operated 3-way valves, as shown in Figure 4.6. The surface water, the pore water in the sand layer and bottom drainage layer were all connected to a standpipe during consolidation of the model soil. To induce excess pore pressures in the sand layer, 3-way valve #1 could be redirected to allow municipal water into the sand layer. Due to evaporation, water could be added from the municipal water supply through 3-way valve #2.

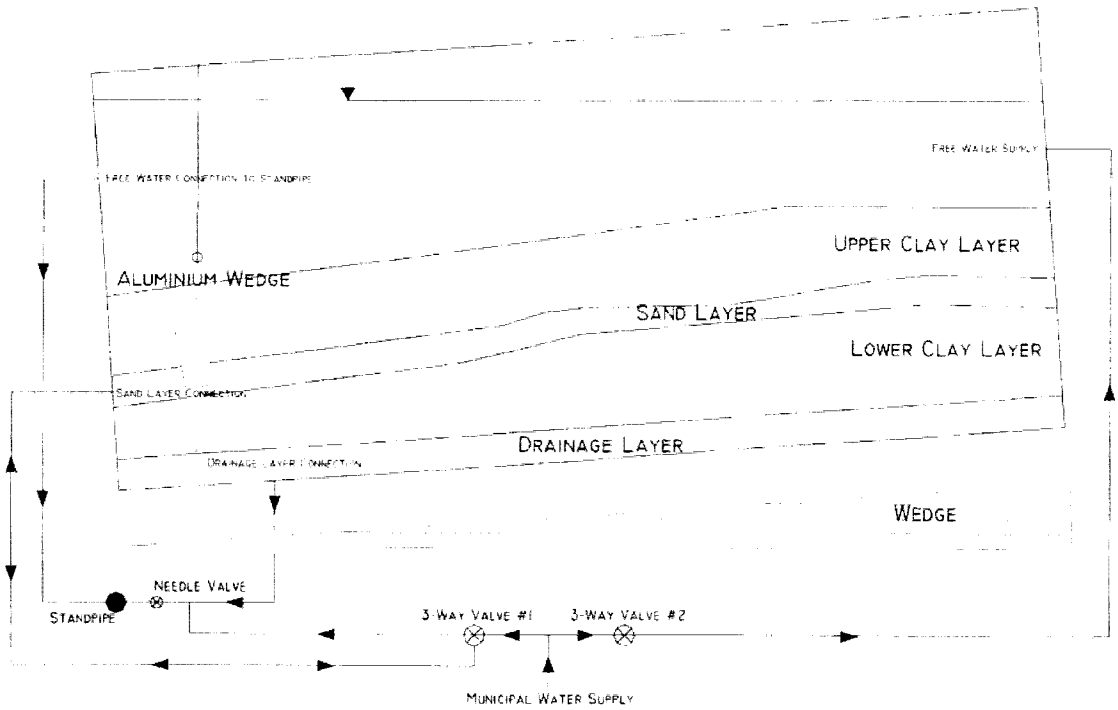

Figure 4.6: Plumbing schematic of SST 1 in plan view.

A servo-motor system, shown in Figure 4.7, was incorporated into the test package to control the vertical movement of the aluminium wedge. The aluminium wedge is a hollow wedge filled with sand to ensure its density was greater than the soil. Its triangular sidewall lengths are 180 mm x 180 mm x 63 mm, with a width across the slope of 295 mm. It was coated with a 2 mm layer of petroleum jelly to reduce side friction and suction forces and was positioned in the toe of the slope. The aluminium wedge was initially proposed to be positioned only in the upper clay layer, however, due to self-weight the wedge and the inability of the servo-motor to maintain the wedges position, it penetrated through the soil profile, as shown in Figure 4.5.

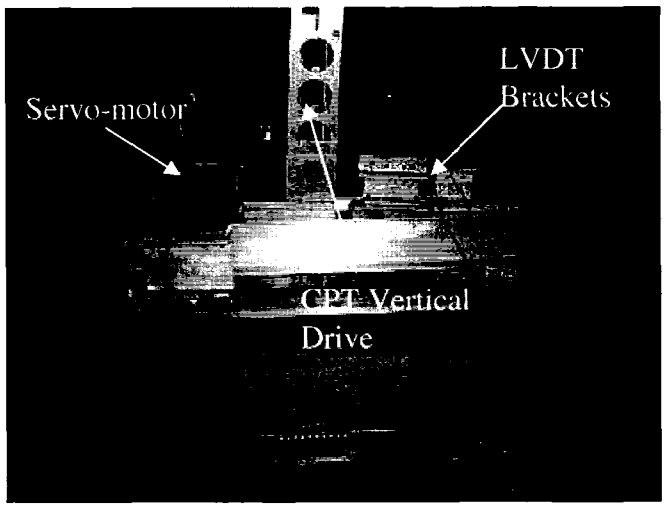

Figure 4.7: Photo of SST 1 model package.

4.3.3 Test Results

Based on the CPT data, shear strength is plotted with increasing depth as shown in Figure 4.8. A target line was incorporated into the plot based the normalized undrained strength of 0.19 described by Bolton et al. (1993). Shear vane test results are also plotted to provide a relative comparison with the CPT results. Hand vane results generally show lower shear strength in post-flight measurements of approximately 50% (Bolton et al., 1993). This is expected, since the hand vanes were carried out at 1 g, after the soil has undergone some swelling and softening due to the removal of overburden pressure.

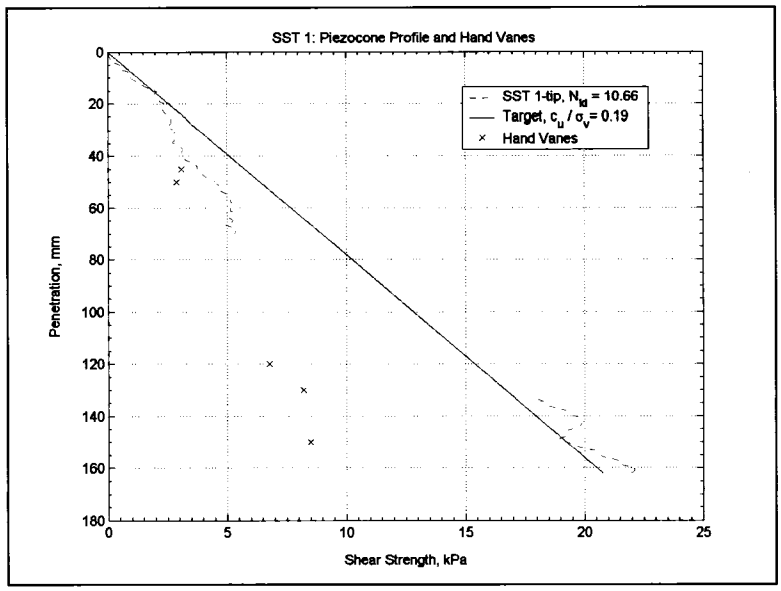

Figure 4.8: Piezocone shear strength and hand vanes with depth of SST 1.

The section removed from the CPT plot reflects the interference from the sand layer. Similar to the sand layer, the top and bottom boundary effects may also influence CPT readings. Based on test results described by Renzi et al. (1994), top boundary effects influence CPT results to a depth of approximately 5.7 cone diameters, which corresponds to a depth of 64 mm for the C-CORE piezocone. They also showed that the bottom boundary effects influence CPT results approximately 1.3 cone diameters from the bottom, corresponding to 15 mm from the model bottom. Although boundary effects significantly affected the CPT results, the shear strength profile can still serve to illustrate consistency in soil strength between centrifuge tests.

After the consolidation phases and CPT were completed, the aluminium wedge was extracted at an average rate of 2.5 mm/s which caused slope failure. The initial

movement of the aluminium wedge can be seen at position A of Figure 4.9. As shown in Figure 4.5, PPT 10 was connected directly to the wedge. The decrease in pore pressure indicates the upward vertical movement of the wedge. At position B, the wedge was completely extracted from the soil. The responses of selected PPTs 2, 3, 8 and 10 are plotted in Figure 4.9 to clearly illustrate the excess pore pressure responses of the critical PPTs during simulation of the submarine slope failure.

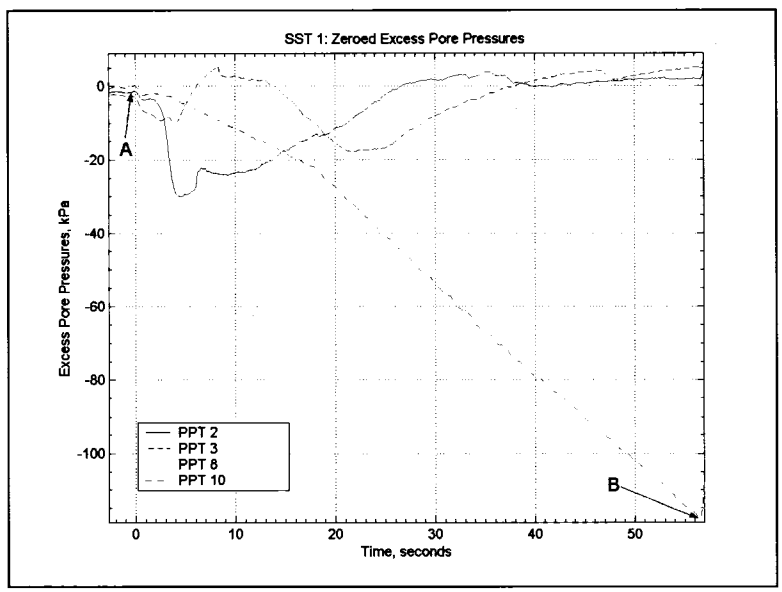

Figure 4.9: Excess pore pressures during aluminium wedge pullout of SST 1.

The pore pressure response of PPT 2 in Figure 4.9 shows that at approximately 4 seconds after the wedge pullout, negative pore pressures of about 30 kPa were measured. The negative pore pressure response may be attributed to the horizontal unloading induced by the lifting of the wedge. The following increase of pore pressure was due to soil shearing. The lag in negative pore pressure displayed by PPT 8 may be associated with a

possible lag in failure due to lower rates of strain deformation that may have occurred upslope, or the time taken for failure to propagate upslope. The negative pore pressure lag response of PPT 3 may be due to shearing in the lower clay layer, caused by loading from the upslope deformation. The fact that the PPTs in the sand layer did not record any positive pore pressures in the sand layer can be accredited to the fact that the sand layer extended directly to the aluminium wedge, therefore, as the wedge was extracted, the sand layer was immediately exposed to hydrostatic conditions.

Figure 4.10 demonstrates that the model surface experienced mass movement. Due to the lack of runout area for the soil to travel, a quantity of remoulded clay accumulated at the base of the slope. Soil movement was also confirmed from the displacement of spaghetti markers.

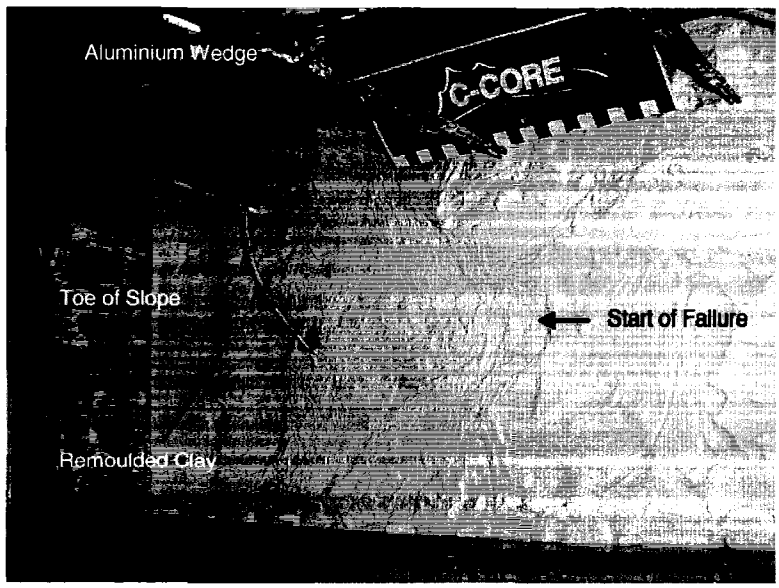

Figure 4.10: Photo of model soil surface after slope failure in SST 1.

An x-ray of the soil model including the soldered spaghetti strands is shown in Figure 4.11. The dots in the upper position of the image are scaling for every 10 mm. Figure 4.11 also displays that the remoulded soil filled the gap created by the removal of the aluminium wedge. The failure plane can be witnessed by the leftward displacement of the solder in the upper clay layer. Also, the slope failure existed primarily in the toe area, and the lower clay layer only showed signs of displacement adjacent to the wedge. Comparisons between the deformation of the spaghetti strands along the Perspex window and the x-rays showed that sidewall boundary did affect the movement of the soil mass.

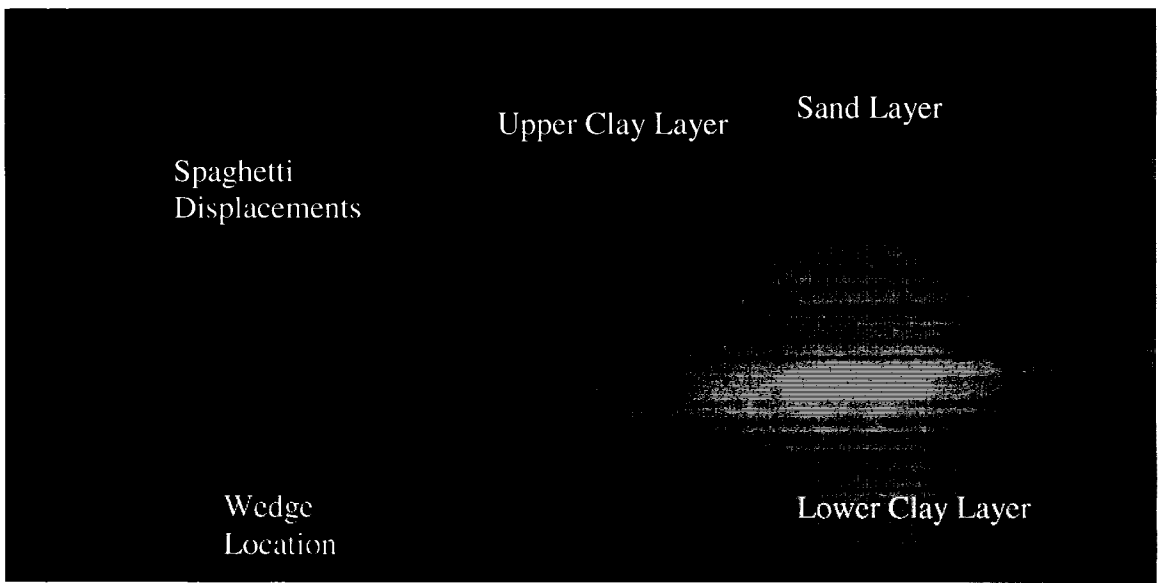

Figure 4.11: X-ray image of toe of model slope in SST 1.

4.3.4 Discussion

Figure 4.12 shows an interpreted shear plane based on the deformation of the spaghetti markers. The shape of the failure surface was constructed from spaghetti marker

positions in the Perspex window and the x-ray image. The markers suggest significant movement in the upper clay layer, and some movement in the sand layer. Figure 4.11 also shows that a secondary slope slump occurred in the lower clay layer, which may have resulted in a retrogressive mechanism if runout of the initial slump was sufficient. This can be confirmed by the lag response of PPT 3 in Figure 4.9. Since this response was subsequent to the initial slope failure, it was not included in the slope stability analysis. In prototype dimensions, the failure surface was approximately 30 m in length and 8 m at maximum depth.

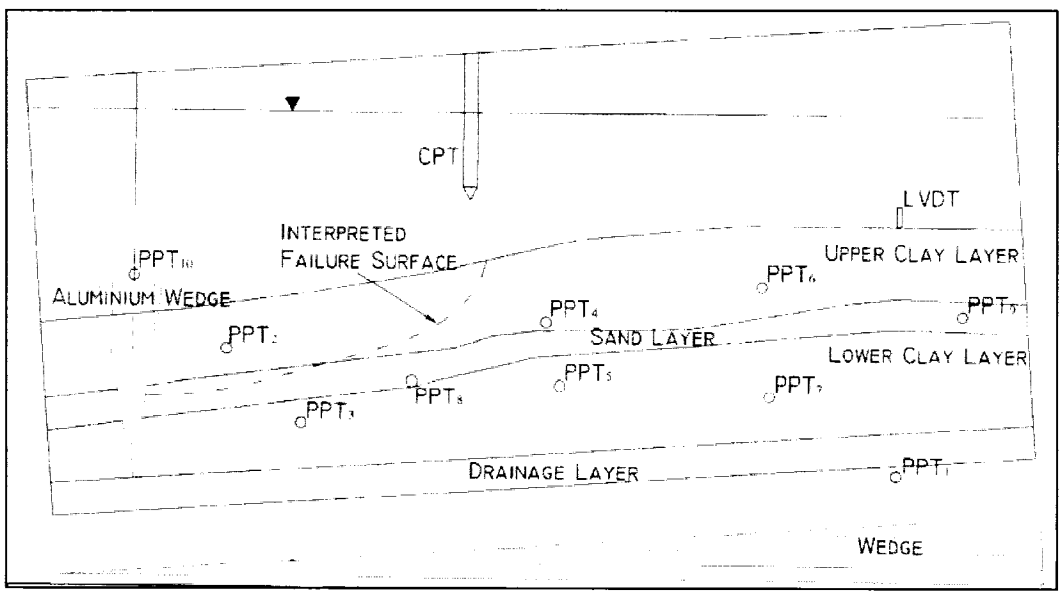

Figure 4.12: SST 1 model soil profile after slope failure.

The failure surface was circular in nature because the centrifuge test design was constructed to minimize boundary effects. Since the centrifuge test was carried out in a strongbox of finite size, the inability of model soils to laterally displace and the effects of

sidewall friction were both a concern. To decrease the effects of slope runout, the failure plane was designed to occur within the strongbox, allowing excess remoulded soil material to fill the gap left by the wedge.

To decrease the effects of sidewall friction, petroleum jelly was used for SST 1. Due to differences of the two failure planes identified from the spaghetti markers, it was clear that the petroleum jelly did not perform as expected. However, it is believed that the centre of the model was minimally affected. To minimize these effects, tests SST 2 and SST 3 utilized a Telfon spray to decrease sidewall friction.

Based on the interpreted failure surface from Figure 4.12, a limit equilibrium slope stability analysis was completed using Geoslope's SLOPE/W software (Geoslope International Ltd., 2004). The geometry of the model was incorporated into the software utilizing prototype dimensions. Within this geometry numerous failure planes corresponding to a range of factors of safety were calculated. All SLOPE/W stability analyses used an anisotropic function to account for the coefficient of lateral earth pressure for kaolin. The anisotropic function accounted for the variation of lateral earth pressure with the changing inclination of each individual slice in the stability analyses. The anisotropic function and the complete test results of all significant slope stability analyses using the SLOPE/W software are presented in Appendix B.

The slope stability analysis was performed using a normalized undrained strength profile of $c_u/\sigma_v^{'} = 0.19$ for the upper and lower clay layers, and a Mohr-Coulomb model for the

sand layer. An important factor not considered in the stability analyses is the effects of the relative density of the sand layer. The relative density of the sand layer was estimated to be loose and therefore an internal friction angle of 35° was used. Due to the limited knowledge of the sand layer's properties, the Mohr-Coulomb failure model was utilized. These models do not consider any complex behaviour characteristics of clay or sand failure.

The recorded PPT responses were not used in the analysis due to the fact that the maximum excess pore pressures necessary to cause slope failure were not recorded by the PPTs. As previously stated, the PPT responses displayed in Figure 4.9 show negative pore pressure responses, which would actually strengthen the slope and increase its stability.

The limit equilibrium analysis used was the Morgenstern-Price method with a constant function, also known as the Spencer method. As previously described in Section 2.2.2.2, the Morgenstern-Price and Spencer methods are techniques that incorporate a failure surface interslice force function, and satisfies both force and moment equations. A constant interslice force function was utilized rather than a specific failure surface function. This was due to the fact that a constant force function is more suitable considering the difficulty and uncertainty of defining a specific interslice force function (Krahn, 2003). Since the failure surface was circular in geometry, an infinite slope analysis was not appropriate for SST 1.

Analysis was initially completed with the failure plane extending through the upper clay layer and the sand layer. Consequently, the frictional resistance of the sand yielded relatively high factors of safety that was not characteristic of the observed slope failure. Based on the stability analysis results and the noncohesive nature of the sand, it is probable that the movement in the sand layer can be attributed to the loss of lateral support as the wedge was extracted. Therefore, it is believed that the slope failure occurred at the interface of the upper clay layer and sand layer.

Figure 4.13 shows the resulting slip circle generation with associated factors of safety. The extraction of the wedge is believed to have caused slope failure, whereby the slumping soil mass fell into the trench created by the wedge. As shown in Figure 4.13, the factors of safety steadily increase until approximately the $Fs = 0.94$ (nearly unity), which results in a stable slope profile. The failure plane corresponding to a $Fs = 0.94$ is close to the location of the interpreted failure surface of Figure 4.12. All figures presenting the stability analysis results using SLOPE/W software are not to scale (NTS).

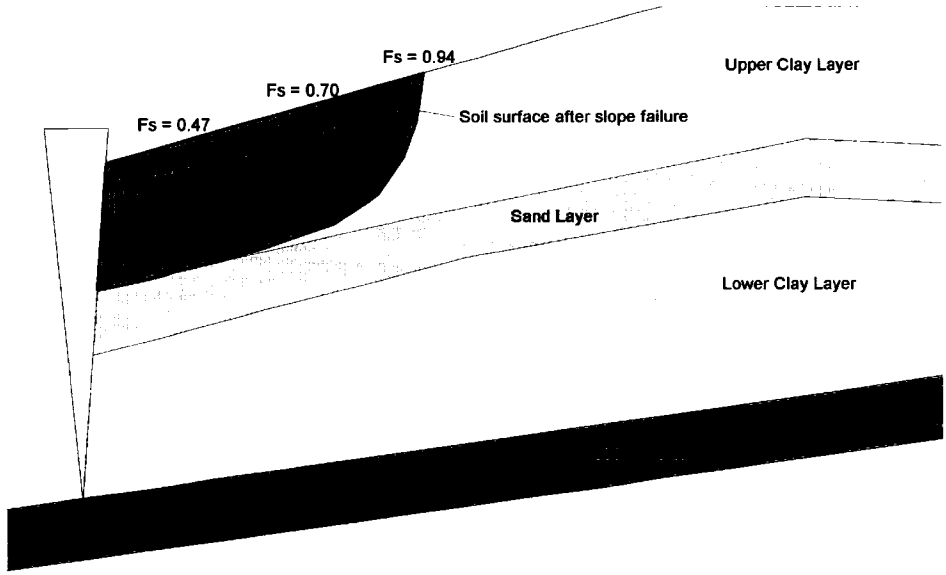

Figure 4.13: Slope stability analysis of SST 1 using SLOPE/W yielding $Fs = 0.94$. (NTS)

The actual factors of safety are influenced by the varying rates of strain deformation within the soil profile and the strain softening that may have both occurred during slope failure. The exposed soil surface due to the wedge removal quickly filled in the gap while the upper portions of the mass movement deformed at a slower rate. As a result, the upper portions of the mass movement were minimally displaced downslope, as can be seen by the soil surface after slope failure shown in Figure 4.13. Due to the lack of runout, the head scarp created from the slope failure was not unloaded, therefore, preventing the upper slope to fail retrogressively. This can be confirmed since the slope angle of the soil surface after initial slope failure was approximately 10-15°, which is stable under normal static conditions. SST 1 demonstrates the significant boundary effects that affect the simulation of slope failures in the centrifuge. If runout was permitted, the slope failure may have simulated retrogressive slope failure. However, the

agreement between the results of the stability analysis and the centrifuge results are satisfactory.

4.4 Slope Stability Test 2

4.4.1 General

Design of Slope Stability Test 2 (SST 2) concentrated on the effect of increased pore water pressure in an embedded sand layer leading to loss of effective stress and slope failure. Slope failure was simulated in the centrifuge by inducing excess pore pressures in the sand layer using a head-leveller. The creation of excess pore pressures in the sand layer may result from several different factors experienced on offshore continental slopes, such as earthquakes, rapid sedimentation, the influence of aquifers, gas charging, and the dissociation of gas hydrates.

4.4.2 Model Preparation and Testing Procedure

Figure 4.14 displays the test package configuration after the addition of the sand layer and clay slurry to the lower clay layer. Figure 4.14 also displays the soil cross-section and positions of the LVDT and PPTs, but excludes the headworks such as the head-leveller assembly, the CPT vertical drive, and LVDT brackets. Figure 4.15 shows the configuration following the rotation of the wedge, and the creation of the 8° slope. The head of the slope was cut to provide a horizontal surface for the LVDT, also clay slurry was added at the toe to create a defined normally consolidated horizontal soil surface.

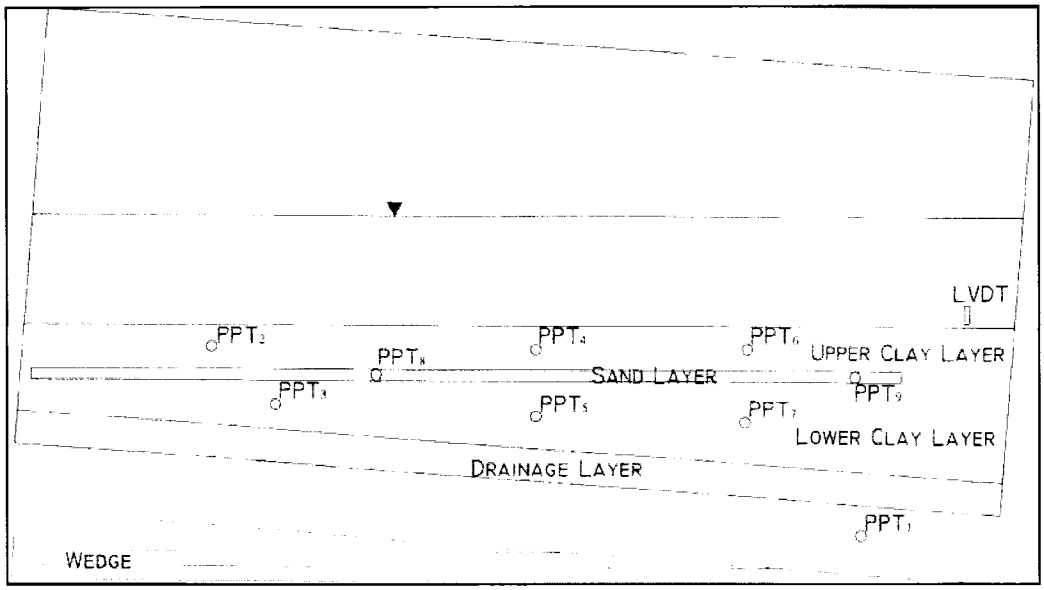

Figure 4.14: SST 2 profile of three soil layers prior to wedge rotation.

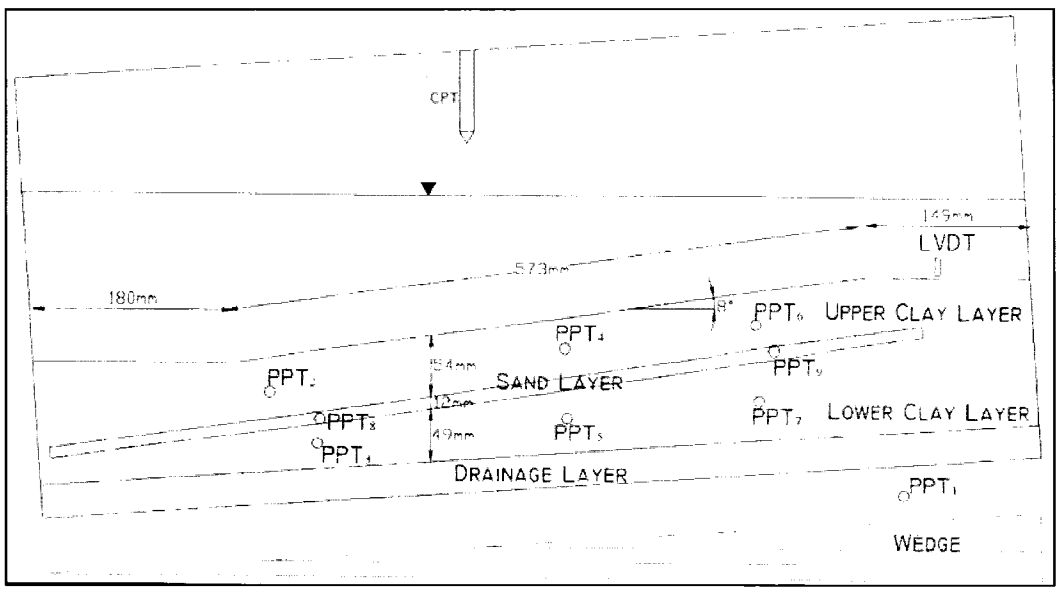

Figure 4.15: SST 2 model slope profile after rotation of wedge.

The creation of a horizontal soil surface was intended to allow a failure surface to occur completely within the strongbox, promoting slope runout. Even though runout could not be modelled properly during the centrifuge test, it was intended that soil movement would allow a well defined failure surface and unload the head scarp, which would possibly cause retrogressive failure of the upslope.

A head-levelling system, shown in Figure 4.16, was located outside the strongbox and controlled the pressure applied to the sand layer by raising or lowering a vertically manoeuvrable standpipe using a winch assembly. The position of the head-leveller was known using a string potentiometer located within the winch. At the start of the test, the head-leveller was approximately the same elevation as the free water in the model.

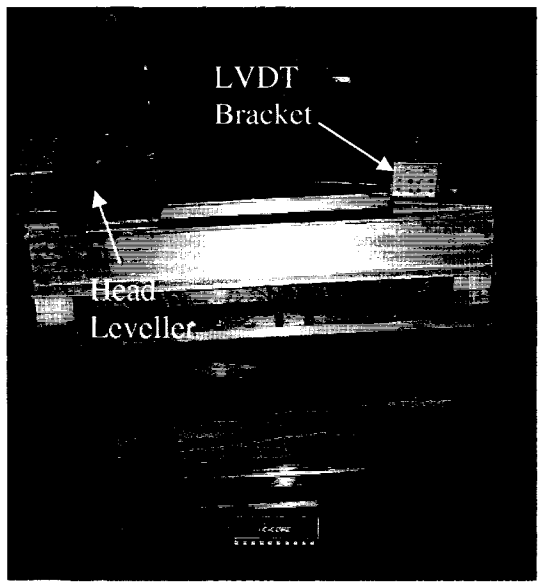

Figure 4.16: Photo of SST 2 model package excluding CPT vertical actuator.

Water flow was again controlled to and from the model package using a system of motor operated 3-way valves, as shown in Figure 4.17. The surface water, the pore water in the sand layer and bottom drainage layer were all connected to a standpipe during consolidation of the model soil. In the sand layer, a small-diameter perforated flexible hose was embedded in the sand and passed through the strongbox at a standard port opening.

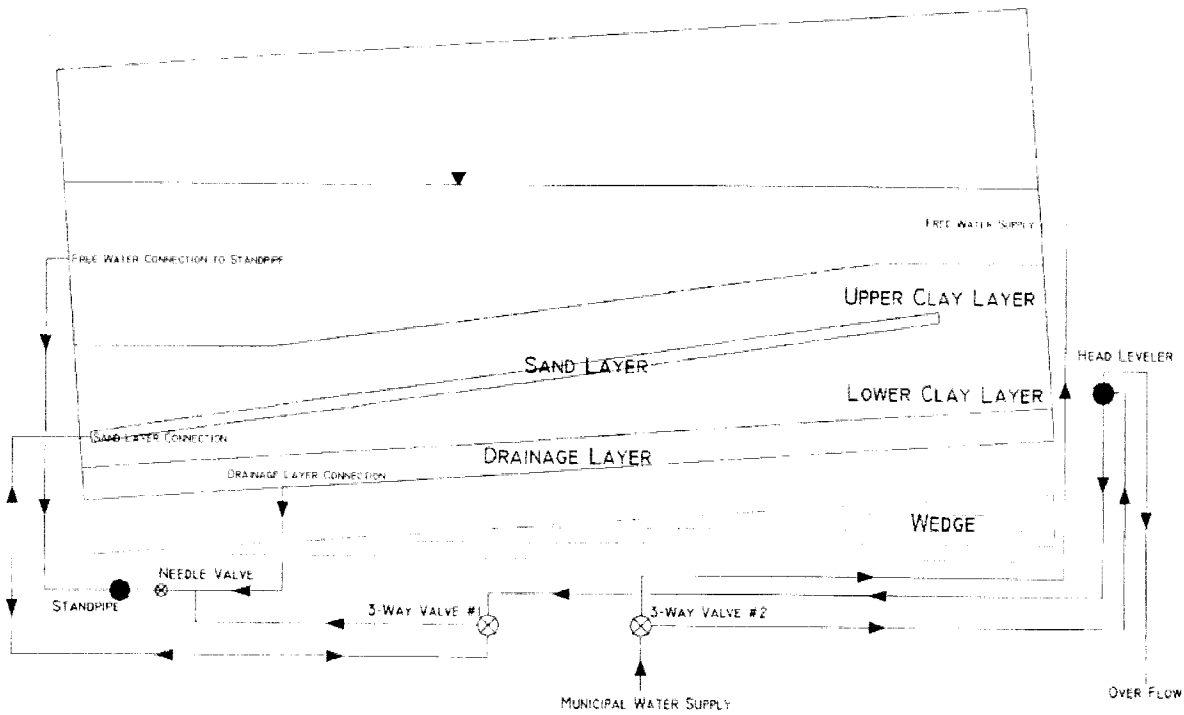

Figure 4.17: Plumbing schematic of SST 2 in plan view.

During consolidation, the sand layer was connected to the hydrostatic surface water, however, the connection did not adequately allow two-way drainage for the upper and lower clay layers. The sand layer and surface water were isolated during testing. At the time of testing, 3-way valve #1 permitted the sand layer and head-leveller to be

connected, which allowed the introduction of excess pore pressures into the sand layer. Through 3-way valve #2, municipal water could be added to the free water or to the head-leveller system.

4.4.3 Test Results

Based on CPT data, shear strength is plotted with increasing depth as shown in Figure 4.18. Target line and hand vane values are plotted to provide a relative comparison with the CPT results. The CPT data below 37 mm was removed due to interference from the sand layer. Furthermore, due to the lower clay layer's relatively thin depth, its CPT data was also not included because of interference from the sand layer. Hand vane results have relatively higher shear strength values than expected. This may be attributed to possible interference from the sand layer, which may have increased soil resistance.

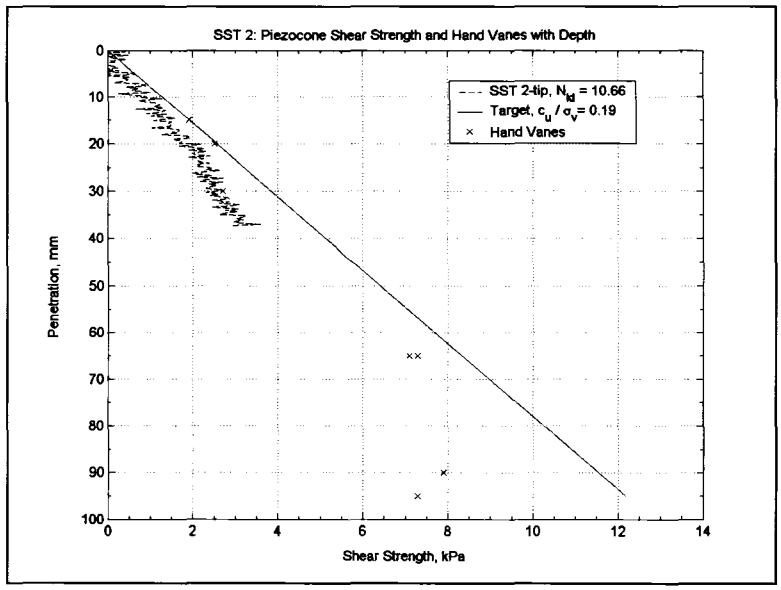

Figure 4.18: Piezocone shear strength and hand vanes with depth of SST 2.

At position A of Figure 4.19, the valve connecting the head-leveller and sand layer was opened. During opening of the valve, the head-leveller was slightly higher in elevation than the surface water, creating an excess pressure head in the sand layer. The increase in pore pressure in the sand layer can be seen by the positive pore pressure responses of PPT 8 and PPT 9 at position B.

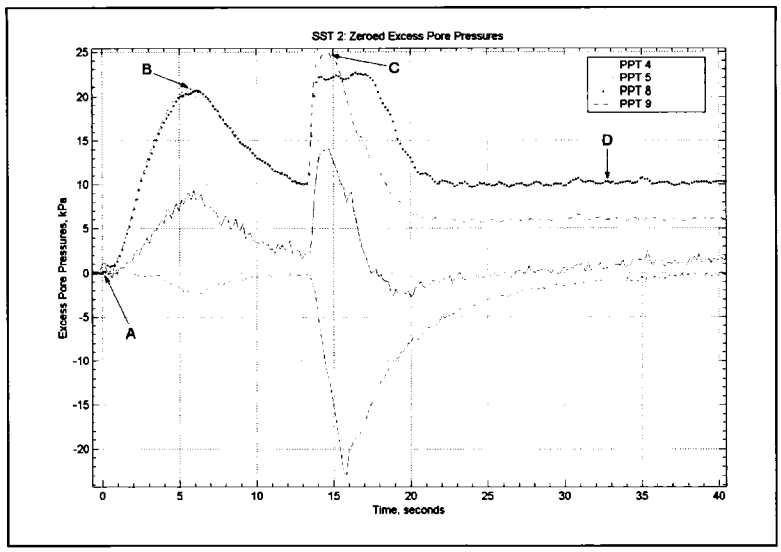

Figure 4.19: Zeroed excess pore pressures during SST 2.

A second increase of pore pressures measured at position C was due to the upward vertical movement of the head-leveller. The decrease in pore pressure of PPT 5 may be attributed to stress relief applied on the lower clay layer. Also at position C, the pressurized water from the sand layer broke through the upper clay layer to the surface water. This was confirmed by the sudden observation of clay suspension in the surface water. The short-circuiting limited the pressures of the injected water in the sand layer, causing it to drop off at position D.

The failure events can be confirmed by corresponding LVDT displacements, as seen in Figure 4.20. Compared to position X, larger soil deformation was observed for the second increase of pore pressure at position Y. Since the second application of water pressure caused larger soil strains and a maximum excess pore pressure of approximately 25 kPa. It is believed that the event at position Y caused slope failure. Slope failure was

verified by the deformation of the spaghetti markers and the change of slope in the negative pore pressure response of PPT 5 at 13.8 seconds of Figure 4.19.

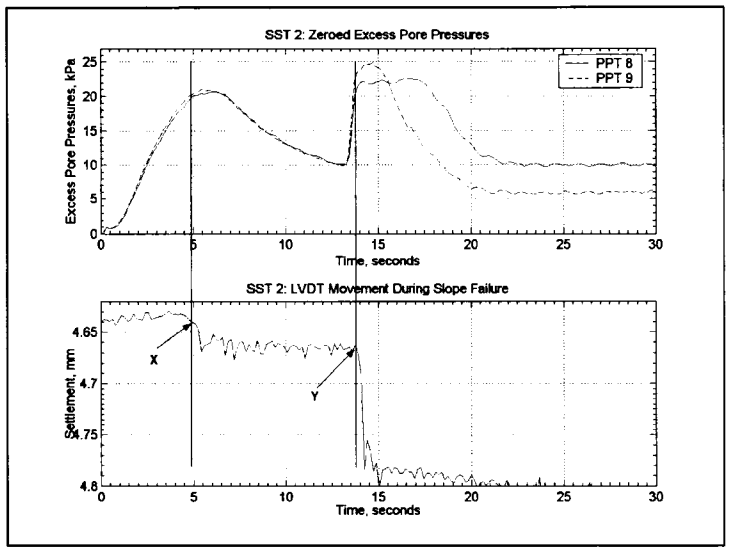

Figure 4.20: SST 2 LVDT displacements corresponding to excess pore pressures.

It can also be seen from Figure 4.20 that the sand layer was shearing during failure due to the vertical surface displacements which correspond to the peak excess pore pressures. From roughly 14 seconds to 17.5 seconds, the excess pore pressures recorded by PPT 9 plateau due to shearing of the sand reaching critical state. At a time of approximately 14 seconds PPT 8 peaked at 25 kPa. The LVDT readings were continuously dropping after 15 seconds, confirming that further soil deformation was occurring.

Figures 4.21a, 4.21b and 4.21c display the deformation of the spaghetti markers, and confirms the slope did experience failure due to applied water pressure in the sand layer. Spaghetti markers indicated movement mainly in the slopes centre of approximately 3-5

mm. Negligible soil movement occurred at the crest and toe of the slope. There was also little sign of remoulded clay or significant changes of slope geometry. The limited soil movement is a function of the constraints imposed by the finite size of the box and the brief time the high pore pressures were maintained before releasing to the surface water.

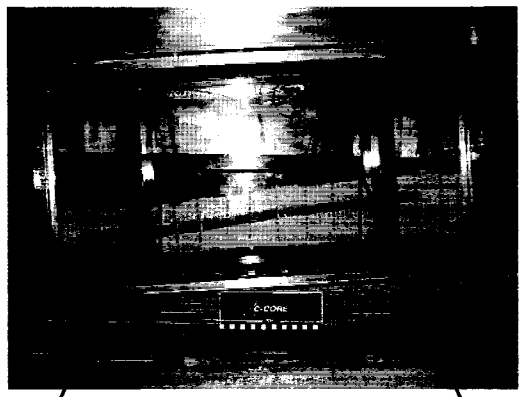

Figure 4.21a: Photo of model after SST 2.

Figure 4.21b: Close up photo of slope after SST 2 showing spaghetti displacements.

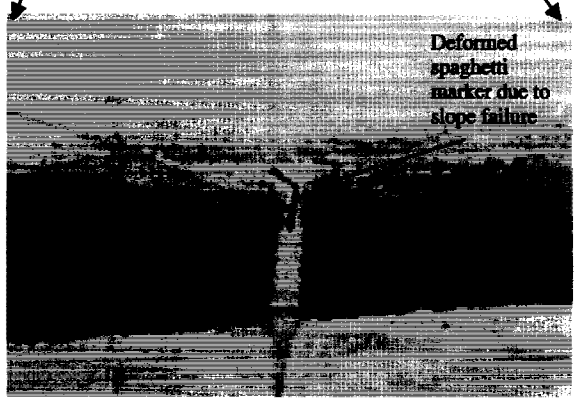

Figure 4.21c: Zoomed photo of one spaghetti strand of SST 2.

X-rays were taken of the soil model, revealing the position of the soldered spaghetti markers as shown in Figure 4.22. The spaghetti strands show clear signs of a slope failure plane along the upper clay layer and sand layer interface. The small leftward displacements in the x-ray image are similar to the spaghetti markers adjacent to the Perspex window. There were no signs of soil displacement in the lower clay layer.

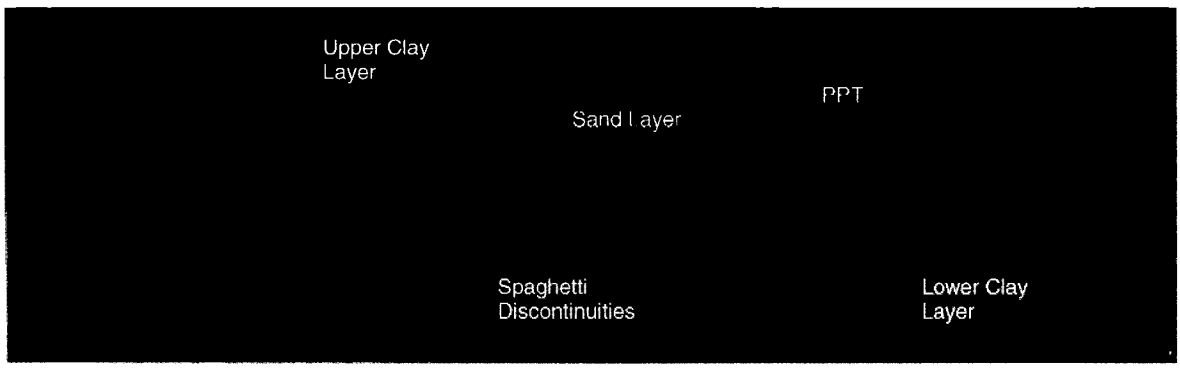

Figure 4.22: SST 2 x-ray image of soil after slope failure.

4.4.4 Discussion

Figure 4.23 shows an interpreted failure plane based on the deformation of the spaghetti markers. The shape of the failure surface was constructed from spaghetti marker positions in the Perspex window and the x-ray image. Comparing the two spaghetti marker positions in the model, the Teflon lubricant satisfactorily decreased the sidewall frictional effects. In prototype dimensions, the failure surface was approximately 50 m in length and 5.4 m at maximum depth.

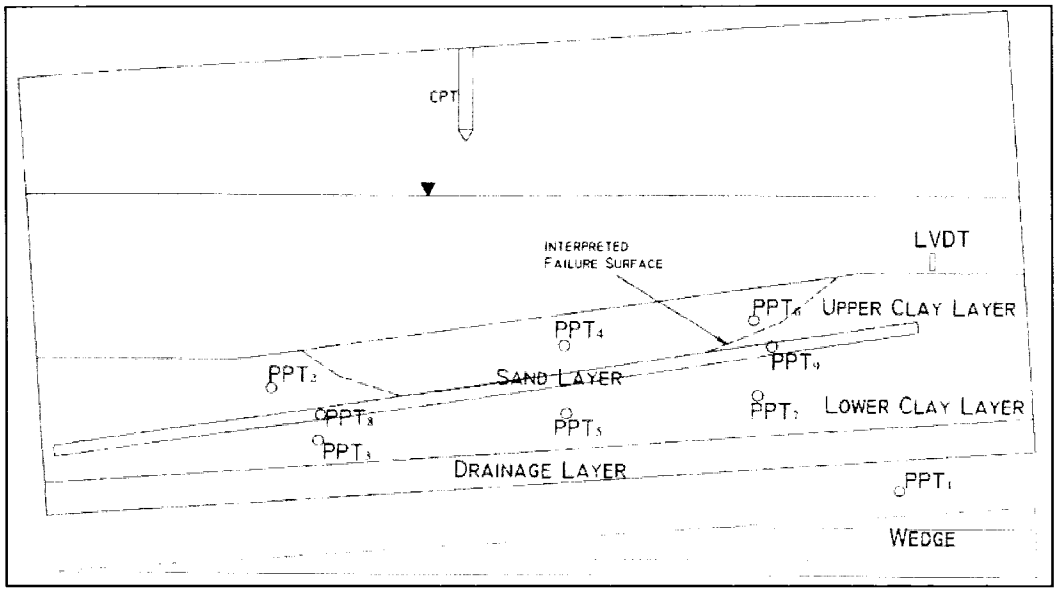

Figure 4.23: SST 2 model soil profile after slope failure.

Based on the interpreted failure surface from Figure 4.23, a slope stability analysis was completed using Geoslope's SLOPE/W software (Geoslope International Ltd., 2004) utilizing Spencer's method. The geometry of the model was incorporated into the software utilizing prototype dimensions.

When comparing the centrifuge results to the SLOPE/W stability analysis, several factors may contribute to differing results. Factors may include the experimental errors associated with measuring the depth of the upper clay layer, the varying gravitation level throughout the model, the fact that PPT calibrations may have slightly changed during testing, the possibly of remaining excess pore pressures due to incomplete consolidation, and the PPT locations may have not been exact. Errors in the assumptions used by the

SLOPE/W software may be another factor. These factors will be discussed in further detail in upcoming sections.

Another major influence on the centrifuge results is the effects of the boundary conditions imposed on the soil model. Slope runout was not permitted in SST 2, demonstrating the difficulty creating slope runout in the centrifuge.

A sensitivity analysis was completed to determine the effects of changing r_u with increasing excess pore pressure for SST 2 and SST 3, as shown in Figure 4.24. Due to the relatively shallow depths of the upper clay layers, it can be observed that small fluctuations of excess pore pressures caused by experimental errors can greatly affect the r_u values. For example, only an increase of 3 kPa in SST 3 can change the r_u value by 0.1.

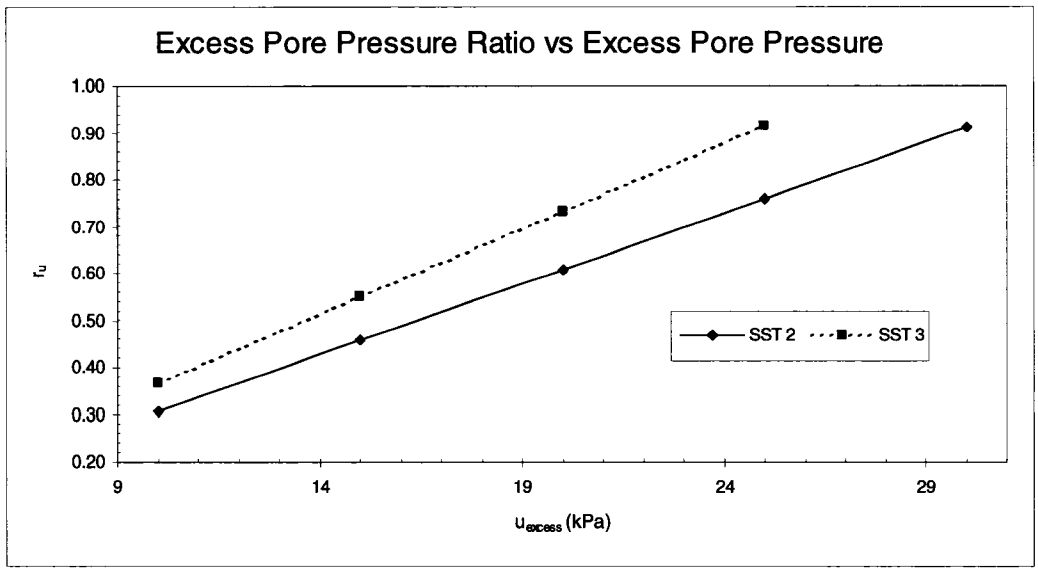

Figure 4.24 Sensitivity analysis of r_u with increasing excess pore pressures for SST 2 and SST 3.

Using the interpreted failure surface from Figure 4.23, two separate analyses were completed. The first analysis assumed that the failure surface along the clay and sand layer interface occurred at the bottom of the clay layer. The second analysis assumed that the failure surface extended down into the top of the sand layer. To complement the analyses, a stability analysis was also completed to search for the critical failure surface of the slope profile using the SLOPE/W software.

For the slope stability analysis, pore pressures measured in the sand layer were defined in terms of r_u. The sand layer was modelled with a cohesionless material with an internal angle of friction of 35°, and the same soil strength models used in SST 1 were applied.

Figure 4.25 shows the results of a stability analysis using SLOPE/W software, where the specified failure surface is extended down into the sand layer. Using a maximum recorded excess pore pressure of approximately 25 kPa, which corresponds to a r_u value of 0.76, a *Fs* of 1.34 was determined. Based on a sensitivity analysis with respect to *Fs* and a varying r_u value, to achieve a factor of safety of unity, a r_u value of 0.85 is required.

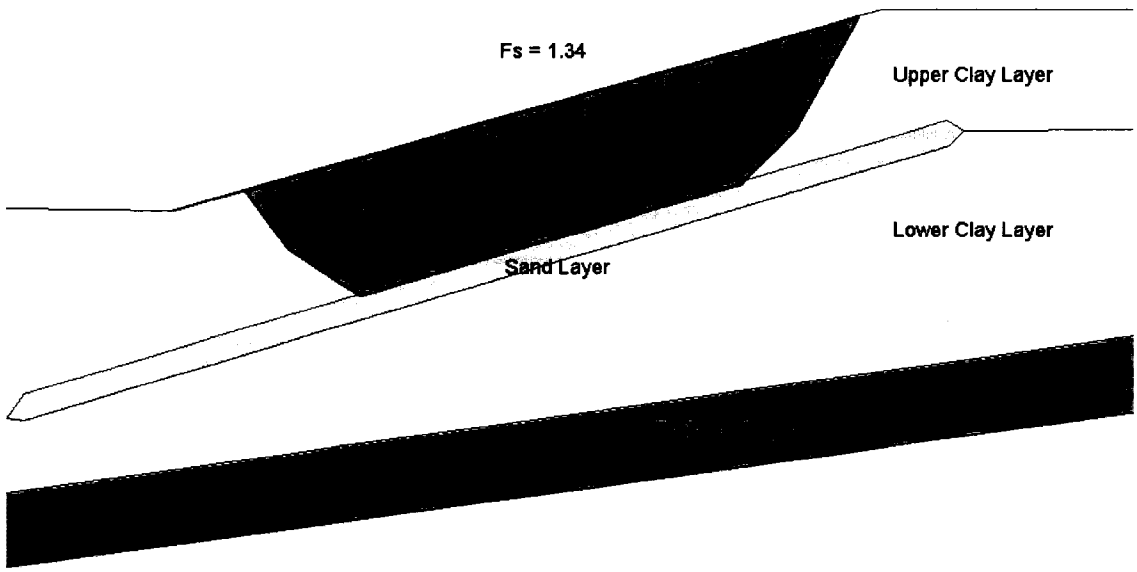

Figure 4.25: SLOPE/W stability analysis of SST 2 using a specified failure surface in the sand layer with a r_u = 0.76 yielding *Fs* = 1.34. (NTS)

A summary of the stability analyses results using the SLOPE/W software is shown in Table 4.3. The table shows that to achieve a factor of safety of unity, for the specified failure surface in the sand layer, only an increase of 3 kPa is required. The difference of 3 kPa can be mainly attributed to the fact that, although the slope profile was 90%

consolidated, there were remaining excess pore pressures persisting from the self weight consolidation.

Table 4.3: Summary of SLOPE/W results of SST 2.

Slip Surface	Passing Through	u_e	r_u	Fs
Specified	Sand layer	25	0.76	1.34
Specified	Sand layer	28	0.85	1.04
Specified	Clay layer	-	-	1.56
Critical surface search	Clay layer	-	-	1.38
Critical surface search	Sand layer	28.3	0.86	1.03

A stability based limit equilibrium analysis defining the failure surface in clay layer demonstrated, as expected, that the factor of safety is independent of the excess pore pressures defined in the sand layer. The stability analyses in the clay layer also demonstrate that the slope model is stable prior to the injection water.

Due to the limitations of the SLOPE/W software, the critical failure surface of the stability analysis was circular in shape for surfaces resulting from critical surface search. The results from the specified failure surface analyses show that the slope stability analysis using Spencer's method of slices reasonably validates the slope failure results from SST 2.

The results completed from the different stability analyses are plotted in Figure 4.26. The plot demonstrates the effect that a varying excess pore pressure ratio has on slope stability. The plot also demonstrates the fundamental differences of each stability

analysis and the independence of the specified failure surface in the clay from varying r_u values. The plot shows that up to a r_u of 0.76 the slope is unaffected by the induced excess pore pressures, however, the slope becomes steadily unstable thereafter.

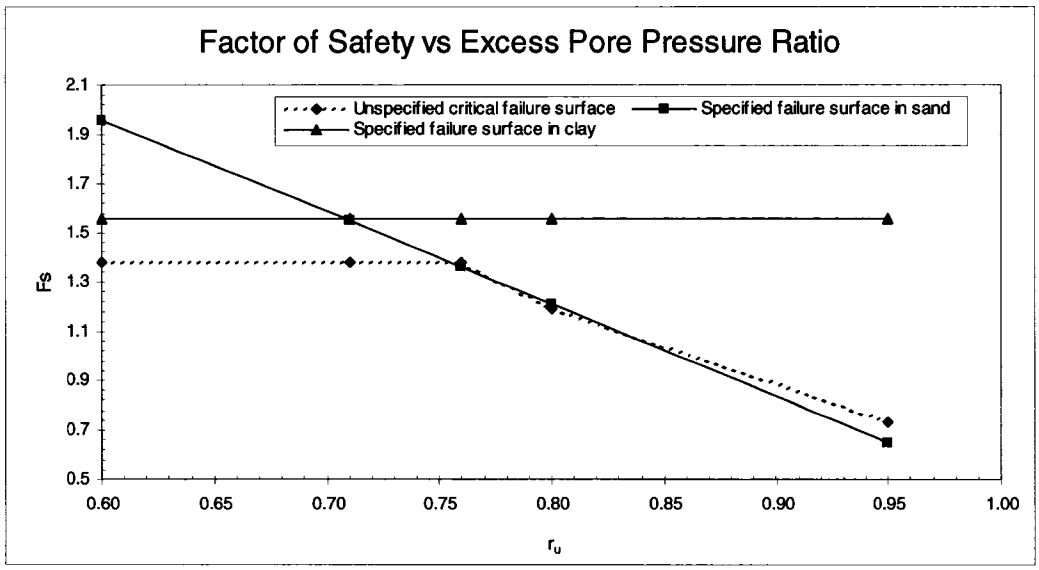

Figure 4.26: Plot of stability analyses factors of safety with varying r_u values for SST 2.

The critical surface search defined by the SLOPE/W software is circular in shape, therefore, its comparison to the failure surface observed in the centrifuge test is not suitable. At a r_u of 0.95 in the plot, it is believed that the critical failure surface has a high factor of safety due to the constrained circular surface used by the SLOPE/W software at such high r_u values. This also can be confirmed by the difference between the factor of safety of the failure surface and the specified failure surface in the clay at a r_u less than 0.76. Since the critical failure surface is relatively shallow compared to the

specified failure surface, its factor of safety is lower. As a result, the unspecified critical failure surface analysis will not be discussed any further.

4.5 Slope Stability Test 3

4.5.1 General

Slope Stability Test 3 (SST 3) continued studying the effects of increased pore water pressure in an embedded sand layer. Results from SST 2 showed that the horizontal toe surface did not promote slope runout as was anticipated. Consequently, model design of SST 3 was similar to SST 2, however, instead of having a horizontal toe surface, the toe of SST 3 was steepened to a 10° slope to allow slope runout. Similar to SST 2, slope failure was simulated in the centrifuge by inducing excess pore pressures in the sand layer using a head-leveller, as shown in Figure 4.16.

4.5.2 Model Preparation and Testing Procedure

The test procedure of SST 3 was identical to SST 2, with the aim of simulating submarine slope failure by increasing the pore pressures in the sand layer. Figure 4.27 displays the test package configuration after the addition of the sand layer and clay slurry to the lower clay layer. Figure 4.27 also displays the soil cross-section and positions of the LVDT and PPTs, but excludes the headworks such as the head-leveller assembly, the CPT vertical drive, and LVDT brackets.

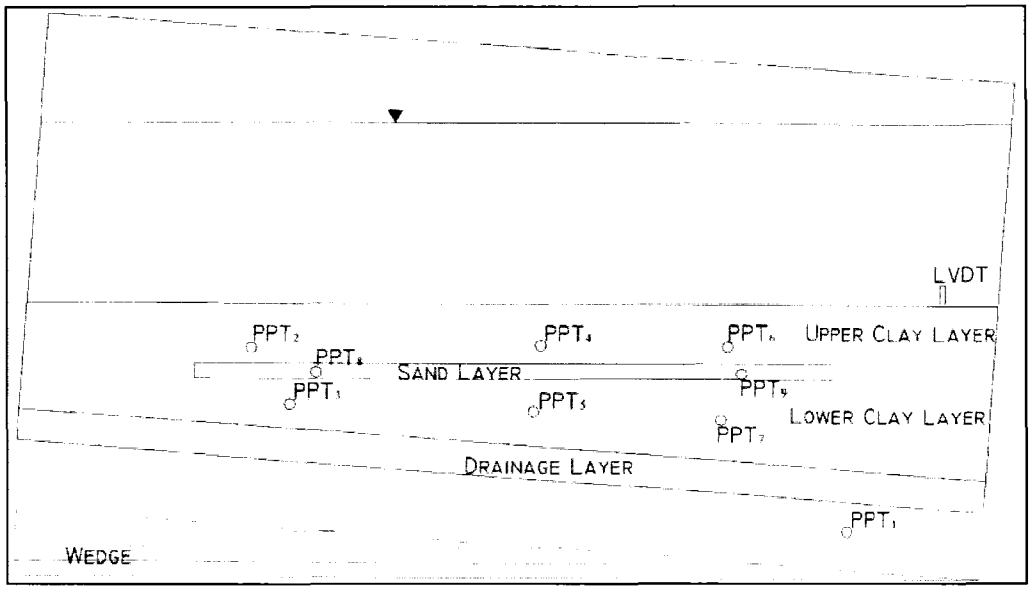

Figure 4.27: SST 3 profile of three soil layers prior to wedge rotation.

Figure 4.28 shows the configuration following the rotation of the wedge, and the creation of the 8° slope. The head of the slope was cut to provide a horizontal surface, and the toe was steepened to a 10° slope. The sand layer was curtailed in the area to ensure that the 10° steepening would not influence the failure mechanism. A total of three LVDTs were included in the test package to better define the soil surface movement during testing.

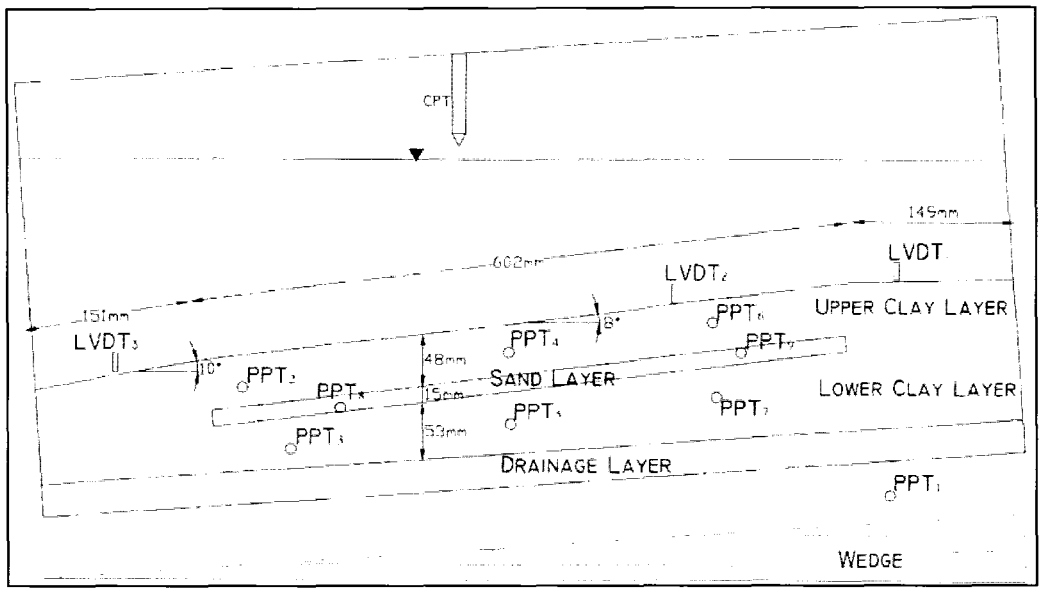

Figure 4.28: SST 3 model slope profile after rotation of wedge.

4.5.3 Test Results

Based on CPT data, shear strength is plotted with increasing depth as shown in Figure 4.29. Target line and hand vane values are plotted to provide a relative comparison with the CPT results. The CPT data below 40 mm was removed due to interference from the sand layer. Similar to SST 2, due to the lower clay layer's relatively thin depth, its CPT data was also not included because of interference from the sand layer. Hand vane results have relatively higher shear strength values at the upper portion of the soil profile, while at lower depths, the hand vane values are approximately 50% of the expected shear strength. Again, the higher shear strength values may be caused by possible interference from the sand layer.

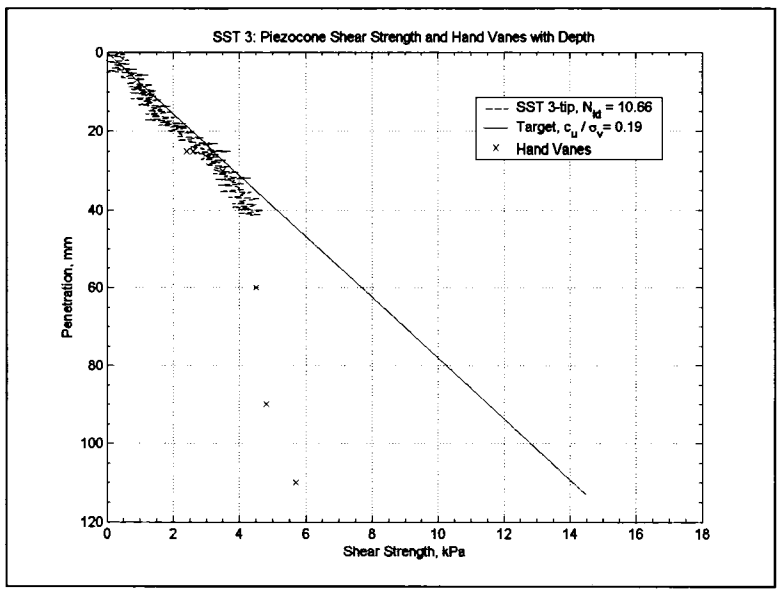

Figure 4.29: Piezocone shear strength and hand vanes with depth of SST 3.

At position A of Figure 4.30, the valve connecting the head-leveller and sand layer was opened. At the start of the test, the head-leveller was lower than the hydrostatic water level inside the model. As a result, the sand layer experienced initial negative excess pore pressures. The decrease in pore pressure in the sand layer can be seen by the negative pore pressure responses of PPT 8 and PPT 9 at position B.

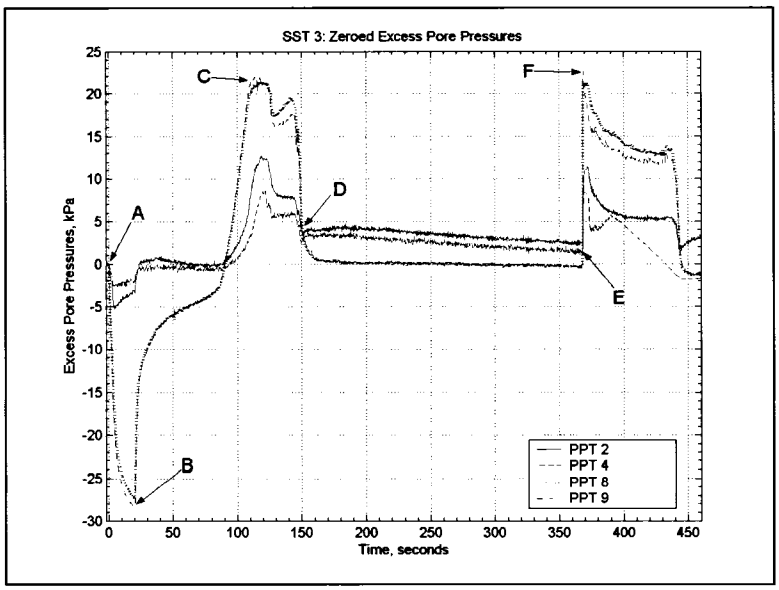

Figure 4.30: Zeroed excess pore pressures during SST 3.

After position B, the steady increase of pore pressures was due to the upward vertical movement of the head-leveller. At position C slope failure was assumed to have occurred, corresponding to a maximum excess pore pressure of approximately 22 kPa in the sand layer. The water supply was turned off at position D. At that time it was not clear whether the slope had failed, since there was no clay suspension observed in the surface water to indicate short-circuiting of the pressurized water from the sand layer. The water was reactivated at position E, and the head-leveller continued upward. At position F, short-circuiting of pressurized water from the sand layer to the surface water occurred. This was confirmed by the sudden observation of clay suspension in the surface water. The water supply was turned off immediately at the sight of the clay suspension.

The failure events can be confirmed by corresponding LVDT displacements, as seen in Figure 4.31. Based on the LVDT responses, it is concluded that slope failure occurred at position A. At position B, the LVDT plot shows that the soil experienced further movement. However, it is believed that the additional soil movement occurred along the same failure plane.

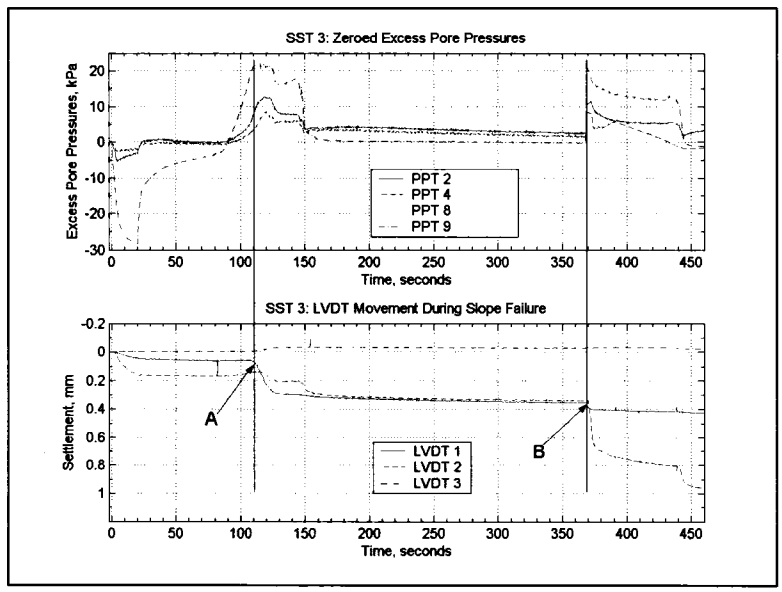

Figure 4.31: SST 3 LVDT displacements corresponding to excess pore pressures.

X-rays were taken of the soil model, revealing the position of the soldered spaghetti markers as shown in Figure 4.32. The spaghetti strands show clear signs of a slope failure plane along the upper clay layer and sand layer interface. Small leftward displacements of approximately 3-5 mm in the x-ray image are similar to the spaghetti markers adjacent to the Perspex window. There were no signs of soil displacement in the

lower clay layer, and negligible soil movement occurred at the crest and toe of the slope. There was also little sign of remoulded clay, or significant changes of slope geometry.

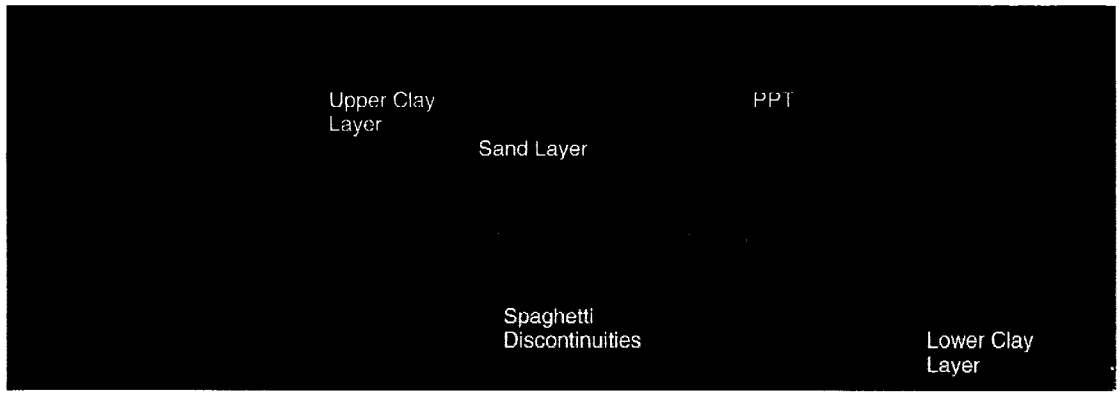

Figure 4.32: SST 3 x-ray image of soil after slope failure.

4.5.4 Discussion

Figure 4.33 shows an interpreted failure plane based on the deformation of the spaghetti markers. The shape of the failure surface was constructed from spaghetti marker positions in the Perspex window and the x-ray image. Similar to SST 2, the Teflon lubricant satisfactorily decreased the sidewall frictional effects. In prototype dimensions, the failure surface was approximately 60 m in length and 4.8 m at maximum depth.

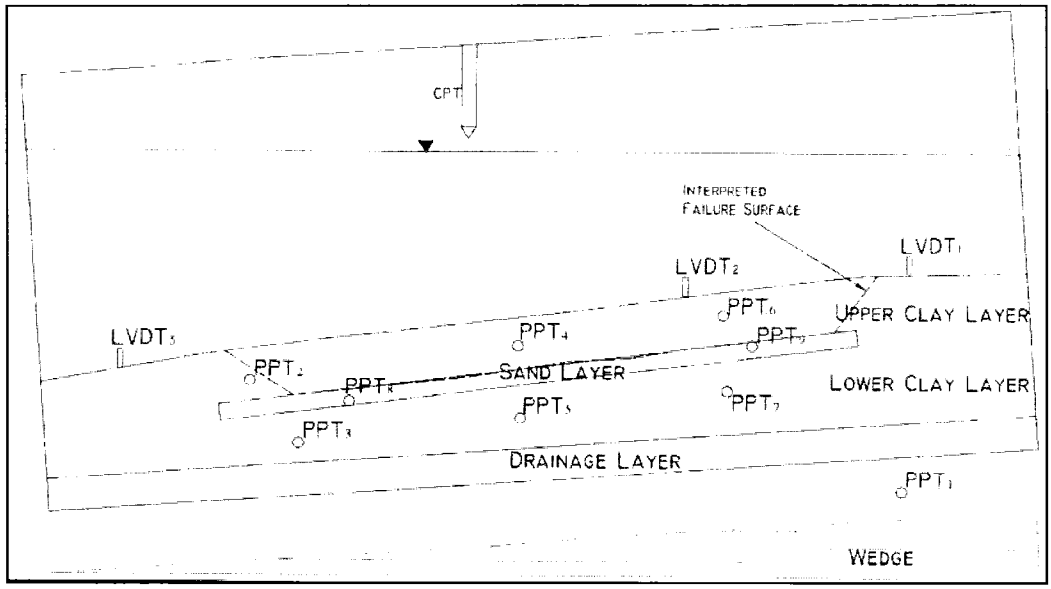

Figure 4.33: SST 3 model soil profile after slope failure.

Based on the interpreted failure surface from Figure 4.33, a slope stability analysis was completed using Geoslope's SLOPE/W software (Geoslope International Ltd., 2004) utilizing Spencer's method. The geometry of the model was incorporated into the software utilizing prototype dimensions.

Using the interpreted failure surface, two separate analyses were completed similar to SST 2. The first analysis assumed that the failure surface along the clay and sand layer interface occurred at the bottom of the clay layer. The second analysis assumed that the failure surface extended down into the top of the sand layer.

For the slope stability analysis, pore pressures measured in the sand layer were defined in terms r_u. The sand layer was modelled with a cohesionless material with an internal angle of friction of 35°, and the same soil strength models used in SST 1 were applied.

Figure 4.34 shows the results of a stability analysis using SLOPE/W software where the specified failure surface is extended down into the sand layer. Using a maximum recorded excess pore pressure of approximately 22 kPa, which corresponds to a r_u value of 0.81, a *Fs* of 1.27 was determined. Based on a sensitivity analysis with respect to *Fs* and a varying r_u value, to achieve a factor of safety of unity, a r_u value of 0.85 is required.

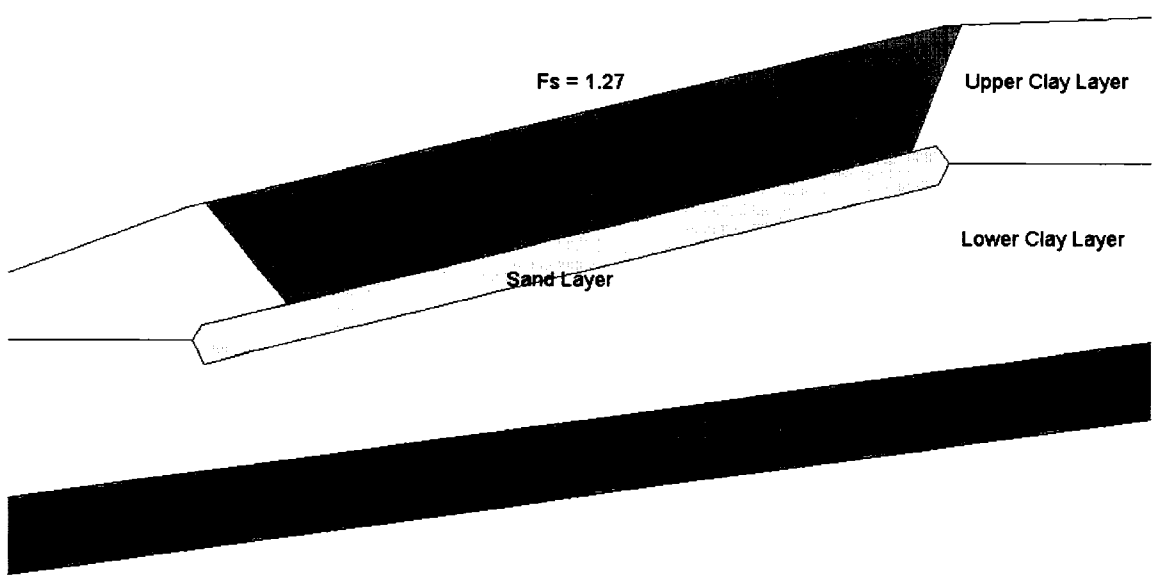

Figure 4.34: SLOPE/W stability analysis of SST 3 using a specified failure surface in the sand layer with a $r_u = 0.81$ yielding $Fs = 1.27$. (NTS)

A summary of the analyses results using the SLOPE/W software is shown in Table 4.4. The table shows that to achieve a factor of safety of unity, for the specified failure surface in the sand layer, only an increase of 1 kPa is required. Unlike SST 2, the soil profile in SST 3 had a higher degree of consolidation. The results of SST 3 are similar to the results of SST 2. The results from the specified failure surface analyses show that the slope stability analysis using Spencer's method of slices validates the results of SST 3.

Table 4.4: Summary of SLOPE/W results of SST 3.

Slip Surface	Passing Through	u_e	r_u	Fs
Specified	sand	22	0.81	1.27
Specified	sand	23	0.85	1.04
Specified	clay	-	-	1.82

The results completed from the different stability analyses are plotted in Figure 4.35. The plot, similar to SST 2, demonstrates the effect that a varying excess pore pressure ratio has on slope stability. For demonstration purposes the critical failure surface is shown to confirm the statements expressed in Section 4.4.4.

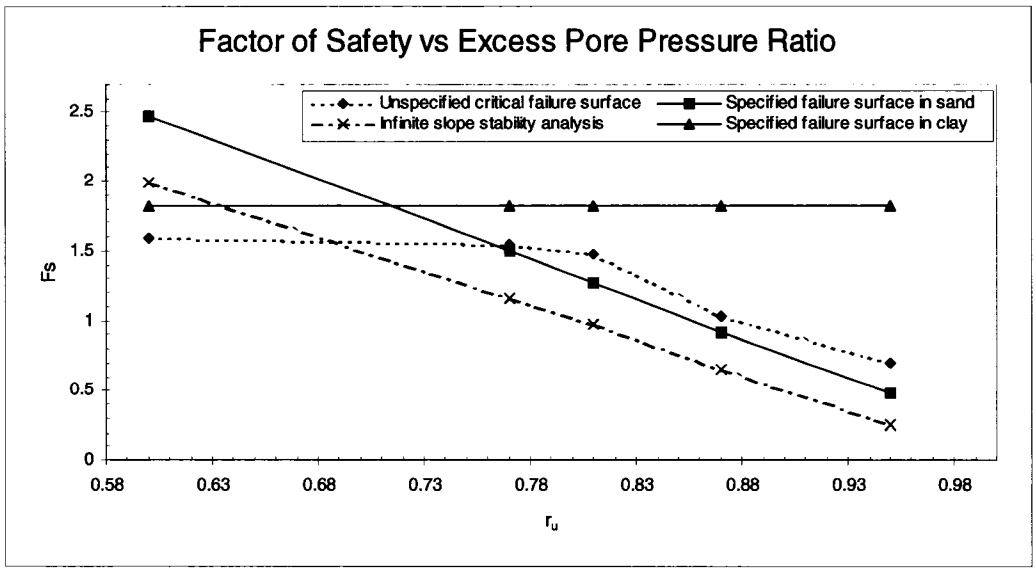

Figure 4.35: Plot of stability analyses factors of safety with varying r_u values for SST 2.

Unfortunately, slope runout was once more not successful. The results of SST 3, again, show the difficulty creating slope runout in the centrifuge and the significant boundary effects caused by the centrifuge strongbox.

4.6 Analysis and Conclusions

Utilizing centrifuge modelling, the effect of excess pore pressures associated with submarine slope failures were investigated. The primary research objectives were to develop methodologies for the modelling of submarine slope failures caused by static loadings on continental slopes, to conduct centrifuge tests simulating the behaviour of submarine slope failures, and to show that the test data obtained reasonably models actual submarine slope failure conditions.

The centrifuge modelling program was carried out at C-CORE's centrifuge centre. Based on previous demonstration tests, the testing program consisted of three centrifuge tests. The first centrifuge test simulated slope failure due to sediment undercutting. The second and third tests both simulated slope failure due to excess pore pressures generated within sediment layering. Table 4.5 displays all centrifuge tests completed by the author in the research program.

Table 4.5: Centrifuge tests completed by the author for the research program.

Centrifuge Test	Centrifuge Test Description
Centrifuge Proof Test	Equipment and related instrumentation was tested in the centrifuge to ensure structural strength for model testing.
Demonstration Test 1	Demonstration test was completed to obtain experience using the centrifuge and determine optimal placement of instrumentation.
Demonstration Test 2	Demonstration test concentrated on causing slope failure by loading an aluminium plate with a vertical actuator on the crest of a submerged slope. Slope failure did not occur, but bearing capacity failure was observed.
Slope Stability Test 1 (SST 1)	SST 1 concentrated on causing slope failure by vertically extracting an aluminium wedge from the toe of a submerged slope. Slope failure did occur.
Slope Stability Test 2 (SST 2)	SST 2 concentrated on causing slope failure by inducing excess pore pressures in an interbedded sand layer of a submerged slope. Slope failure did occur.
Slope Stability Test 3 (SST 3)	SST 3 concentrated on causing slope failure by inducing excess pore pressures in an interbedded sand layer of a submerged slope. Slope failure did occur.

The failure mechanisms associated with each centrifuge test were specifically chosen to simulate possible offshore slope failure conditions. The extraction of an aluminium wedge in SST 1 created an immediate exposed soil surface that initiated slope failure. This method was intended to simulate soil undercutting created by several natural conditions, however, it is believed that the steep soil surface limited the simulation of physical conditions. Due to the steep near vertical exposed soil surface, the centrifuge test more closely simulated slope failure due to an exposed head scarp created by a downslope mass movement, rather than erosion due to ocean currents or diapirism.

Slope stability analysis using Spencer's method of slices was completed to evaluate the results from SST 1. The results from the stability analysis compared favourably to the data obtained from the centrifuge tests. Analyses also showed that lower factors of safety within the mass movement indicate probable variations in the rates of strain deformation and strain softening.

Due to the lack of runout, the head scarp created from the slope failure was not unloaded, therefore, preventing the upper slope to develop a retrogressive failure. As a result, the upper portions of the mass movement were minimally displaced downslope. This can be confirmed since the slope angle of the soil surface after slope failure was approximately 10-15°, which is stable under normal static conditions.

The eight PPTs located in the soil model of SST 1, showed that negative excess pore pressures were generated during slope failure. The negative excess pore pressures were probably caused by the soil shearing during slope failure.

SST 1 demonstrates the significant boundary effects that control the simulation of slope failures in the centrifuge. If runout was permitted, the slope failure may have developed into a retrogressive slope failure. The slope failure triggering mechanism was very different from SST 2 and SST 3. Overall, the stability analysis and the centrifuge results of SST 1 are satisfactorily in good agreement with each other.

As previously mentioned, discrepancies between the centrifuge results and the stability analysis can be accredited to several factors. For example, each model soil profile prior to slope failure was estimated after slope failure had occurred. The final positions of the instrumentation and the soil profiles were carefully recorded after each centrifuge test, however, errors of several millimetres was possible. The spaghetti markers provided reasonably defined failure surfaces, however, minor variations of the defined failure plane can yield various factors of safety when using limit equilibrium methods. The varying gravitation level throughout the model, the fact that PPT calibrations may have slightly changed during testing, the possibly of remaining excess pore pressures due to incomplete consolidation, and errors in the assumptions used by the SLOPE/W software are all additional factors that may lead to discrepancies of results.

The unique stress history of the soil model was not considered in limit equilibrium analyses. Although the soil profile was considered to be normally consolidated, the rotation on the 4° plywood wedge changed the direction of the principal stresses acting of the soil profile. Prior to the wedge rotation, the principal stresses were acting perpendicular to the soil surface. After the wedge was rotated and the 8° slope was created, the principal stresses that were previously acting on the soil slope were also rotated 8°. These effects were not considered in the slope stability analyses.

A significant factor that may have affected the centrifuge results are the artificial boundaries created by the finite size of the model package. Boundary effects are always a major concern in centrifuge modelling. Due to the neglect of three-dimensional boundary effects it would be expected that the limit equilibrium slope stability analysis would provide a lowerbound estimate. However, the stability analysis of SST 2 and SST 3 did not provide a lower bound estimate.

As previously stated, the results of the three centrifuge tests were noticeably affected by boundary conditions imposed by the centrifuge strongbox. It is quite possible that the high excess pore pressures experienced in SST 2 and SST 3 may be a result of the boundary conditions imposed on the model slope. Since the boundary conditions in the model restricted slope failure, greater excess pore pressures may have been needed to cause slope failure.

An infinite slope stability analysis was performed for SST 2 and SST 3 to demonstrate the influence of the head and toe boundary effects. Since both centrifuge tests have similar properties, only one analysis was necessary. Morgenstern's infinite slope stability equation (Equation 2.11) was used. Morgenstern (1967) proposed standard infinite slope stability equations for large, shallow submarine slopes that assess the factor of safety of a particular slope accounting for pore water pressure at the base of the strata. As previously defined, the factor of safety can be expressed as,

$$Fs = \frac{\tan\phi'}{\tan\beta}(1 - r_u).$$

Using a r_u value of 0.81, an infinite slope analysis resulted in a Fs of approximately unity. Similar to the SLOPE/W stability analysis using the specified failure surface in the sand layer, the infinite slope analysis completed utilizes the sand's internal friction angle as the resisting soil parameter.

Figure 4.36 shows the relationship of the factor of safety with varying r_u using the specified failure surface for SST 3 compared to the infinite slope analysis. The graph clearly shows that according to Spencer's method of slices with a specified failure surface extending into the sand layer, the model slope becomes unstable at a r_u of approximately 0.86. The infinite slope analysis is unstable at a r_u of 0.81.

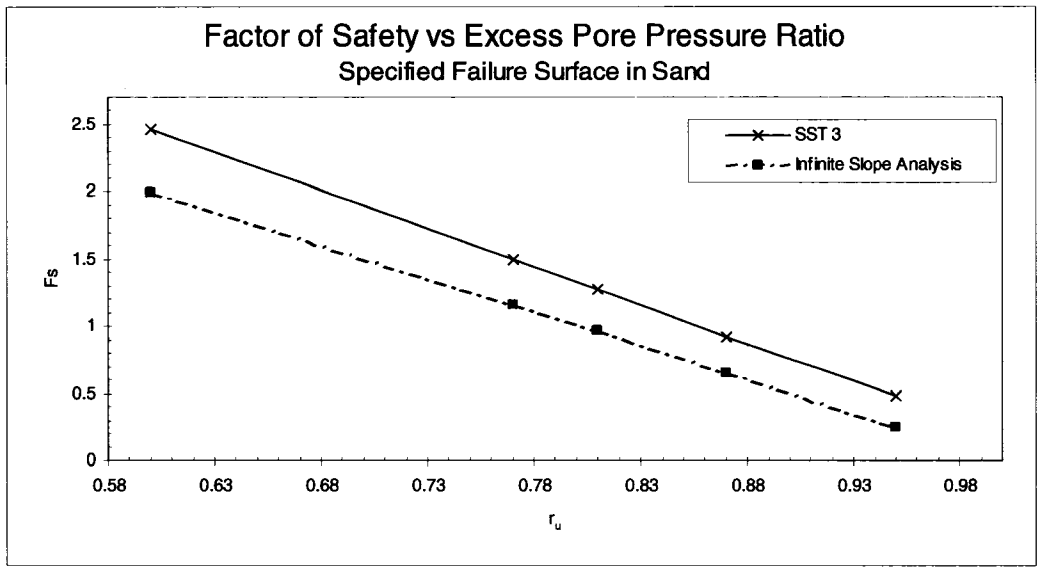

Figure 4.36: Plot of specified failure surface and infinite slope analyses with varying r_u values for SST 3 SLOPE/W analysis and an infinite slope analysis.

Although infinite slope stability analyses are often conservative, there is a significant difference between the two lines shown in Figure 4.36. The difference is believed to illustrate the boundary effects imposed on the stability analysis and model slopes. Since the infinite slope analysis completed does not account for the head and toe boundary conditions, a lower r_u value is required to cause slope instability. This shows that the stability analysis using the SLOPE/W software accounts for the boundary effects experienced in the centrifuge test. As a result, it can be stated that the SLOPE/W software is an acceptable method to assess the stability of the centrifuge tests.

The centrifuge results and stability analyses show that due to significant boundary effects caused by the centrifuge strongbox, very high excess pore pressures are required to

initiate slope failures in the centrifuge. Also, the slope angle of the model slope is relatively high compared to most continental slopes. Based on Morgenstern's infinite slope equation, to achieve a factor of safety of unity using a r_u of 0.85, a slope angle of 6° is required. This demonstrates that the high excess pore pressures recorded in SST 3 that caused slope failure, would cause instability in a 6° slope using infinite slope analysis. Nevertheless, the infinite slope analysis shows that very high excess pore pressures are still required to cause slope instability in the absence of the centrifuge boundary conditions.

To confirm that the high r_u values generated in SST 2 and SST 3 are actually simulating natural conditions a literature review was completed. Unfortunately, there is limited published literature that describes the measured excess pore pressures in natural conditions. One was presented in Section 2.3.14, which stated that based on numerical simulation and sediment sampling of the 0.5°- 2° slope, excess pore pressures of 20 to 30% above hydrostatic were predicted at the time of the Storegga slide. Although these excess pore pressures are high, they are not equivalent to the high r_u values experienced by the submarine slope failures simulated in SST 2 and SST 3. Also, the slope of the Storegga slide region was much less than the 8° model slope used. Since the author is not aware of any submarine sediment stability studies to explain the high r_u values witnessed in the centrifuge, other literature and research studies will be used to verify the centrifuge results.

Lee (2003) describes a detailed slope stability analysis using SLOPE/W software on the normally consolidated Hudson Apron sediments, which lie mostly on a 4° slope. Studying the factors that could create high excess pore pressures, Lee (2003) studied underconsolidation, groundwater seepage from a nearby coastal aquifer, gas-hydrate dissociation, and earthquake loading. The analysis showed that very high excess pore pressures would be required to generate instability. The excess pore pressures were equivalent to a r_u value between 0.8 and 0.9. Lee (2003) concluded that in order to create such high excess pore pressures, more than one strength reduction factor would be required to cause slope instability. Considering the centrifuge model slope was 8°, these r_u values compare well with the 0.76 and 0.81 recorded for SST 2 and SST 3, respectively.

To further validate the r_u values experienced in the centrifuge, an infinite slope analysis described by Quéméneur et al. (1998) on the Gabon continental slope was performed. Based on their results, the critical r_u value due to vertical seepage forces was estimated to be 0.691 for a 8° slope. This value also demonstrates that very high r_u values are needed to cause slope instability under those conditions.

Along with limit equilibrium studies, finite element studies of submarine slope failure have also shown that very high excess pore pressures are required to cause slope instability. Azizian and Popescu (2003) simulate earthquake-induced retrogressive sliding using finite element methods on layered soil profiles of loose silt and sand. Using

a seafloor slope of 2°, the stability study determined that r_u values greater than 0.75 were predicted during slope failure simulation. Based on an infinite slope analysis completed using the centrifuge soil properties, a r_u value of 0.95 is required to cause instability of a 2° slope.

Similar to the numerical studies previously discussed, centrifuge studies have also been completed to assess the excess pore pressures associated with submarine slope stability. Malvick et al. (2002) describe a centrifuge study where slope failure due to earthquake loading was simulated in the centrifuge. The 31° model sand slope included embedded silt seams to impede drainage along a potential failure surface. Centrifuge results show that r_u values ranging from 0.50 to 0.90 were experienced during slope failure. Even though the model slope was quite steep, the r_u values are still quite high, similar to the r_u values witnessed during SST 2 and SST 3.

The high r_u values obtained from the centrifuge testing cannot be confirmed from actual submarine conditions. However, based on previous numerical and physical modelling, the r_u values obtained in SST 2 and SST 3 can be linked to actual excess pore pressure conditions.

Although, the centrifuge research program did simulate submarine slope failures, it was limited in assessing some important factors that affect submarine slope stability on continental slopes. For instance, the 8° slope angle used in the centrifuge models was

relatively steep for continental slopes and it is not clear the effects that soil layering, retrogressive failure, and strain-softening may have caused to the model slope.

Based on their study of the Storegga slide complex, Bryn et al. (2004) state that high excess pore pressures were necessary to cause local instability which initiated the regional slide complex. However, a combination of events such as retrogressive failure, weak soil layers, and strain softening with progressive failure are all important factors that contributed to the extremely large slide complex.

Since the strain-softening behaviour of marine clays is the most important factor in the understanding of the failure and retrogressive slide processes in low angle slopes of the continental margin (Bryn et al., 2004), the slope stability behaviour of very low slopes may not have been effectively modelled. Although strain-softening behaviour was not effectively modelled in the centrifuge, it is an essential concept that must be considered. Slope runout was prohibited due to the finite size of the centrifuge model. Consequently, the ability to simulate large soil strains and retrogressive slope failure in the centrifuge was not possible.

Another limiting factor associated with the centrifuge testing program was the relatively small size of the slope failures. Continental slope mass movements can cover area's 100's km^2 at depths of 100's of meters, but the model size restrictions only allowed the slope failure surfaces to be 50 to 60 m of prototype length and the prototype depths of the centrifuge models ranged from 4.8 to 7.6 m. It is believed that the centrifuge models

simulated localized slope failure, while the ability of the model slope to fail retrogressively was not possible. As a result, it is difficult to conclude that the small local slope failures created in the centrifuge tests are applicable to very large mass movements.

Based on the literature presented in this Section, it can be implied that the r_u values experienced during slope failure in the centrifuge tests are in agreement with numerical and physical modelling results obtained by other authors. Unfortunately, the literature is based on numerical and physical modelling. Since the effects of retrogressive failure, soil layering, and strain-softening cannot be reasonably concluded, it is not clear if the results of the centrifuge research program accurately model actual submarine slope failure conditions which occur on continental slopes. However, it is believed the centrifuge tests reasonably simulated localized submarine slope failure conditions and triggering conditions.

Overall, the centrifuge research program developed new methodologies for the modelling of submarine slope failures caused by static loadings. The program also demonstrated that stability analyses using limit equilibrium methods reasonably predicted the centrifuge results.

5.0 CONCLUSIONS

This thesis describes a research program utilizing centrifuge modelling to provide further insight into the understanding and mechanics associated with submarine slope failures on continental slopes. The primary research objectives were to develop methodologies for the modelling of submarine slope failures caused by static loadings, conduct centrifuge tests investigating the behaviour of submarine slope failures and show that the test data obtained reasonably simulates actual submarine slope failure conditions.

After many decades of research, the conditions leading to failure, as well as the triggering of many large submarine slides throughout the world are still not fully understood. Centrifuge modelling is one particular tool that can provide information into the mechanisms associated with submarine slope failures. Centrifuge modeling is a method for reduced-scale physical modelling of gravity-dependent phenomena, such as submarine slope failures. A centrifuge modelling program was carried out at C-CORE's centrifuge centre to study the mechanisms associated with submarine slope failures.

Based on experience developed from previous demonstration tests, the testing program consisted of three centrifuge tests. The centrifuge tests simulated the failure of submarine slopes caused by sediment undercutting and excess pore pressure generation within an interbedded sand layer. Slope stability analyses using limit equilibrium methods were completed to evaluate the results from the centrifuge tests.

The design of SST 1 concentrated on soil undercutting leading to slope failure. The primary triggering mechanism was designed to simulate sediment undercutting by vertically extracting an aluminium wedge that was embedded in the toe of the slope. The extraction of an aluminium wedge in SST 1 created an immediate exposed soil surface that initiated slope failure. The steep near vertical exposed soil surface, the centrifuge test more closely simulated slope failure due to an exposed head scarp created by a downslope mass movement. Slope stability analysis using SLOPE/W software was completed to evaluate the results from SST 1. The results from the stability analysis compared favourably to the data obtained from the centrifuge tests.

Design of SST 2 and SST 3 both concentrated on the effect of increased pore water pressures in an interbedded sand layer leading to loss of effective stress and slope failure. Slope failure was simulated in the centrifuge by artificially inducing excess pore pressures in the model sand layer. The creation of excess pore pressures was intended to simulate several different offshore continental slope strength reduction mechanisms, such as earthquakes, rapid sedimentation, the influence of aquifers, gas charging and the dissociation of gas hydrates.

A slope stability analysis was completed for both tests using an infinite slope stability analysis and SLOPE/W software. The results from the stability analyses satisfactorily predicted the results of SST 2 and SST 3. Infinite slope analysis showed that the boundary conditions affected the stability of the centrifuge model slope. Both tests

demonstrated that very high excess pore pressure ratios are required to simulate submarine slope failure in the centrifuge.

Due to limited published literature, it was difficult to compare the excess pore pressures recorded in the centrifuge tests to the natural seabed conditions. Therefore, numerical and physical modelling was used to validate the centrifuge results. Using the modelling, it was shown that such high excess pore pressures resulting from this study are possible.

The centrifuge research program completed was limited in assessing some of the factors that affect submarine slopes stability on continental slopes. Even though the limit equilibrium analyses reasonably predicted the centrifuge results, the effects of retrogressive failure, soil layering, and strain-softening cannot be concluded. However, it is believed the centrifuge tests reasonably simulated localized submarine slope failure conditions and conditions for slope failure initiation.

Overall, the centrifuge research program did develop new methodologies for the modelling of submarine slope failures caused by static loadings. The program also demonstrated that stability analyses using limit equilibrium methods reasonably predicted the centrifuge results.

6.0 RECOMMENDATIONS

Experience gained from the centrifuge testing and the limit equilibrium stability analysis has lead to several recommendations for further work. The recommendations proposed cover several areas of interest.

Further centrifuge testing should be conducted to continue studying the behaviour of static loading failure mechanisms associated with submarine slopes. New techniques simulating different failure mechanisms should be development. These techniques may simulate oversteepening, ocean current sediment erosion, glacial loading and slope failure due to creep. They also should be developed to minimize boundary effects.

Different soil profiles with varying soil types should be used to simulate different sediment properties and layering conditions. Since the offshore environment has a diversified and continuously changing stratigraphy, various types of soil models may be suitable. Different slope angles are also suggested. For instance, a low-sloped submarine slope model may be able to model strain-softening and retrogressive failure more effectively. The soil depth of the upper clay layer should be increased to more accurately define the excess pore pressure ratios at failure.

Due to the shallow depths of the soil profiles and the interference created by bottom boundary effects and the sand layer the CPT results are not reliable. A method of

accurately determining the strength characteristics of the soil profile would be useful in the stability analysis of future centrifuge studies.

The relative density of the sand layer was estimated for the centrifuge tests. It is recommended that sand raining procedures be used so that soil strength parameters can be more confidently defined for slope stability analyses. Also, the spaghetti strands in the soil profile should be positioned closer to allow for a better defined failure plane.

When the pressurization of the sand layer was carried out during centrifuge testing, it was not known if the slope had failed until clay suspension was witnessed in the surface water. It is recommended at the time of testing that the PPTs in the sand layer and a LVDT should be plotted separately in real time to confirm that slope failure had occurred. A high-speed digital camera is also recommended. It would allow slope failure to be captured frame by frame, permitting for more detailed analysis.

The effects of side wall friction should also be studied in further detail. It is believed that the Teflon spray worked reasonably well for the clay layers, but the sand layer still may be influenced by the effects of side wall friction. Due to the granular nature of the model sand, it is possible that the sand penetrated the Teflon coating.

To compare with the limit equilibrium analysis completed, a finite element analysis of the centrifuge tests would be useful to confirm the results of the limit equilibrium analysis. Furthermore, a finite element analysis could assess the effects of the unique stress history

experienced by the centrifuge model. Comparing a straightforward finite element analysis and a finite element analysis accounting for the unique stress history could determine the effects.

The study of triggering mechanisms associated with continental slope failure using centrifuge modelling is still in its early stages. Further centrifuge testing would give insight into future usefulness of studying the behaviour of submarine slope failures. Further centrifuge testing and analysis is recommended.

7.0 REFERENCES

Almagor, G. (1980). Halokinetic deep-seated slumping on the Mediterranean slope of northern Sinai and southern Israel. *Marine Geotechnology*, Vol. 4. pp. 83-105.

Al-Tabba, A. (1987). *Permeability and Stress-Strain Response of Speswhite Kaolin*. Ph. D. Thesis, University of Cambridge.

Arulanandan, K., Manzari, M., Zeng, X., Fagan, M., Scott, R.F., & Tan, T.S. (1994). What the VELACS project has revealed. *In.* Centrifuge 94. Leung, Lee, & Tan (eds.). Rotterdam: Balkema. pp. 25-32.

Astaneh, S.M.F., Ko, H.-Y. & Sture, S. (1994). Assessment of earthquake effects on soil embankment. *In.* Centrifuge 94. Leung, Lee, & Tan (eds.). Rotterdam: Balkema. pp. 221-226.

Atigh, E. & Byrne, P.M. (2004). Liquefaction flow of submarine slopes under partially undrained conditions: and effective stress approach. *Canadian Geotechnical Journal.* Vol. 41. pp. 154-165.

Azizian, A. & Popescu, R. (2001). Backanalysis of the 1929 Grand Banks submarine slope failure. *2nd Joint IAH and CGS Groundwater Conference: An Earth Odyssey.* Calgary, Canada. pp. 808-815.

Azizian, A. & Popescu, R. (2003). Finite element simulation of retrogressive failure of submarine slopes. *In.* Submarine Mass Movements and Their Consequences. J. Locat and J. Mienert, (eds.). Kluwer Academic Publishers. pp. 11-20.

Baraza, J., Lee, H.J., Kayen, R.E. & Hampton, M.A. (1990). Geotechnical characteristics and slope stability on the Ebro margin, western Mediterranean. *Marine Geology.* Vol. 95. pp. 379-393.

Barnes, P.M., Cheung, K.C., Smits, A.P., Almagor, G., Read, S.A.L., Barker, P.R. & Froggatt, P. (1991). Geotechnical analysis of the Kidnappers slide, upper continental slope, New Zealand. *Marine Geotechnology.* Vol. 10. pp. 159-188.

Biscontin, G., Pestana, J.M. & Nadim, F. (2003). Seismic triggering of submarine slides in soft cohesive soil deposits. *Marine Geology.* Vol. 3417. pp. 1-14.

Bishop, A.W. (1955). The use of the slip circle in the stability analysis of slopes. *Geotechnique.* Vol. 5. pp. 7-17.

Bolton, M.D., Gui, M.W. & Phillips, R. (1993). Review of miniature soil probes for model tests. *Proceedings of the 11th South East Asian Geotechnical Conference.* Singapore. pp. 1-6.

Booker, J.R., Balaam, N.P. & Davis, E.H. (1985a). The behaviour of an elastic non-homogeneous half-space: part I line and point loads. *International Journal of Numerical and Analytical Methods in Geomechanics.* Vol. 9, No. 4. pp. 353-367.

Booker, J.R., Balaam, N.P. & Davis, E.H. (1985b). The behaviour of an elastic non-homogeneous half-space: part II circular and strip footings. *International Journal of Numerical and Analytical Methods in Geomechanics.* Vol. 9, No. 4. pp. 369-381.

Booth, J.S. & Garrison, L.E. (1978). A geologic and geotechnical analysis of the upper continental slope adjacent to the Mississippi delta. *Proceedings of the 10th Annual Offshore Technology Conference.* Houston, USA. OTC 3165. pp. 1019-1028.

Boulanger, E., Konrad, J.-M., Locat, J. & Lee, H.J. (1998). Cyclic behaviour of Eel river sediments: a possible explanation for the paucity of submarine landslide features. *American Geophysical Union San Francisco, EOS*, Abstract.

Bryant, W.R., Bean, D., Liu, J.Y. & Dunlap, W. (2000). Geotechnical stratigraphy of sediments of the northwest Gulf of Mexico continental slope. *Proceedings of the Annual Offshore Technology Conference.* Houston, USA. OTC 12104. pp. 549-558.

Bryn, P., Kvalstad, T.J., Guttormsen, T.R., Kjærnes, P.A., Jund, J.K., Nadim, F. & Olsen, J. (2004). Storegga slide risk assessment. *Proceedings of the Annual Offshore Technology Conference.* Houston, USA. OTC 16560. pp. 1-14.

Bryn, P., Solheim, A., Berg, K., Lien, R., Forsberg, C.F., Haflidason, H., Ottesen, D. & Rise, L. (2003). The Storegga slide complex: repeated large scale sliding in response to climatic cyclicity. *In.* Submarine Mass Movements and Their Consequences. Locat, J. & Mienert, J. (eds.). Kluwer Academic Publishers. pp. 215-222.

Bugge T., Befring, S., Belderson, R.H., Eidvin, T., Jansen, E., Kenyon, N.H., Holtedahl, H. & Sejrup, H.P. (1987). A giant three-staged submarine slide off Norway. *Geo-Marine Letters.* Vol. 7. pp. 191-198.

Carlson, P.R., Karl, H.A., Edwards, B.D., Gardner, J.V. & Hall, R. (1993). Mass movement related to large submarine canyons along the Beringian margin, Alaska. *In.* Submarine Landslides: Selected Studies in the U.S. Exclusive Economic Zone. W.C. Schwab, H.J. Lee & D.C Twichell (eds.), U.S. Geological Survey Bulletin, 2002. pp. 104-116.

Casas, D., Ercilla, G., Alonso, B., Baraza, J., Lee, H.J. & Maldonado, A. (2003). Submarine mass movements on the Ebro slope. *In.* Submarine Mass Movements and

Their Consequences. Locat, J. & Mienert, J. (eds.). Kluwer Academic Publishers. pp. 393-400.

Cayocca, F., Cochonat, P., Bourillet, J.-F. & Quéméneur, P. (1998). Submarine slope failure related to fluid migration processes (continental slope of Gulf of Guinea). Online Source: http://www.ifremer.fr/drogm/Realisation/Publi/Poster/Images/gabon.pdf. Retrieved on February 2003.

C-CORE. (2004). *Earthquake induced damage mitigation from soil liquefaction: data report – centrifuge test CT1.* C-CORE Report R-04-010-145.

C-CORE. (2005). *Centrifuge modelling of pipeline stress due to heavy equipment encroachment.* C-CORE Report R-02-018-609v1.0.

Christian H.A., Mulder T. & Courtney R.C. (1995). Seabed slope instability on the Fraser River delta. *GSC Open File 2412,* Vancouver, British Columbia, Canada..

Clark, J.I. & Guigne, J.Y. (1988). Marine geotechnical engineering in Canada. *Canadian Geotechnical Journal.* Vol. 25. pp. 179-198.

Coleman, J.M. & Prior, D.B. (1978). Submarine landslides in the Mississippi river delta. *Proceedings of the 10th Annual Offshore Technology Conference.* Houston, USA. OTC 3170.

Dimakis, P., Elverhøi, A., Høeg, K., Solheim, A., Harbitz, C., Laberg, J.S., Vorren, T.O., & Marr, J. (2000). Submarine slope stability on high-latitude glaciated Svalbard-Barents Sea margin. *Marine Geology.* Vol. 162. pp. 303-316.

Driscoll, N,W., Weissel, J.K., & Goff, J.A. (2000). Potential for large-scale submarine slope failure and tsunami generation along the U.S. mid-Atlantic coast. *Geology.* Vol. 28, No. 5. pp. 407-410.

Edwards, B.D., Field, M.E. & Clukey, E.C. (1980). Geological and geotechnical analysis of a submarine slump, California borderland. *Proceedings of the 12th Annual Offshore Technology Conference.* Houston, USA. OTC 3726. pp. 399-410.

Evans, D., King, E.L., Kenyon, N.H., Brett, C. & Wallis, D. (1996). Evidence for long-term instability in the Storegga slide region off western Norway. *Marine Geology,* Vol. 130. pp. 281-292.

Fellenius, W. (1936). Calculation of the stability of earth dams. *Proceedings of the Second Congress on Large Dams.* Vol. 4. pp. 445-463.

Finn, W.D.L. (2002). State of the art for the evaluation of seismic liquefaction potential. *Computers and Geotechnics*, Vol. 29. pp. 329-341.

Fredlund, D.G. & Krahn, J. (1976). Comparison of slope stability methods of analysis. *Canadian Geotechnical Journal*. Vol. 14. pp. 429-439.

Fredlund, D.G., Krahn, J. & Pufahl, D.E. (1981). The relationship between limit equilibrium slope stability methods. *Proc. 10th International Conference on Soil Mechanics and Foundations Engineering*, Stockholm. Vol. 3. pp. 409-416.

Fuglsang, L.D. & Ovesen, N.K. (1988). The application of the theory of modelling to centrifuge studies. *In.* Centrifuges in Soil Mechanics. Craig, James and Schofield (eds). Balkema, Rotterdam (1988).

Gardner, J.V., Prior, D.B. & Field, M.E. (1999). Humboldt slide - a large shear-dominated retrogressive slope failure. *Marine Geology*. Vol. 154. pp. 323-338.

Geoslope International Ltd. (2004). *Slope-W Version 5.19*. Geoslope International, Calgary, Canada.

Hampton, M.A., Bouma, A.H., Carlson, P.R., Molnia, B.F., Clukey, E.C., & Sangrey, D.A. (1978). Quantitative study of slope instability in the Gulf of Alaska. *Proceedings of the 10th Annual Offshore Technology Conference*. Houston, USA. OTC 3314. pp. 2307-2319.

Hampton, M.A., Lee, H.J. & Locat, J. (1996). Submarine landslides. *Review of Geophysics*. Vol. 34, No. 1. pp. 33-59.

Hsiao, S.V. & Shemdin, O.H. (1980). Interaction of ocean waves with a soft bottom. *Journal of Physical Oceanography*. Vol. 10. pp. 605-610.

Hurley, S.J. (1999). *Development of a settling column and associated primary consolidation monitoring systems for the use in a geotechnical centrifuge*. Master of Engineering Thesis, Memorial University of Newfoundland.

Ishihara, K. (1977). Pore water pressure response and liquefaction of sand deposits during earthquakes. *Proceedings of the DM SR77*. Karlsruhe, Germany. Vol. 2. pp. 161-193.

Janbu, N. (1954). Application of composite slip surfaces for stability analysis, *Proc. European Conf. on Stability of Earth Slopes*, Stockholm. pp. 43-49.

Johns, M.W., Prior, D.B., Bornhold, B.D., Coleman, J.M. & Bryant, W.R. (1986). Geotechnical aspects of a submarine slope failure, Kitmat fjord, British Columbia. *Marine Geotechnology*. Vol. 6, No. 3. pp. 243-279.

Khoo, E., Okumura, T. & Lee, F.H. (1994). Side friction effects in plain strain models. *In.* Centrifuge 94. Leung, Lee, & Tan (eds.). Rotterdam: Balkema. pp. 115-120.

Krahn, J. (2003). The 2001 R.M. Hardy lecture: The limits of limit equilibrium analyses. *Canadian Geotechnical Journal.* Vol. 40. pp. 643-660.

Laberg, J.S. & Vorren, T.O. (2000). The Trænadjupet slide, offshore Norway—morphology, evaluation and triggering mechanisms. *Marine Geology.* Vol. 171. pp. 95-114.

Laberg, J.S., Vorren, T.O., Dowdeswell, J.A., Kenyon, N.H. & Taylor, J. (2000). The Andøya Slide and the Andøya canyon, north-eastern Norwegian-Greenland sea. *Marine Geology.* Vol. 162. pp. 259-275.

Laberg, J.S., Vorren, T.O., Mienert, J., Haflidason, H., Bryn, P. & Lien, R. (2003). Preconditions leading to the Holocene Trænadjupet slide offshore Norway. *In.* Submarine Mass Movements and Their Consequences. Locat, J. & Mienert, J. (eds.). Kluwer Academic Publishers. pp. 247-254.

Lee, H.J. (2003). Factors influencing occurrence, scale, mobility, runout, and morphology of mass movements on the continental slope. Online source: www.onr.navy.mil/sci_tech/ ocean/reports/docs/mg/00/lee.pdf. Retrieved on 20/01/2005.

Lee, H.J. & Edwards, B.D. (1986). Regional method to assess offshore slope stability. *Journal of Geotechnical Engineering.* Vol. 112, No. 5. pp. 489-509.

Lee, H.J., Locat, L., Dartnell, P., Israel, K. & Wong, F. (1999). Regional variability of slope stability: application to the Eel margin, California. *Marine Geology.* Vol. 154. pp. 305-321.

Leynaud, D. & Mienert, J. (2003). Slope stability assessment of the Trænadjupet slide area offshore the mid-Norwegian margin. *In.* Submarine Mass Movements and Their Consequences. Locat, J. & Mienert, J. (eds.). Kluwer Academic Publishers. pp. 255-265.

Lin, L. (1995). *Strength characteristics of a modelling silty clay.* Master of Engineering Thesis, Memorial University of Newfoundland.

Locat, J. & Lee, H.J. (2000). Submarine landslides: advances and challenges. *Proceedings of the 8th International Symposium on Landslides.* Cardiff, UK. pp. 1-30.

Logan, D.L. (2002). *A first course in the finite element method 3rd Ed.* Wadsworth Group, USA.

Lynett, P., Liu, P.L.-F. & Synolakis, C.E. (2003). Numerical modeling of tsunami generation by subaerial and submerged landslides. *In.* Submarine Mass Movements and Their Consequences. Locat, J. & Mienert, J. (eds.). Kluwer Academic Publishers. pp. 77-84.

Malvick, E.J., Kulasingam, R., Kutter, B.L., & Boulanger, R.W. (2002). Void redistribution and localized shear strains in slopes during liquefaction. *In.* Int. Conf. Physical Modelling Geotechnics-ICPMG '02. Phillips, R., Guo, P.J. & Popescu, R. (eds.). St. John's, Canada. pp. 495-500.

Mello, U.T. & Pratson, L.F. (1999). Regional slope stability and slope-failure mechanics from the two-dimensional state of stress in an infinite slope. *Marine Geology.* Vol. 154. pp. 339-356.

Menard, H.W. (1964). *Marine geology of the pacific.* McGraw-Hill, New York.

Milne, J. (1897). Suboceanic changes. *Geography Journal.* Vol. 10. pp. 129-146 and 259-289.

Miyamoto, J., Sassa, S. & Sekiguchi, H. (2002). Wave-induced liquefaction and changes in void ratio profile with depth. *In.* Int. Conf. Physical Modelling Geotechnics-ICPMG '02. Phillips, R., Guo, P.J. & Popescu, R. (eds.). St. John's, Canada. pp. 259-264.

Moore, J.G., Clague, D.A., Holcomb, R.T., Lipman, P.W., Normark, W.R. & Torresan, M.T. (1989). Prodigious submarine landslides on the Hawaiian ridge. *Journal of Geophysical Research.* Vol. 94, No. 17. pp. 465-484.

Morgenstern, N.R. (1967). Submarine slumping and the initiation of turbidity currents. *In.* Marine Geotechnique. Richards, A.F. (ed.), Urbana: University of Illinois Press. pp. 189-220.

Morgenstern, N.R. & Price, V.E. (1965). The analysis of the stability of general slip surfaces. *Geotechnique.* Vol. 15. pp. 70-93.

Mulder, T. & Cochonat, P. (1996). Classification of offshore mass movements. *Journal of Sedimentary Research.* Vol. 66, No. 1. pp. 43-57.

Mulder, T. & Moran, K. (1995). Relationship among submarine instabilities, sea-level variations and the presence of an ice sheet on the continental shelf: an example from the Verrill canyon area, Scotian shelf. *Paleoceanography.* Vol. 10. pp. 137-154.

Nagase, H., Ko, H.-Y., Law, H.K. & Pak, R.Y.S. (1994). Permanent displacement of sloping ground due to liquefaction. *In.* Centrifuge 94. Leung, Lee, & Tan (eds.). Rotterdam: Balkema. pp. 239-244.

Olsen, H.W., McGregor, B.A., Booth, J.S., Cardinell, A.P., & Rice, T.L. (1982). Stability of near-surface sediment on the mid-Atlantic upper continental slope. *Proceedings of the 14th Annual Offshore Technology Conference.* Houston, USA. OTC 4303. pp. 21-35.

Phillips, R. (2001). Simulating submarine slope stability initiation using centrifuge model testing. *2nd Joint IAH and CGS Groundwater Conference: An Earth Odyssey.* pp. 802-806.

Phillips, R. & Byrne, P.M. (1995). Modelling flowslides due to static loading. *Transportation Research Record.* Vol. 1504. pp. 12-21.

Phillips, R., Clark, J.I., Paulin, M.J., Meaney, R., Millan, D.E.L. & Tuff, K. (1994). Canadian national centrifuge centre with cold regions capabilities. *In.* Centrifuge 94. Leung, Lee, & Tan (eds.). Rotterdam: Balkema. pp. 57-62.

Pickrill, R., Piper, D.J.W., Collins, J., Kleiner, A. & Gee L. (2001). Scotian slope mapping project: the benefits of an integrated regional high-resolution multibeam survey. *Proceedings of the 2001 Offshore Technology Conference.* Houston, USA. OTC 12995. pp. 1-11.

Piper, D.J.W., Cochonat, P. & Morrison, M.L. (1999). The sequence of events around the epicentre of the 1929 Grand Banks earthquake: initiation of debris flows and turbidity current inferred from sidescan sonar. *Sedimentology.* Vol. 46. pp. 79-97.

Piper, D.J.W. & McCall, C. (2003). A synthesis of the distribution of submarine mass movements on the eastern Canadian margin. *EGS, AGU, and EUG Joint Assembly.* Nice, France. pp. 291-298.

Poulos, H.G. (1988). *Marine Geotechnics.* Unwin Hyman. London, UK.

Prior, D.B. & Coleman, J.M. (1978). Disintegrative retrogressive landslides on very-low-angle subaqueous slopes, Mississippi delta. *Marine Geotechnology.* Vol. 3. pp. 37-60.

Prior, D.B. & Coleman, J.M. (1984). Submarine slope instability. *In.* Slope Instability. Brunsden, D. & Prior, D.B. (eds). John Wiley & Sons Ltd. pp. 419-455.

Puzrin, A.M., Germanovich, L.N. & Kim, S. (2004). Catastrophic failure of submerged slopes in normally consolidated sediments. *Géotechnique.* Vol. 54, No. 10. pp. 631-643.

Quéméneur, P., Tisot, J.P., & Cochonat, P. (1998). Limit equilibrium conditions for deep sea sediments and infinite plane failure analysis, offshore Gabon. *Marine Georesources and Geotechnology.* Vol. 16. pp. 179-199.

Rahman, M.S. & Jaber, W.Y. (1991). Submarine landslide: elements of analysis. *Marine Geology*. Vol. 10. pp. 97-124.

Renzi, R., Corté, J.F., Rault, G., Bagge, G., Gui, M. & Laue, J. (1994). Cone penetration tests in the centrifuge: experience of five laboratories. *In*. Centrifuge 94. Leung, Lee, & Tan (eds.). Rotterdam: Balkema. pp. 221-226.

Robb, J.M. (1984). Spring sapping on the lower continental slope, offshore New Jersey. *Geology*. Vol. 12. pp. 278-282.

Robertson, P.K. & Campanella, R.G. (1985). Liquefaction potential of sands using the CPT. *Journal of Geotechnical Engineering, ASCE.* Vol. 111, No. 3. pp. 384-403.

Robertson, P.K. & Wride, C.E. (1998). Evaluating cyclic liquefaction potential using the cone penetration test. *Canadian Geotechnical Journal*. Vol. 35. pp. 442-459.

Sangrey, D.A. & Marks, D.L. (1981). Hindcasting evaluation of slope stability in the Baltimore canyon trough area. *Proceedings of the 13th Annual Offshore Technology Conference*. Houston, USA. OTC 3976. pp. 241-248.

Santamarina, J.C. & Goodings, D.J. (1989). Centrifuge modelling: a study of similarity. *Geotechnical Testing Journal, ASTM*. Vol. 12. pp. 163-166.

Sassa, S. & Sekiguchi, H. (1999). Wave-induced liquefaction of beds of sand in a centrifuge. *Geotechnique*. Vol. 49, No. 4. pp. 621-638.

Schofield, A.N. (1980). Cambridge geotechnical centrifuge operations. *Geotechnique*. Vol. 30, No. 3. pp. 227-268.

Schwab, W.C., Danforth, W.W., Scanlon, K.M. & Masson, D.G. (1991). A giant submarine slope failure on the northern insular slope of Puerto Rico. *Marine Geology*. Vol. 96. pp. 237-246.

Seed, H.B. & Idriss, I.M. (1971). Simplified procedure for evaluating soil liquefaction potential. *Journal of Soil Mechanics and Foundations Division, ASCE*. Vol. 97. pp. 1249-1273.

Seed, H.B., Idriss, I.M & Arango, I. (1983). Evaluation of liquefaction potential using field performance data. *Journal of Geotechnical Engineering*. Vol. 109, No. 3. pp. 458-482.

Seed, H.B. & Rahman, M.S. (1978). Wave-induced pore pressure in relation to ocean floor stability of cohesionless soils. *Marine Geotechnology*. Vol. 3. pp. 123-150.

Seed, H.B., Tokimatsu, K., Harder, L.F. & Chung, R.M. (1984). *The influence of SPT procedures in soil liquefaction resistance evaluations*. Earthquake Engineering Research Center. Berkeley, California. Report No. UCB/EERC-84/15.

Sekiguchi, H., Kita, K. & Okamoto, O. (1993). Centrifuge modelling of wave-induced instability of sand beds. *Proc. 3rd NTU-KU-KAIST Trilateral Seminar/Workshop on Civil Engineering*. pp. 199-204.

Sekiguchi, H., Sassa, S., Sugioka, K. & Miyamoto, J. (2000). Wave induced liquefaction, flow deformation and particle transport in sand beds. *GeoEng 2000*, Melbourne.

Shepard, F.P. (1963). *Submarine geology*. Harper-Collins, New York. pp. 557.

Small, J.C. & Booker, J.R. (1982). Finite layer analysis of primary and secondary consolidation. *Proceedings of the 3rd International Symposium on Numerical Methods in Geomechanics*. Edmonton, Canada. pp. 365-371.

Spencer, E. (1967). A method of analysis of the stability of embankments assuming parallel inter-slice forces. *Geotechnique*. Vol. 17. pp. 11-26.

Sultan, N., Cochonat, P., Foucher, J.P., Mienert, J., Haflidason, H. & Sejrup, H.P. (2003). Effect of gas hydrates dissociation on seafloor slope stability. *In.* Submarine Mass Movements and Their Consequences. Locat, J. & Mienert, J. (eds). Kluwer Academic Publishers. pp. 103-111.

Take, W.A. & Bolton, M.D. (2002). An atmospheric chamber for the investigation of the effect of seasonal moisture changes on clay slopes. *In.* Int. Conf. Physical Modelling Geotechnics-ICPMG '02. Phillips, R., Guo, P.J. & Popescu, R. (eds.). St. John's, Canada. pp. 765-770.

Taniguchi, E., Koga, Y., Morimoto, I. & Yasuda, Y. (1988). Centrifugal model tests on reinforced embankments by non-woven fabric. *Proceedings of the International Conference on Geotechnical Centrifuge Modelling*, Paris. pp. 253-258.

Taylor, R.N. (1994). Centrifuges in modelling: principles and scale effects. *In.* Geotechnical Centrifuge Technology. Taylor, R.N. (ed). Blackie Academic & Professional, London, UK.

Terzaghi, K. (1956). Varieties of submarine slope failures. *Proceedings of the 8th Texas Conference on Soil Mechanics and Foundation Engineering*. Austin, USA.

Towhata, I. & Ryull, K.S. (1990). Undrained strength of underconsolidated clays and its application to stability analysis of submarine slopes under rapid sedimentation. *Soils and Foundations*. Vol. 30, No. 1. pp. 100-114.

Trifunac, M.D. & Todorovska, M.I. (2003). Tsunami source parameters of submarine earthquakes and slides. *In.* Submarine Mass Movements and Their Consequences. Locat, J. & Mienert, J. (eds.). Kluwer Academic Publishers. pp. 121-128.

Tripsanas, E.K., Bryant, W.R., Prior, D.B. & Phaneuf, B.A. (2003). Interplay between salt activities and slope instabilities, Bryant canyon area, northwest Gulf of Mexico. *In.* Submarine Mass Movements and Their Consequences. Locat, J. & Mienert, J. (eds.). Kluwer Academic Publishers. pp. 307-315.

Vaid, Y.P. & Sivathayalan, S. (1996). Static and cyclic liquefaction potential of Fraser Delta sand in simple shear and triaxial tests. *Canadian Geotechnical Journal.* Vol. 33. pp. 281-289.

Walder, J.S. & Watts, P. (2003). Evaluating tsunami hazards from debris flows. *In.* Submarine Mass Movements and Their Consequences. Locat, J. & Mienert, J. (eds.). Kluwer Academic Publishers. pp. 155-162.

Watts, P. (2003). Probabilistic analyses of landslide tsunami hazards. *In.* Submarine Mass Movements and Their Consequences. Locat, J. & Mienert, J. (eds.). Kluwer Academic Publishers. pp. 163-170.

Whitman, R.V. & Bailey, W.A. (1967). Use of computer for slope stability analysis. *Journal of the Soil Mechanics and Foundation Division, ASCE.* Vol. 93. (SM4).

Yamamoto, T. (1978). Sea bed instability from waves. *Proceedings of the 10th Annual Offshore Technology Conference.* Houston, USA. OTC 3262.

Youd, T.L., Idriss, I.M., Andrus, R.D., Arango, I., Castro, G., Christian, J.T., Dobry, R., Finn, W.D.L., Harder, L.F., Hynes, M.E., Ishihara, K., Koester, J.P, Liao, S.S.C., Marcuson, W.F., Martin, G.R., Mitchel, J.K., Moriwaki, Y., Power, M.S., Robertson, P.K., Seed, R.B. & Stokoe, K.H. (2001). Liquefaction resistance of soils: summary report from the 1996 NCEER and 1998 NCEER/NSF workshops on evaluation of liquefaction resistance of soils. *Journal of Geotechnical and Geoenvironmental Engineering.* Vol. 127, No. 10. pp. 817-833.

Zen, K. & Yamakazi, H. (1991). Field observation and analysis of wave-induced liquefaction in seabed. *Soils and Foundations.* Vol. 21, No. 4. pp. 161-179.

Zhou, S.H., Liu, J.G., Wang, B.L., Yang, L.C. & Gong, Q.M. (2002). Centrifuge model test on the stability of underwater slope. *In.* Int. Conf. Physical Modelling Geotechnics-ICPMG '02. Phillips, R., Guo, P.J. & Popescu, R. (eds.). St. John's, Canada. pp. 759-764.

Appendix A

Testing Instrument Specifications

DRUCK PDCR 81 Miniature Pore Pressure Transducer

PDCR 81

Figure A1: Image of DRUCK PDCR 81 miniature pore pressure transducer.

Dimensions:	6.5 x 11.7 mm
Operating Pressure Ranges:	100 and 200 psi
Excitation Voltage:	5 volts 6 ma nominal
Output Voltage:	75 mV
Zero Offset:	± 10 mV maximum
Span Setting:	± 20% of nominal output
Output Impedence:	1000 ohms
Load Impedence:	Greater than 100 kohms
Resolution:	Infinite
Operating Temperature:	-5 ^{O} to 250°F
Mechanical Shock:	1000 g for 1 ms in each axes will not affect calibration
Weight:	1.05 oz with 15 feet of cable

For additional information consult:
http://www.druck.com/usa/products/MiniatureSeries.pdf

Trans-Tek Series 240 General Purpose CV LVDT

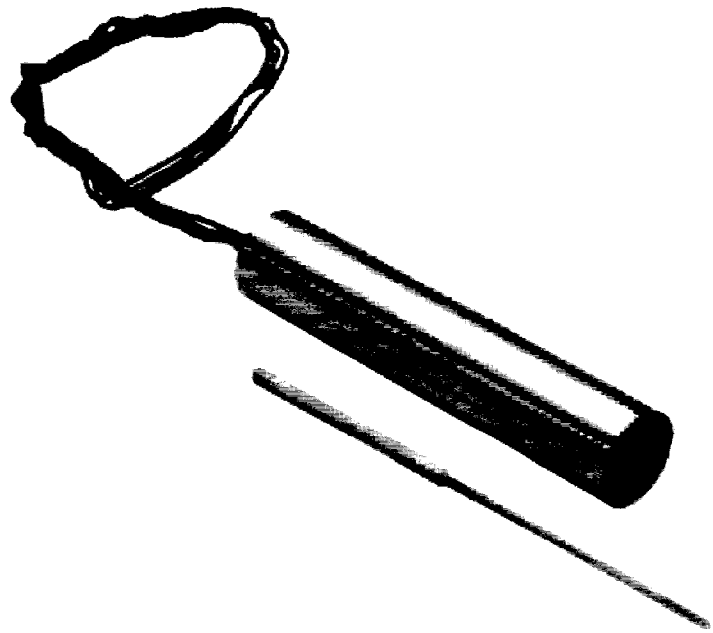

Figure A2: Image of Trans-Tek Series 240 general purpose CV LVDT.

Working Range:	± 25.4 mm
Maximum Working Range:	± 38.1 mm
Input:	6 to 30 VDC
Nominal Output:	4.6 to 24.8 VDC
Input Current:	8.3 – 52 mA
Non-Linearity:	± 0.5% over working range, ± 1% over usable range
Internal Carrier Frequency:	3200 Hz
% Ripple:	0.8
Output Impedance:	5600 Ohms
Frequency Response:	100 Hz
Temperature Range:	-54 to 121°C
Resolution:	Infinite

For additional information consult:
http://www.transtekinc.com/Catalog_PDFs-01/LVDTs/Ser240_01F.pdf

Fugro 1 cm^2 Miniature Piezocone Type: F0.5CKEW2/V

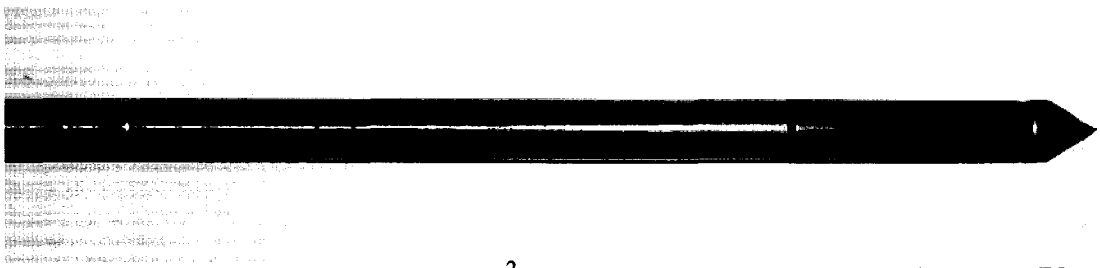

Figure A3: Image of Fugro 1 cm^2 miniature piezocone type: F0.5CKEW2/V.

Pore Pressure Transducer:	Kulite type XCM-3-50BAR serial #L27-80
Piezocone Tip Area:	1 cm^2
Piezocone OD:	11.3 mm
Friction Sleeve Area:	15 cm^2

Table A1: Fugro 1 cm^2 miniature piezocone specifications.

	Load limit	Zero at no load	Zero under 2.5 MPa Pressure	Output under load Zero pressure
Cone load cell	9 kN	-4.7 mV	21.4 mV	831.3 mV @ 5.0 kN
Cone+Friction load cell	9 kN	13.3 mV	30.8 mV	821.2 mV @ 5.0 kN
Pore pressure transducer	10.0 MPa	36.2 mV	737.6 mV	

Appendix B

Results from Slope Stability Analyses

Tabulated results of the slope stability analysis are presented. Utilizing Geoslope's SLOPE/W software, the factor of safety was calculated for each slope using Spencer's method of limit equilibrium. The tables provide the results calculated for each slice. The shear mobilization in the tables represent the shear stresses developed in the slope. All analyses used an anisotropic function shown in Figure B1. The anisotropic function accounted for the variation of lateral earth pressure with the changing inclination of each individual slice in the stability analyses. This function accounted for the fact that Speswhite kaolin clay has a coefficient of lateral earth pressure of 0.64 (Al-Tabba, 1987) and that as the slope becomes inclined the effect of lateral earth pressure decreases.

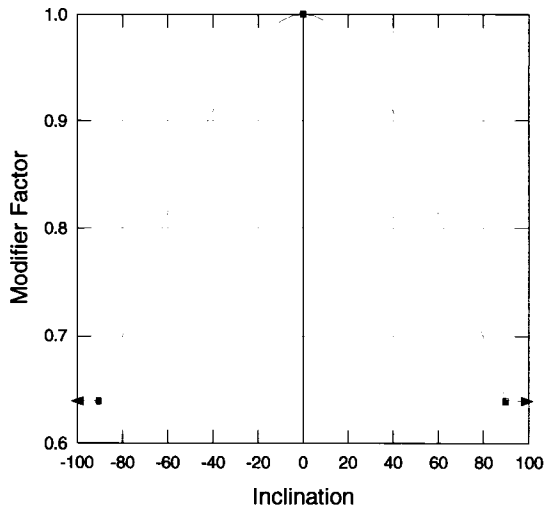

Figure B1: Anisotropic function used in all SLOPE/W analyses.

Slope Stability Test 1

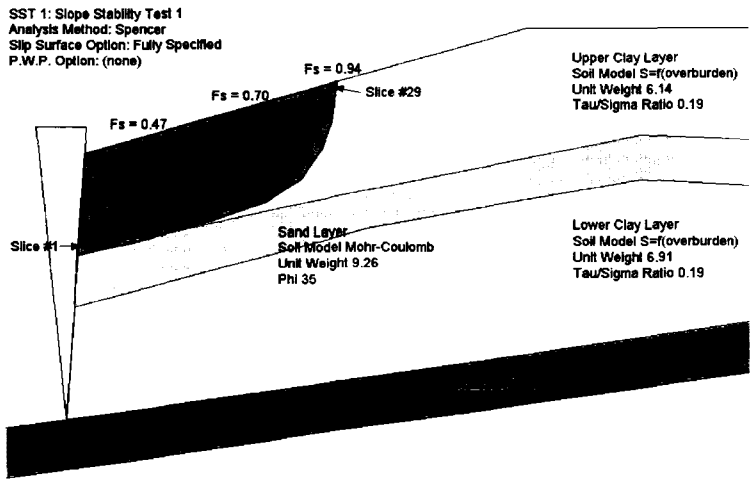

Figure B2: Slope stability analysis of SST 1 using SLOPE/W yielding $Fs = 0.94$. (NTS)

Table B1: Results from the slope stability analysis of SST 1.

Slice #	Cohesive Strength (kPa)	Frictional Strength (kPa)	Shear Strength (kPa)	Shear Mobilization (kPa)	Phi (degrees)	Excess Pore Water Pressures (kPa)
1	3.48	0.00	3.48	3.71	0.00	0.00
2	6.98	0.00	6.98	7.43	0.00	0.00
3	7.02	0.00	7.02	7.47	0.00	0.00
4	7.06	0.00	7.06	7.51	0.00	0.00
5	7.10	0.00	7.10	7.55	0.00	0.00
6	7.12	0.00	7.12	7.58	0.00	0.00
7	7.14	0.00	7.14	7.60	0.00	0.00
8	7.15	0.00	7.15	7.61	0.00	0.00
9	7.17	0.00	7.17	7.63	0.00	0.00
10	7.19	0.00	7.19	7.65	0.00	0.00
11	7.20	0.00	7.20	7.67	0.00	0.00
12	7.22	0.00	7.22	7.68	0.00	0.00
13	7.24	0.00	7.24	7.70	0.00	0.00
14	7.25	0.00	7.25	7.72	0.00	0.00
15	7.24	0.00	7.24	7.71	0.00	0.00
16	7.21	0.00	7.21	7.67	0.00	0.00
17	7.17	0.00	7.17	7.63	0.00	0.00
18	7.14	0.00	7.14	7.60	0.00	0.00
19	7.10	0.00	7.10	7.56	0.00	0.00
20	7.07	0.00	7.07	7.52	0.00	0.00
21	7.03	0.00	7.03	7.48	0.00	0.00
22	6.89	0.00	6.89	7.34	0.00	0.00
23	6.65	0.00	6.65	7.08	0.00	0.00
24	6.41	0.00	6.41	6.82	0.00	0.00
25	6.17	0.00	6.17	6.56	0.00	0.00
26	5.62	0.00	5.62	5.98	0.00	0.00
27	4.78	0.00	4.78	5.08	0.00	0.00
28	3.51	0.00	3.51	3.74	0.00	0.00
29	1.34	0.00	1.34	1.42	0.00	0.00

Slope Stability Test 2

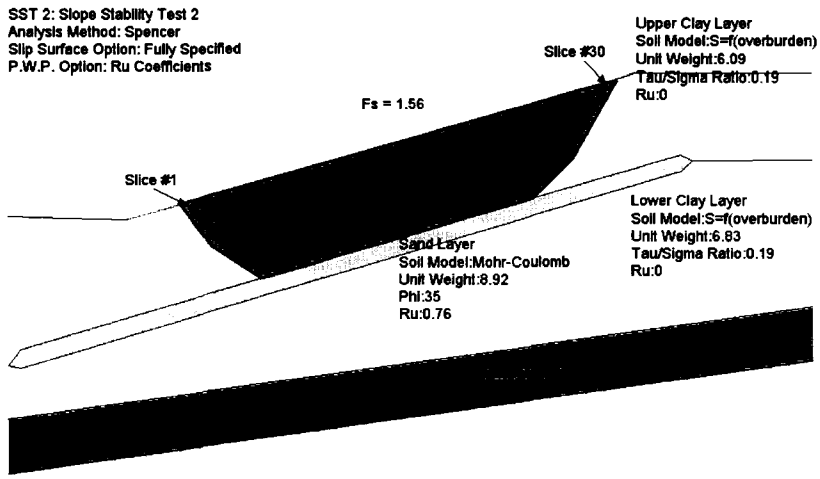

Figure B3: SLOPE/W stability analysis of SST 2 using a specified failure surface in the clay layer with a $r_u = 0.76$ yielding $Fs = 1.56$. (NTS)

Table B2: Results from the SLOPE/W stability analysis of SST 2 using a specified failure surface in the clay layer with a $r_u = 0.76$ yielding $Fs = 1.56$.

Slice #	Cohesive Strength (kPa)	Frictional Strength (kPa)	Shear Strength (kPa)	Shear Mobilization (kPa)	Phi (degrees)	Excess Pore Water Pressures (kPa)
1	0.83	0.00	0.83	0.53	0.00	0.00
2	2.49	0.00	2.49	1.60	0.00	0.00
3	3.82	0.00	3.82	2.45	0.00	0.00
4	4.81	0.00	4.81	3.09	0.00	0.00
5	5.80	0.00	5.80	3.73	0.00	0.00
6	6.30	0.00	6.30	4.05	0.00	0.00
7	6.29	0.00	6.29	4.04	0.00	0.00
8	6.28	0.00	6.28	4.04	0.00	0.00
9	6.27	0.00	6.27	4.03	0.00	0.00
10	6.26	0.00	6.26	4.03	0.00	0.00
11	6.25	0.00	6.25	4.02	0.00	0.00
12	6.25	0.00	6.25	4.01	0.00	0.00
13	6.24	0.00	6.24	4.01	0.00	0.00
14	6.23	0.00	6.23	4.00	0.00	0.00
15	6.22	0.00	6.22	4.00	0.00	0.00
16	6.21	0.00	6.21	3.99	0.00	0.00
17	6.20	0.00	6.20	3.99	0.00	0.00
18	6.19	0.00	6.19	3.98	0.00	0.00
19	6.19	0.00	6.19	3.98	0.00	0.00
20	6.18	0.00	6.18	3.97	0.00	0.00
21	6.17	0.00	6.17	3.97	0.00	0.00
22	6.16	0.00	6.16	3.96	0.00	0.00
23	6.15	0.00	6.15	3.95	0.00	0.00
24	6.14	0.00	6.14	3.95	0.00	0.00
25	5.84	0.00	5.84	3.75	0.00	0.00
26	5.23	0.00	5.23	3.36	0.00	0.00
27	4.62	0.00	4.62	2.97	0.00	0.00
28	3.60	0.00	3.60	2.31	0.00	0.00
29	2.16	0.00	2.16	1.39	0.00	0.00
30	0.72	0.00	0.72	0.46	0.00	0.00

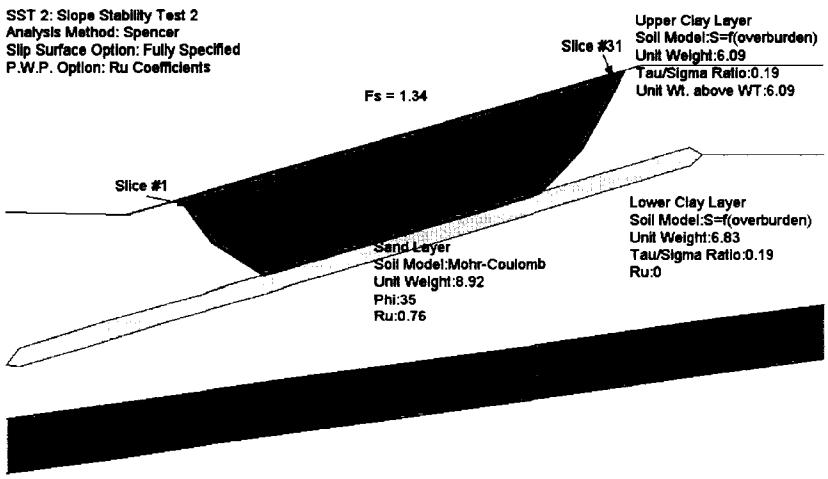

Figure B4: SLOPE/W stability analysis of SST 2 using a specified failure surface in the sand layer with a $r_u = 0.76$ yielding $Fs = 1.34$. (NTS)

Table B3: Results from the SLOPE/W stability analysis of SST 2 using a specified failure surface in the sand layer with a $r_u = 0.76$ yielding $Fs = 1.34$.

Slice #	Cohesive Strength (kPa)	Frictional Strength (kPa)	Shear Strength (kPa)	Shear Mobilization (kPa)	Phi (degrees)	Excess Pore Water Pressures (kPa)
1	0.77	0.00	0.77	0.58	0.00	0.00
2	2.32	0.00	2.32	1.74	0.00	0.00
3	3.74	0.00	3.74	2.80	0.00	0.00
4	4.73	0.00	4.73	3.54	0.00	0.00
5	5.71	0.00	5.71	4.28	0.00	0.00
6	6.30	0.00	6.30	4.71	0.00	0.00
7	0.00	5.11	5.11	3.83	35.00	25.27
8	0.00	5.10	5.10	3.82	35.00	25.24
9	0.00	5.10	5.10	3.82	35.00	25.21
10	0.00	5.09	5.09	3.81	35.00	25.18
11	0.00	5.09	5.09	3.81	35.00	25.16
12	0.00	5.08	5.08	3.80	35.00	25.13
13	0.00	5.08	5.08	3.80	35.00	25.10
14	0.00	5.07	5.07	3.80	35.00	25.07
15	0.00	5.06	5.06	3.79	35.00	25.04
16	0.00	5.06	5.06	3.79	35.00	25.01
17	0.00	5.05	5.05	3.78	35.00	24.99
18	0.00	5.05	5.05	3.78	35.00	24.96
19	0.00	5.04	5.04	3.77	35.00	24.93
20	0.00	5.04	5.04	3.77	35.00	24.90
21	0.00	5.03	5.03	3.77	35.00	24.87
22	0.00	5.02	5.02	3.76	35.00	24.85
23	0.00	5.02	5.02	3.76	35.00	24.82
24	0.00	5.01	5.01	3.75	35.00	24.79
25	0.00	3.43	3.43	2.57	35.00	24.69
26	5.59	0.00	5.59	4.18	0.00	0.00
27	5.00	0.00	5.00	3.74	0.00	0.00
28	4.42	0.00	4.42	3.31	0.00	0.00
29	3.23	0.00	3.23	2.42	0.00	0.00
30	1.94	0.00	1.94	1.45	0.00	0.00
31	0.65	0.00	0.65	0.48	0.00	0.00

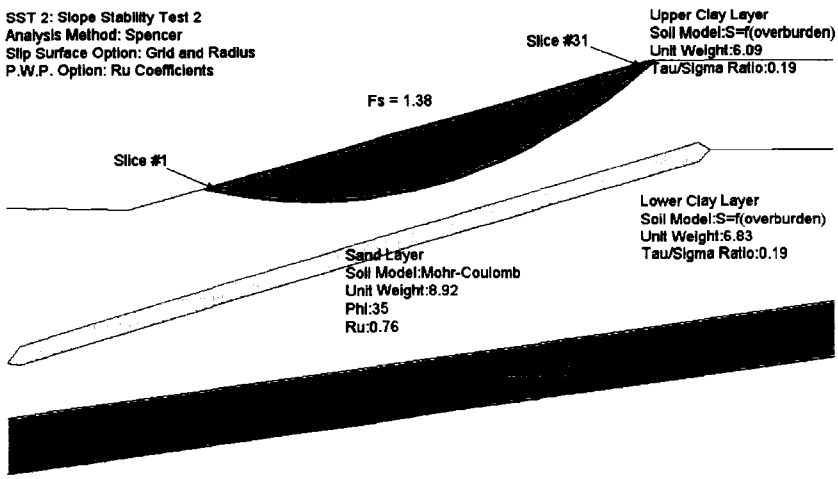

Figure B5: Critical slope stability analysis of SST 2 using SLOPE/W with a $r_u = 0.76$ yielding $Fs = 1.38$. (NTS)

Table B4: Results from the critical slope stability analysis of SST 2 using SLOPE/W with a $r_u = 0.76$ yielding $Fs = 1.38$

Slice #	Cohesive Strength (kPa)	Frictional Strength (kPa)	Shear Strength (kPa)	Shear Mobilization (kPa)	Phi (degrees)	Excess Pore Water Pressures (kPa)
1	0.24	0.00	0.24	0.18	0.00	0.00
2	0.71	0.00	0.71	0.51	0.00	0.00
3	1.14	0.00	1.14	0.82	0.00	0.00
4	1.54	0.00	1.54	1.11	0.00	0.00
5	1.91	0.00	1.91	1.38	0.00	0.00
6	2.25	0.00	2.25	1.62	0.00	0.00
7	2.55	0.00	2.55	1.84	0.00	0.00
8	2.82	0.00	2.82	2.04	0.00	0.00
9	3.06	0.00	3.06	2.21	0.00	0.00
10	3.27	0.00	3.27	2.36	0.00	0.00
11	3.45	0.00	3.45	2.49	0.00	0.00
12	3.59	0.00	3.59	2.60	0.00	0.00
13	3.70	0.00	3.70	2.68	0.00	0.00
14	3.78	0.00	3.78	2.73	0.00	0.00
15	3.83	0.00	3.83	2.76	0.00	0.00
16	3.84	0.00	3.84	2.77	0.00	0.00
17	3.82	0.00	3.82	2.76	0.00	0.00
18	3.77	0.00	3.77	2.72	0.00	0.00
19	3.68	0.00	3.68	2.66	0.00	0.00
20	3.56	0.00	3.56	2.57	0.00	0.00
21	3.40	0.00	3.40	2.46	0.00	0.00
22	3.22	0.00	3.22	2.32	0.00	0.00
23	2.99	0.00	2.99	2.16	0.00	0.00
24	2.74	0.00	2.74	1.98	0.00	0.00
25	2.45	0.00	2.45	1.77	0.00	0.00
26	2.12	0.00	2.12	1.53	0.00	0.00
27	1.76	0.00	1.76	1.27	0.00	0.00
28	1.36	0.00	1.36	0.98	0.00	0.00
29	0.93	0.00	0.93	0.67	0.00	0.00
30	0.46	0.00	0.46	0.33	0.00	0.00
31	0.11	0.00	0.11	0.08	0.00	0.00

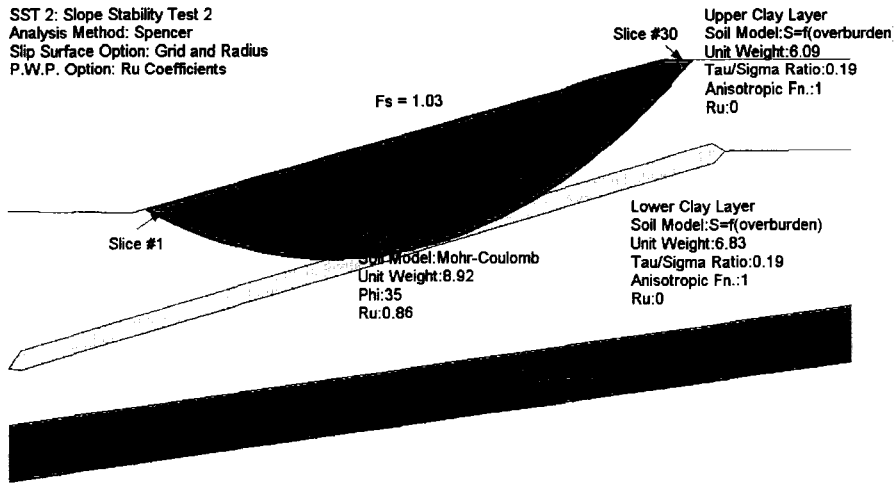

Figure B6: Critical slope stability analysis of SST 2 using SLOPE/W with a $r_u = 0.86$ yielding $Fs = 1.03$. (NTS)

Table B5: Results from the critical slope stability analysis of SST 2 using SLOPE/W with $r_u = 0.86$ yielding $Fs = 1.03$

Slice #	Cohesive Strength (kPa)	Frictional Strength (kPa)	Shear Strength (kPa)	Shear Mobilization (kPa)	Phi (degrees)	Excess Pore Water Pressures (kPa)
1	0.46	0.00	0.46	0.45	0.00	0.00
2	1.33	0.00	1.33	1.30	0.00	0.00
3	2.14	0.00	2.14	2.09	0.00	0.00
4	2.90	0.00	2.90	2.82	0.00	0.00
5	3.59	0.00	3.59	3.49	0.00	0.00
6	4.22	0.00	4.22	4.10	0.00	0.00
7	4.78	0.00	4.79	4.66	0.00	0.00
8	5.29	0.00	5.29	5.15	0.00	0.00
9	5.74	0.00	5.74	5.59	0.00	0.00
10	6.12	0.00	6.12	5.96	0.00	0.00
11	0.00	3.51	3.51	3.41	35.00	29.50
12	0.00	3.59	3.59	3.49	35.00	31.25
13	0.00	3.61	3.61	3.52	35.00	32.61
14	0.00	3.59	3.59	3.49	35.00	33.57
15	0.00	3.52	3.52	3.43	35.00	34.14
16	0.00	3.42	3.42	3.33	35.00	34.31
17	0.00	3.28	3.28	3.19	35.00	34.08
18	0.00	3.10	3.10	3.02	35.00	33.44
19	0.00	2.89	2.89	2.82	35.00	32.40
20	0.00	2.66	2.66	2.59	35.00	30.92
21	0.00	2.41	2.41	2.34	35.00	29.03
22	5.87	0.00	5.87	5.71	0.00	0.00
23	5.44	0.00	5.44	5.29	0.00	0.00
24	4.94	0.00	4.94	4.81	0.00	0.00
25	4.38	0.00	4.38	4.26	0.00	0.00
26	3.75	0.00	3.75	3.65	0.00	0.00
27	3.05	0.00	3.05	2.97	0.00	0.00
28	2.29	0.00	2.29	2.23	0.00	0.00
29	1.42	0.00	1.42	1.39	0.00	0.00
30	0.49	0.00	0.49	0.47	0.00	0.00

Slope Stability Test 3

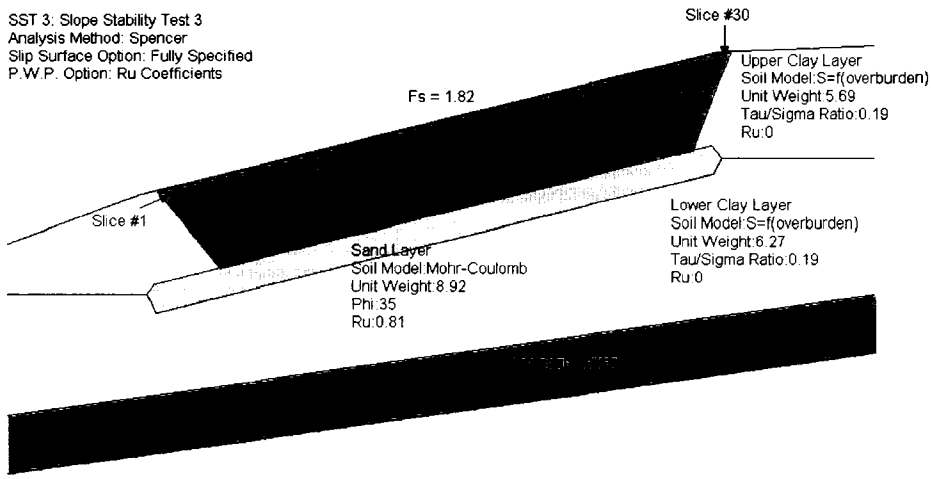

Figure B7: SLOPE/W stability analysis of SST 3 using a specified failure surface in the clay layer with a $r_u = 0.81$ yielding $Fs = 1.82$. (NTS)

Table B6: Results from the SLOPE/W stability analysis of SST 2 using a specified failure surface in the clay layer with a $r_u = 0.81$ yielding $Fs = 1.82$.

Slice #	Cohesive Strength (kPa)	Frictional Strength (kPa)	Shear Strength (kPa)	Shear Mobilization (kPa)	Phi (degrees)	Excess Pore Water Pressures (kPa)
1	0.81	0.00	0.81	0.44	0.00	0.00
2	2.42	0.00	2.42	1.33	0.00	0.00
3	4.03	0.00	4.03	2.22	0.00	0.00
4	5.12	0.00	5.12	2.82	0.00	0.00
5	5.12	0.00	5.12	2.82	0.00	0.00
6	5.12	0.00	5.12	2.82	0.00	0.00
7	5.12	0.00	5.12	2.82	0.00	0.00
8	5.11	0.00	5.11	2.82	0.00	0.00
9	5.11	0.00	5.11	2.82	0.00	0.00
10	5.11	0.00	5.11	2.81	0.00	0.00
11	5.11	0.00	5.11	2.81	0.00	0.00
12	5.11	0.00	5.11	2.81	0.00	0.00
13	5.10	0.00	5.10	2.81	0.00	0.00
14	5.10	0.00	5.10	2.81	0.00	0.00
15	5.10	0.00	5.10	2.81	0.00	0.00
16	5.10	0.00	5.10	2.81	0.00	0.00
17	5.10	0.00	5.10	2.81	0.00	0.00
18	5.09	0.00	5.09	2.81	0.00	0.00
19	5.09	0.00	5.09	2.80	0.00	0.00
20	5.09	0.00	5.09	2.80	0.00	0.00
21	5.09	0.00	5.09	2.80	0.00	0.00
22	5.09	0.00	5.09	2.80	0.00	0.00
23	5.08	0.00	5.08	2.80	0.00	0.00
24	5.08	0.00	5.08	2.80	0.00	0.00
25	5.08	0.00	5.08	2.80	0.00	0.00
26	5.08	0.00	5.08	2.80	0.00	0.00
27	5.08	0.00	5.08	2.80	0.00	0.00
28	5.07	0.00	5.07	2.79	0.00	0.00
29	2.86	0.00	2.86	1.58	0.00	0.00
30	0.70	0.00	0.70	0.38	0.00	0.00

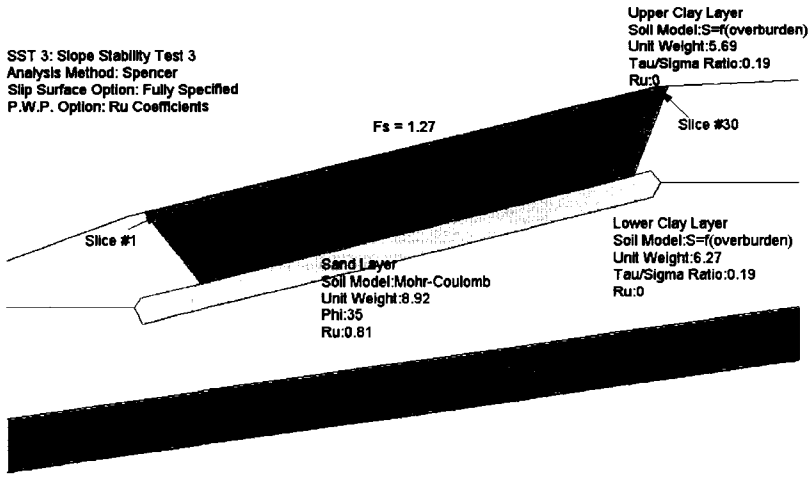

Figure B8: SLOPE/W stability analysis of SST 3 using a specified failure surface in the sand layer with a $r_u = 0.81$ yielding $Fs = 1.27$. (NTS)

Table B7: Results from the SLOPE/W stability analysis of SST 3 using a specified failure surface in the sand layer with a $r_u = 0.81$ yielding $Fs = 1.27$.

Slice #	Cohesive Strength (kPa)	Frictional Strength (kPa)	Shear Strength (kPa)	Shear Mobilization (kPa)	Phi (degrees)	Excess Pore Water Pressures (kPa)
1	0.81	0.00	0.81	0.64	0.00	0.00
2	2.42	0.00	2.42	1.91	0.00	0.00
3	4.04	0.00	4.04	3.18	0.00	0.00
4	0.00	3.34	3.34	2.63	35.00	21.96
5	0.00	3.33	3.33	2.63	35.00	21.95
6	0.00	3.33	3.33	2.63	35.00	21.94
7	0.00	3.33	3.33	2.62	35.00	21.93
8	0.00	3.33	3.33	2.62	35.00	21.91
9	0.00	3.32	3.32	2.62	35.00	21.90
10	0.00	3.32	3.32	2.62	35.00	21.89
11	0.00	3.32	3.32	2.62	35.00	21.88
12	0.00	3.32	3.32	2.62	35.00	21.87
13	0.00	3.32	3.32	2.62	35.00	21.86
14	0.00	3.32	3.32	2.62	35.00	21.85
15	0.00	3.32	3.32	2.62	35.00	21.84
16	0.00	3.31	3.31	2.61	35.00	21.83
17	0.00	3.31	3.31	2.61	35.00	21.82
18	0.00	3.31	3.31	2.61	35.00	21.81
19	0.00	3.31	3.31	2.61	35.00	21.80
20	0.00	3.31	3.31	2.61	35.00	21.79
21	0.00	3.31	3.31	2.61	35.00	21.78
22	0.00	3.30	3.30	2.61	35.00	21.77
23	0.00	3.30	3.30	2.61	35.00	21.76
24	0.00	3.30	3.30	2.60	35.00	21.75
25	0.00	3.30	3.30	2.60	35.00	21.74
26	0.00	3.30	3.30	2.60	35.00	21.73
27	0.00	3.30	3.30	2.60	35.00	21.72
28	0.00	3.29	3.29	2.60	35.00	21.71
29	2.86	0.00	2.86	2.26	0.00	0.00
30	0.70	0.00	0.70	0.55	0.00	0.00

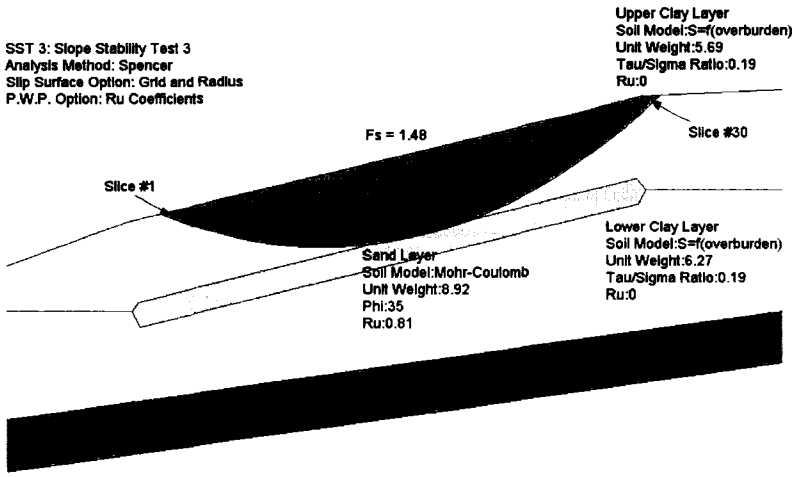

Figure B9: Critical slope stability analysis of SST 3 using SLOPE/W with a $r_u = 0.81$ yielding $Fs = 1.48$. (NTS)

Table B8: Results from the critical slope stability analysis of SST 3 using SLOPE/W with a $r_u = 0.81$ yielding $Fs = 1.48$.

Slice #	Cohesive Strength (kPa)	Frictional Strength (kPa)	Shear Strength (kPa)	Shear Mobilization (kPa)	Phi (degrees)	Excess Pore Water Pressures (kPa)
1	0.33	0.00	0.33	0.22	0.00	0.00
2	0.95	0.00	0.95	0.64	0.00	0.00
3	1.52	0.00	1.52	1.03	0.00	0.00
4	2.06	0.00	2.06	1.39	0.00	0.00
5	2.56	0.00	2.56	1.73	0.00	0.00
6	3.02	0.00	3.02	2.04	0.00	0.00
7	3.43	0.00	3.43	2.32	0.00	0.00
8	3.81	0.00	3.81	2.57	0.00	0.00
9	4.14	0.00	4.14	2.79	0.00	0.00
10	4.43	0.00	4.43	2.99	0.00	0.00
11	4.68	0.00	4.68	3.16	0.00	0.00
12	4.89	0.00	4.89	3.30	0.00	0.00
13	5.05	0.00	5.05	3.41	0.00	0.00
14	0.00	3.57	3.57	2.41	35.00	22.25
15	0.00	3.59	3.59	2.42	35.00	22.83
16	0.00	3.57	3.57	2.41	35.00	23.12
17	0.00	3.50	3.50	2.36	35.00	23.12
18	0.00	3.39	3.39	2.29	35.00	22.81
19	0.00	3.24	3.24	2.18	35.00	22.20
20	4.99	0.00	4.99	3.37	0.00	0.00
21	4.79	0.00	4.79	3.23	0.00	0.00
22	4.53	0.00	4.53	3.06	0.00	0.00
23	4.22	0.00	4.22	2.85	0.00	0.00
24	3.87	0.00	3.87	2.61	0.00	0.00
25	3.45	0.00	3.45	2.33	0.00	0.00
26	2.99	0.00	2.99	2.02	0.00	0.00
27	2.47	0.00	2.47	1.67	0.00	0.00
28	1.90	0.00	1.90	1.28	0.00	0.00
29	1.27	0.00	1.27	0.86	0.00	0.00
30	0.47	0.00	0.47	0.32	0.00	0.00

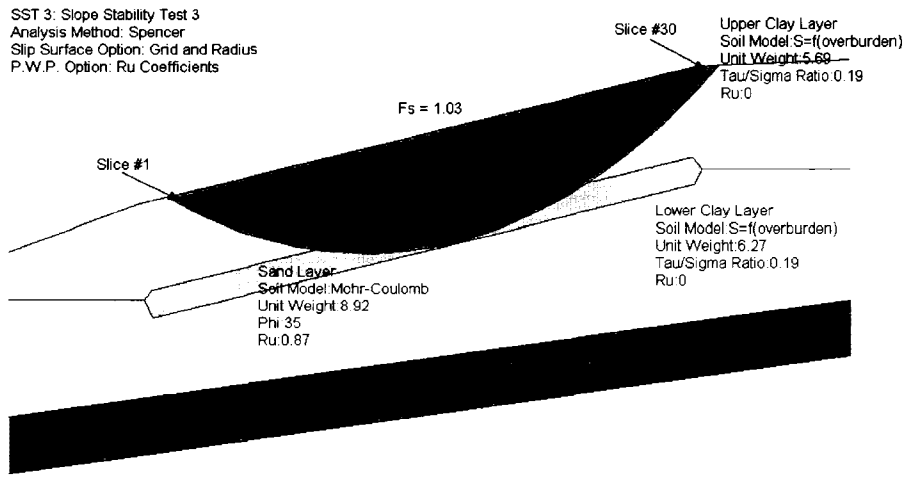

Figure B10: Critical slope stability analysis of SST 3 using SLOPE/W with a $r_u = 0.87$ yielding $Fs = 1.03$. (NTS)

Table B9: Results from the critical slope stability analysis of SST 3 using SLOPE/W with a $r_u = 0.87$ yielding $Fs = 1.03$

Slice #	Cohesive Strength (kPa)	Frictional Strength (kPa)	Shear Strength (kPa)	Shear Mobilization (kPa)	Phi (degrees)	Excess Pore Water Pressures (kPa)
1	0.43	0.00	0.43	0.41	0.00	0.00
2	1.24	0.00	1.24	1.20	0.00	0.00
3	1.99	0.00	1.99	1.94	0.00	0.00
4	2.69	0.00	2.69	2.61	0.00	0.00
5	3.33	0.00	3.33	3.24	0.00	0.00
6	3.92	0.00	3.92	3.81	0.00	0.00
7	4.44	0.00	4.44	4.32	0.00	0.00
8	4.91	0.00	4.92	4.78	0.00	0.00
9	0.00	2.97	2.97	2.88	35.00	24.90
10	0.00	3.15	3.15	3.07	35.00	27.39
11	0.00	3.29	3.29	3.19	35.00	29.50
12	0.00	3.37	3.37	3.27	35.00	31.23
13	0.00	3.40	3.40	3.30	35.00	32.59
14	0.00	3.39	3.39	3.29	35.00	33.56
15	0.00	3.33	3.33	3.24	35.00	34.16
16	0.00	3.25	3.25	3.15	35.00	34.38
17	0.00	3.12	3.12	3.04	35.00	34.21
18	0.00	2.97	2.97	2.89	35.00	33.65
19	0.00	2.79	2.79	2.71	35.00	32.70
20	0.00	2.59	2.59	2.51	35.00	31.34
21	0.00	2.36	2.36	2.29	35.00	29.58
22	0.00	2.11	2.11	2.05	35.00	27.41
23	0.00	1.84	1.84	1.79	35.00	24.81
24	4.77	0.00	4.77	4.63	0.00	0.00
25	4.26	0.00	4.26	4.14	0.00	0.00
26	3.69	0.00	3.69	3.58	0.00	0.00
27	3.05	0.00	3.05	2.96	0.00	0.00
28	2.35	0.00	2.35	2.28	0.00	0.00
29	1.58	0.00	1.58	1.53	0.00	0.00
30	0.59	0.00	0.59	0.58	0.00	0.00